

Anatomical, Morphometrical and Biomechanical Studies
of Barn Owls' and Pigeons' Wings

Von der Fakultät für Mathematik, Informatik und Naturwissenschaften
der RWTH Aachen University zur Erlangung des akademischen Grades
eines Doktors der Naturwissenschaften genehmigte Dissertation

vorgelegt von
Diplom-Biologe
Thomas Willem Bachmann
aus Bonn

Berichter: Universitätsprofessor Dr. Hermann Wagner
Universitätsprofessor Dr. Werner Baumgartner

Tag der mündlichen Prüfung: 21.05.2010

Diese Dissertation ist auf den Internetseiten der Hochschulbibliothek online verfügbar.

Wenn einer, der mit Mühe kaum
gekrochen ist auf einen Baum,
schon meint, dass er ein Vöglein wär'
so irrt sich der.

(Wilhelm Busch)

Meiner Familie gewidmet

Contents

1	Introduction	1
1.1	Fundamentals of bird flight	1
1.2	A silent hunter - The barn owl (<i>Tyto alba</i>)	2
1.3	Specialisations of the owl's plumage	4
1.4	Objective and organisation of the thesis	5
2	Anatomical Characterisation of Barn Owl's and Pigeon's Wings	6
2.1	Introduction	6
2.2	Materials and Methods	7
2.2.1	Specimens and preparation (for 2D analysis)	7
2.2.2	Morphometrics	8
2.2.3	3D-analysis and profile measurements	9
2.2.4	Computed tomography and 3D-reconstruction of internal wing structures	10
2.3	Results	10
2.3.1	Wing anatomy of barn owls and pigeons	10
2.3.2	Morphometrics	14
2.3.3	Aerodynamic parameters of wing profiles	15
2.3.4	Barn owl	15
2.3.5	Pigeon	19
2.3.6	Comparison between barn owl and pigeon	22
2.4	Discussion	24
2.4.1	Reconstruction of a three-dimensional wing	24
2.4.2	Are barn owl wings adapted to low-speed flight?	24
2.4.3	Aerodynamic properties of the wing	26
2.5	Conclusions	27
3	3D Reconstruction and Investigation of Plumage Specifics of Barn Owls	28
3.1	Introduction	28
3.2	Materials and Methods	29
3.2.1	Confocal laser scanning microscopy and 3D reconstruction	29
3.2.2	Feather material	29
3.2.3	Serrations of the barn owl's 10 th primary	29
3.2.4	Fringes of barn owls' remiges	32
3.2.5	Velvet-like dorsal surface of barn owls' remiges	33
3.3	Results	35
3.3.1	Serrations	35
3.3.2	Fringes	41
3.3.3	Velvet-like dorsal surface	44
3.4	Discussion	47
3.4.1	Serrations	47
3.4.2	Fringes	49
3.4.3	Velvet-like dorsal surface	50

3.4.4	Confocal laser scanning microscopy in comparison to other volume based methods	51
3.5	Conclusions	53
4	Material Properties of Barn Owls' and Pigeons' Feathers	54
4.1	Introduction	54
4.2	Materials and Methods	55
4.2.1	Two-point bending test	55
4.2.2	Determination of the second moment of area	57
4.2.3	Calculation of the Young's modulus	58
4.2.4	Nanoindentation	59
4.3	Results	61
4.3.1	Young's modulus of barn owl's and pigeon's feather keratin	61
4.3.2	Geometry of the rachis of barn owls' and pigeons' 4 th primaries	63
4.4	Discussion	68
4.4.1	A critical view on the methods used	68
4.4.2	Young's modulus of feather keratin and the geometry of the feather shaft	69
4.5	Conclusions	71
5	General Discussion	72
5.1	Wings	72
5.2	Feathers	74
5.2.1	Serrations	74
5.2.2	Velvet-like dorsal texture	75
5.2.3	Fringes	76
5.3	Material properties and geometry of the feather shafts	76
5.4	Hunting strategy of barn owls	77
5.5	Ecological niche	78
5.6	Conclusions	79
6	Summary	80
7	Zusammenfassung	81
	References	83
	Danksagung	90
	Curriculum vitae	91

1 Introduction

Owls (*Strigiformes*) have evolved a slow and silent flight to detect and localise potential prey in flight using acoustic information. An understanding of the mechanisms underlying silent flight may be an inspiration for the development of engineering solutions for noise reduction in today's world. Urbanisation and the increasing demand for air freight and renewable energy have led to a dramatic increase of noise pollution in the last decades. At ground level, airplanes produce an intense noise by their high lift configurations of the wings. Furthermore, wind farms are constantly upgraded. Their noise emission does not only annoy humans, but also disturbs migratory animals such as birds, or in case of offshore wind farms, whales and fish. How flight noise is efficiently reduced is shown by owls. These birds evolved noise reduction and noise suppressing devices during their long period of evolution. The transformation of the underlying mechanisms to modern air crafts and wings of wind power plants would help to reduce noise pollution drastically. This thesis provides a comprehensive study of the flight apparatus of the barn owl (*Tyto alba*) as a fundamental basis for studying silent flight.

1.1 Fundamentals of bird flight

In the course of evolution some reptiles developed feathers and conquered the air for locomotion [66, 67, 72]. The evolution of feathers and the transformation of the forelimb from a device for terrestrial locomotion into a wing were explicit features that split *archosaurs*, respectively the class *aves*, from other taxa [55]. Due to different birds' needs, a great variability of wing planforms has evolved. Wings can be long or short, narrow or broad, thick or thin [52, 81]. Furthermore, they can have a pointed wing tip, or a round taper, which may be smooth or fingered [20, 53, 71]. Considering this variety, each wing appears to be perfectly adapted to the particular species and the ecological niche it uses. However, all wings have at least one aerodynamic feature in common: they are cambered to the dorsal side. Only curved wings are able to produce enough lift in order to get birds airborne. Bird wings are mostly cambered in proximal regions of the wing. Thickness as well as camber decrease towards the wing tip [12, 41, 52, 61, 64]. The reduction of mass causes a decrease of inertia, which allows the bird to beat its wings at high frequencies. A higher mass at the wing tip would increase the inertia and much more energy would be needed for flapping flight [81].

Wings produce lift because the air flows faster on the dorsal than on the ventral side. This phenomenon is due to the dorsal cambering and can be most easily understood for gliding flight, which resembles the situation in a conventional aircraft. The faster movement on the dorsal side is accompanied by a pressure reduction (suction) [80, 81]. In this way wings produce lift. In flapping flight the aerodynamic circumstances are much more complex and hard to measure, since different forces act on the wing. These forces depend on the flow direction of the air, the angle of attack and the drag of the wing [1, 9, 10, 49, 52, 61, 76, 88, 89, 91, 93]. Explanations in the following chapters refer only to the gliding flight.

A bird has to counteract gravity in order to become airborne. Consequently, flight consumes a lot of energy, especially during take-off and landing [75, 88, 89]. Birds achieve high lift either by an intense beating of the wings or by forming wings with high lift properties [1, 10, 60, 71]. A high-lift configuration is achieved by a high camber and a large wing area that results in a low wing loading [80].

Apart from gravity, birds have to deal with a further force, the drag. Drag is the resistance of the body and the wings while moving in air. It comprises three components: First, the friction between the air flow and the body, second, the drag of the bird's body and leading edges of the wings and third, the induced drag. The induced drag is the component of drag force on the bird's wing that is 'induced' by lift and associated with the tip vortices that are formed at the tip of a wing [80]. To reduce the induced drag, birds evolved different wings and wing tip endings depending on their living conditions [53]. Birds with elongated wings and pointed wing tips, such as the albatross (*Diomedea exulans*), or birds with broad wings and fingered wing tips, such as the condor (*Vultur gryphus*) are perfectly adapted to gliding flight, but in different habitats. A round or rather elliptic wing planform, as it is found in owls, is also effective in gliding flight in the low flight speed range [81].

1.2 A silent hunter - The barn owl (*Tyto alba*)

Barn owls have an almost global distribution [87], which is reflected in the existence of many subspecies. For the purpose of the presented studies, the American subspecies *Tyto alba pratincola* was investigated and most subsequent descriptions and comments will refer to this subspecies. In urban areas, barn owls nest in barns and churches. Hereby, in many countries, these birds were named after their nesting places (UK, USA: *barn owl*, NL: *kerkuil*). In the German language this bird is named after the characteristic facial ruff (*Schleiereule*). Originally barn owls nested in cavities and depended upon fissures in cliffs or tree holes. Such nesting sites are still found in California (USA).

Barn owls are medium-sized birds with a mean body weight of about 450 g. Although the appearance of barn owls suggests a large bird, the thorax is quite small (Fig. 1). The large body volume is reached by the feathers and downs. Barn owls' wings [39] and legs are elongated (Fig. 1 right), by which owls are able to fly in suitable open habitats and dive into long vegetation to catch prey [17]. Those subspecies that are adapted to more wooded environments have shorter wings [87]. The colouring of barn owls varies between individuals and subspecies. Head, back and the dorsal surfaces of the wings and the tail are brownish golden, with some tendencies to a dark grey, but always with dark brown, white and almost black marks. All parts that are subjected to the ground during flight, such as the neck, the underside, the legs, the lower side of the wings and the tail, are mostly white or light brown with small black dots. Females tend to be darker than males [87].



Figure 1: *Habitus and skeleton of an adult barn owl (Tyto alba pratincola)*

Barn owls spend a high proportion of their time searching for prey, either sitting on a perch, or flying slowly over fields and vegetation [56, 87]. Several anatomical and behavioural adaptations to the hunting strategy in this bird have been reported [4, 31, 43, 46, 62, 69, 87, 94]. The prey of the barn owl, small voles and mice [87], is mainly active at night. Although adapted to the twilight, the visual perception of barn owls is limited in terms of visual resolution and contrast sensitivity [32]. However, by rustling through leaves and by squeaking, mice emit noise [99], which can be detected by the owl even at absolute darkness [42, 46, 69]. One conspicuous specialisation is the facial ruff with its specialised feathers that directs the sound towards the ears like a dish antenna [43]. Asymmetrically arranged ear flaps in front of the outer ear canals help the owl with discrimination of sound sources in elevation [34, 94]. Furthermore, nuclei in the brain that process acoustic information are enlarged compared with other similar-sized birds [42, 45, 48, 97]. With this set of adaptations, barn owls are able to detect and localise their prey precisely by acoustic information.

Nevertheless, to be able to utilise these specialisations, owls should not produce noise during flight. On the one hand, noise emitted by prey would be masked by the owl's own noise. On the other hand, prey might be warned by the approaching owl. Consequently, owls rely on a silent flight, which is achieved by further adaptations of the wing and the plumage.

1.3 Specialisations of the owl's plumage

Feathers are the main components of a bird's wing [4, 18]. Interaction with the air flow during flight and protection against cold, heat and wetness are some functions to mention. Furthermore, wings are used for display or camouflage by some birds [18].

A feather consists of a central shaft (rachis) and two laterally attached vanes [4, 18, 72]. Vanes are formed by barbs that are in turn connected via hook and bow radiates [4, 72]. While each feather is inserted with its calamus (basal part of the rachis) into the integument of the wing, all remiges are additionally associated with the underlying skeleton [16, 72]. Secondary remiges are connected to the posterior edge of the ulna; primary remiges are supported by bones of the hand and fingers. Coverts arise from the anterior integument membrane, forming smooth and closed upper and lower wing surfaces. As mentioned above, wing feathers interact with the air flow during flight. Furthermore, lift and drag are influenced by the feather's bending behaviour under incident flow and by their surface and edge appearance.

In barn owls, several plumage specialisations have been reported that influence the flow over the wing: The dorsal surfaces of the feathers have an increased roughness formed by elongations of hook radiates, called pennula [4, 31, 51, 62]. The 10th primary and 10th greater primary covert, which form the leading edge of the distal wing, are equipped with serrations at the outer vanes [4, 31, 62]. Last but not least, every single feather of the wing is surrounded by a fringed structure due to unconnected barb endings [4, 31]. These plumage specifics have been implicated in noise suppression during flight [31, 47, 62] by damping noise above 2 kHz [51, 62]. Thus, flight noise is reduced within the typical hearing spectrum of the owl's prey [62, 99] and within the owl's own best hearing range as well [25, 44].

Although two-dimensional information about the feather specifics are available [4] and few experiments have been performed to understand the mechanisms underlying silent flight [2, 31, 35, 36, 41, 51, 52, 62, 79, 86], the aerodynamics and acoustical features implemented by barn owls are yet poorly understood.

1.4 Objective and organisation of the thesis

The objective of this thesis was to provide quantitative two- and three-dimensional characterisations of wings and feathers of barn owls (*Tyto alba*) using modern 3D-imaging techniques and -analysis. These characterisations shall then be used to understand the mechanisms underlying silent flight. In order to emphasise wing specifics found in barn owls, the same measurements were performed at a further bird species, the pigeon (*Columba livia*), that has a similar body weight but shows a different flight style and living conditions. Since the anatomical investigations are based on only two species, this thesis has not the pretension of a comparative morphological study. It was rather aimed to understand the different requirements on the flight apparatus (wing anatomy, feather appearance, material properties) of the two bird species investigated here, with a main focus on the barn owl.

The core of this thesis comprises three different studies. Chapters two to four present the results of these three studies. Methodological approaches of the relevant studies are introduced in the particular chapters. Wings of barn owls and pigeons are anatomically characterised using two- and three-dimensionally measuring methods in chapter two. By this approach profile characteristics and aerodynamic properties of the wings were revealed. The results are discussed with respect to the flight style and living conditions of the particular bird species. In chapter three a morphometric three-dimensional description of the plumage specialisations of barn owls is given. High-resolution microscopical techniques were used to collect three-dimensional information of these structures, which in turn allow speculations about possible functions. Material properties of feather keratin of barn owls and pigeons are presented in chapter four. Mechanical measurements were used to determine the second moment of area of rachises and the Young's modulus of feather keratin. This study addresses the question whether material or geometrical properties are responsible for the bending behaviour of the investigated feathers. After these chapters, a general discussion reviews the main findings with respect to their influence on the flow field and to noise suppression during flight. A summary of the thesis is presented in the last chapter.

2 Anatomical Characterisation of Barn Owl's and Pigeon's Wings

2.1 Introduction

Wings of birds were already taken as role models in early aviation attempts. Unfortunately, copying the natural structure alone was not successful (see for example the work of *Leonardo da Vinci* and other visionaries of aviation). Early publications of the three-dimensional wing structure of birds were mainly suggestions. This can be seen for example in the drawings of a flying stork by Otto Lilienthal in 1889 [50]. Later investigations [12, 52, 59, 61, 64] of the wing as a three-dimensional object were more precise, but were partially hampered by problems due to fixation, drying processes or the accuracy of the measuring setup. For example, small metal brads were used to frame profiles of bird wings by Nachtigall et al. [61]. Although these authors provided important data of the wing geometry, only limited information was gained due to the small number of brads and measured profiles. Modern imaging techniques allow the digitising of the whole surface of a wing, which results in a precise point cloud with high spatial resolution. In contrast, two-dimensional information of the wing, such as wing area and wing span, are more easily obtained and many bird species were investigated and compared in the past [1, 39, 53, 63, 88, 95].

The aim of this study was to quantitatively describe the wing anatomy of two species of birds, barn owls and pigeons, with a similar body weight, but with a different flight style and different requirements on their flight apparatus. The anatomical characterisations of barn owl and pigeon wings presented here are based on two- and three-dimensional data.

Flight speed and flight style are affected by wing anatomy, body size and body mass. Wing loading, the loaded weight of the bird divided by the wing area, correlates with the flight speed, the dynamics of lift and the turning radius of flying birds [1, 39, 53, 63, 92, 95]. Species living or hunting within vegetation show low wing loadings, guaranteeing slow flight and tight turning radii [39, 63]. Another characteristic of wing anatomy is the aspect ratio, the wing span divided by the mean wing chord. A low aspect ratio indicates broad wings, which allow low-speed flight and guarantee high manoeuvrability. A high aspect ratio stands for narrow and long wings and is typically correlated with higher flight speeds [39, 53]. Furthermore, profile characteristics such as camber and thickness distribution have a great impact on the flight performance.

Since barn owls detect their prey by hearing, they need to reduce flight noise. Flying slowly is one means in this direction. To provide enough lift at low-speed, the wing need to be highly cambered [80]. However, the flow over highly cambered wings tends to separate more easily with a resulting negative impact on the lift distribution.

Pigeons are known as fast and persistent flying birds [5, 9, 24, 61, 70, 71]. Their wings should be smaller in size to reduce drag at high velocities. These birds have to beat their wings at high frequencies in order to reach the high flight speed. Consequently, the inertia of the tip should be reduced to save energy. However, other parameters such as angle of attack, free stream velocity, surface quality and thickness distribution influence the flight performance of a wing as well.

Non-invasive imaging techniques, such as computed tomography (CT) may now be used to investigate the skeletal elements, muscles and ligaments in high-resolution and thus to specify structures that are involved in forming camber and thickness. Furthermore, digitising via laser scanning or modern photogrammetry allows a much more precise and fast description of the three-dimensional wing anatomy. Liu et al. [52] investigated several bird wings via laser scanning and provided a mathematical method to describe aerodynamic relevant parameters such as thickness and camber. These authors used separated and dried wings for their studies. Such wings show many differences to the wing geometry and characteristics of living and free gliding birds. Additionally, Liu et al. [52] did not take the dependence of wing area and wing span on flight style and flying speed into account. Other authors [49, 71] have provided such data, but did not present three-dimensional information.

In the following barn owl's and pigeon's wings are characterised with respect to their aerodynamic properties. Those structures that are responsible for forming the aerodynamic properties are determined with modern three-dimensional visualisation methods.

2.2 Materials and Methods

2.2.1 Specimens and preparation (for 2D analysis)

Wings of barn owls (*Tyto alba pratincola*) and pigeons (*Columba livia*) were carefully prepared to carry out the anatomical investigations. Barn owl wings were obtained from specimens of the institute's own colony that had been sacrificed for other experiments under a permit of the local authorities (Landespräsidium für Natur, Umwelt und Verbraucherschutz Nordrhein Westfalen, Recklinghausen, Germany (LANUV)). Ten wings of six different barn owls were prepared (six were separated, four still connected to the bird's body). Five pigeons were received from a breeder and prepared specifically for this and other studies under another permit from LANUV. Thus, ten pigeon wings (eight were separated, two still connected to the bird's body) were obtained. All wings were manually extended until they were fully sprawled out. Photos of free gliding pigeons and barn owls were used as a template in the process of preparation and fixation. The wings were fixed with needles on Styrofoam. Immediately after preparation digital images were made with an 8-megapixel digital camera (Canon EOS 350D, Canon Lens 50 mm, Canon Inc., Tokio, Japan) from dorsal and ventral. Graphic software (Adobe Photoshop CS, Adobe Systems, San Jose, California, USA and ImageJ, National Institutes of Health, USA) was used to collect the morphometric data.

The skeletal elements of a birds forearm (ulna and radius) indicate how much the bird is moving its wing in flight [23]. A higher bowing of these bones suggests more muscle mass and thus a stronger movement. To specify the bowing of ulna and radius, the skeletal elements were measured. Therefore, four wings per species were dissected and the ratio of the length of ulna to the maximum distance between ulna and radius was calculated to specify the curving.

2.2.2 Morphometrics

Wing morphometry measurements were performed at digital images of fully extended and fixed wings. The length of the wing was measured as the distance of the outermost feather's tip (barn owl 10th primary, pigeon 9th primary) to the proximal humerus (Fig. 2). Usually the length of wing is measured as the half wing span, the half distance between both wing tips [88]. At the separated wings, wing span was measured by adding the lengths of both wings plus the body width. The body width was measured in one specimen of both species (barn owl 10 cm, pigeon 9.5 cm). Wing area was measured by counting the relevant pixels with a given size. Millimetre paper placed on the wing's surface was taken as reference. The root box was calculated by multiplying the body width with the root chord of the wing. Body mass was obtained using a digital scale. For a detailed depiction of the measured 2D parameters see Figure 2.

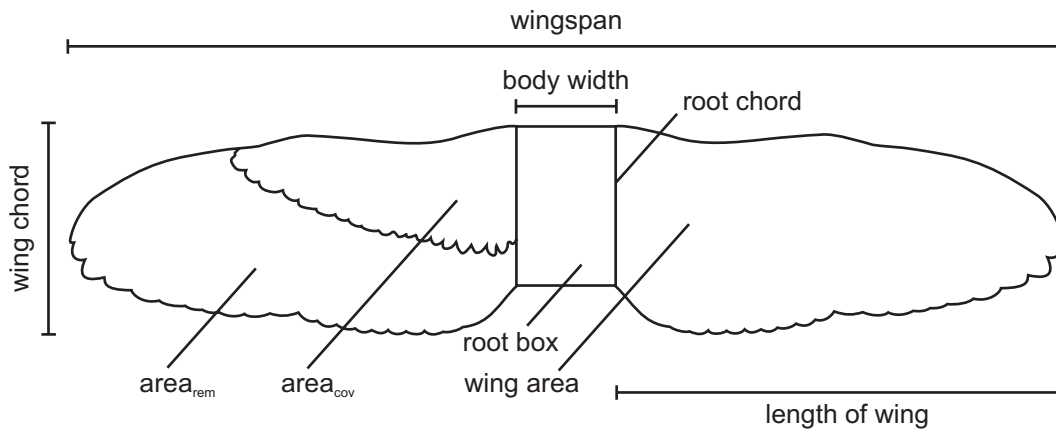


Figure 2: *Measured morphometric characteristics of wings - Wing span (twice the length of wing plus body width), length of wing (distance between the tip of the outermost remex and the proximal humerus), wing chord (distance between leading and trailing edge of the expanded wing), wing area (area of the expanded wing), area_{rem} (area formed by remiges), area_{cov} (area formed by coverts), root box (area of the body, calculated as body width multiplied with root chord).*

Wing loading was calculated for each species and specimen according to the formula: $(\text{body mass} \times 9.81 \text{ m s}^{-2}) / (\text{both single wing areas added})$. The area between both wings covering the body was not taken into account. Aspect ratio was calculated according to the formula: $(\text{wingspan}^2) / (\text{wing area})$.

The morphometric analysis of the bones was performed at fixed bones of the institute's own collection. A digital vernier calliper was used to obtain the length, thickness and distance of ulna and radius.

2.2.3 3D-analysis and profile measurements

Three dead barn owls and one dead pigeon were mounted in gliding flight position by fixing the body and wrist with wires and rods in a metal frame. Digital images of gliding barn owls and pigeons were used as templates to set the position and geometry of the bird and its wings. Two barn owl specimens and the pigeon specimen were frozen for 6 months, but completely defrosted for the measurements; one barn owl specimen was recently dead (twelve hours). The wings of the fixed birds were then digitised with an optical digitiser ATOS I (GOM Optical Measuring Techniques, Brunswick, Germany). Afterwards the point clouds were transformed into polygon meshes and analysed with Matlab (The MathsWorks, Inc., Natick, USA). Polygon meshes describe the surface by triangles. A typical wing scan consists of about 200,000 triangles. Every triangle consists of the three corners and a normal vector to specify the in- or outside. A plane with a constant span wise coordinate was chosen for the extraction of a profile. While all triangles of the wing's digital model that were cut by the plane were identified, those points on the edge of each triangle that lay in the plane were interpolated. The interpolated points formed the local profile of the wing and were used to determine the local chord length, thickness and camber in dependence of the chordwise position and the leading edge position of the wing.

The position of the leading edge and the local chord length were extracted from every profile. Chord length was determined by measuring the distance between the most anterior and most posterior point on the wing profile. The foremost point of the profile was the position of the leading edge. To extract the camber line and the thickness distribution, the profiles were divided into an upper and lower side. The distance between the upper and lower side defined the thickness. Adding half the thickness to the lower side resulted in the camber line. Using the extracted data, it was possible to determine the position of maximum camber and maximum thickness. Figure 3 shows an overview of the measured parameters.

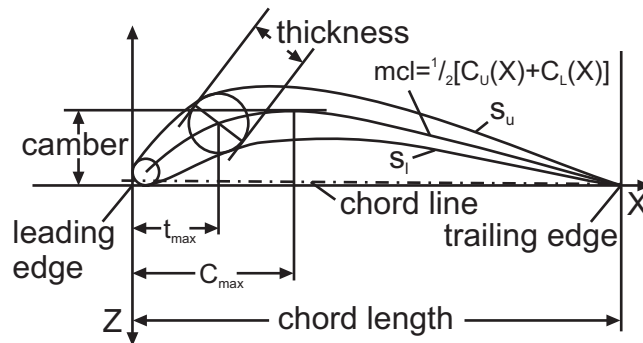


Figure 3: *Parameters of wing profiles - Camber (C), mean camber line (mcl), point of maximum camber (C_{max}), chord length (c), chord line, thickness (t), point of maximum thickness (t_{max}), upper and lower surface (S_u , S_l). Modified after Nachtigall and Klimbingat [59].*

2.2.4 Computed tomography and 3D-reconstruction of internal wing structures

Computed tomography measurements were performed in close cooperation with Dr. Georg Mühlenbruch from the Department of Diagnostic and Interventional Radiology of the RWTH Aachen University Hospital.

One recently dead barn owl (8 hours) was fixed on a Styrofoam plate with both wings spread laterally. The plate was centrally positioned in a clinical 16-slice Computed Tomography Scanner (Somatom Sensation 16, Siemens, Erlangen, Germany). After performing a scanogram with a table feed of 12 mm per rotation with a rotation time of 0.5 s, a standard chest CT protocol with a collimation of 16 x 0.75 mm was applied. An effective tube current-time product of 100 mAs_{eff} and a tube voltage of 120 kVp were chosen. Very thin image reconstruction was performed using a sharp convolution kernel, especially designed for visualisation of bones (Siemens B60) at a slice thickness of 0.75 mm with an overlapping increment of 0.5 mm. All reconstructed images were stored in DICOM-format on a mobile hard disc and transferred to a dedicated post-processing workstation for further analysis and 3D-reconstruction. The grey value of each voxel codes the mean material density. Different structures such as bones, muscles, skin and feather rachises were separated by labelling the material-characterising grey value using the software AMIRA 4.1 (Mercury Computer Systems GmbH, Berlin, Germany). A surface of the marked voxels was generated and smoothed for better visualisation.

2.3 Results

This chapter is based on the two- and three-dimensional analysis of barn owl and pigeon wings. The basic characteristics for comparison with values from the literature, and the analysis of the novel three-dimensional properties of the wings will be described.

2.3.1 Wing anatomy of barn owls and pigeons

Skeletal elements of barn owl wings were obtained from computer tomographical images and the reconstructed skeletal elements (Fig. 4C). Since pigeon wings have already been described before [5, 12, 61, 64], only a photograph of a pigeon wing is presented here (Fig. 5).

The main flight muscles of the breast were attached only to the humerus. These muscles, the *Musculus pectoralis* and *Musculus supracoracoideus*, were involved in moving the wing up and down in flapping flight. At the proximal end of the humerus these muscles were attached at two large crests of bone. Since the humerus has to withstand high forces, it was thick and strong, but hollow and pneumatic in the two species. A pneumatic foramen at the ventral side of the proximal humerus was found in the two species as well. This foramen enables gas exchange.

Ulna and radius, building the forearm, were bowed. To specify this bowing, the ratio of the length of ulna to the maximum distance between ulna and radius was calculated. In barn owls the ratio was 8.95 (with SD of 0.44, n=4), while it was 4.31 (with SD of 0.12, n=4) in pigeons (Table 1). Besides the stronger bowing, the bones of pigeon's wings were more robust and thicker in relation to their size. For example the thickness of ulna and radius were in the same range in the two species (thickness of ulna: 5 mm, thickness of

radius: 3 mm, Table 1), but the bones of barn owls were almost twice as long as those of pigeons (e.g. length of ulna: barn owl 106.6 mm; pigeon 62.4 mm, Table 1).

Table 1: *Morphometric characteristics of wings of barn owls (*Tyto alba pratincola*; $N = 4$) and pigeons (*Columba livia*; $N = 4$)*

		<i>barn owl</i>	<i>pigeon</i>
		mean +/- SD	mean +/- SD
wingspan	[cm]	101 +/- 3	68 +/- 2
length of wing	[cm]	45.3 +/- 1.9	29.2 +/- 1.1
mean wing chord	[cm]	17.1 +/- 3.0	9.8 +/- 3.5
wing area (single wing)	[cm ²]	705.7 +/- 78.9	279.4 +/- 20.4
ratio of area ^{rem} to area _{cov}		1.71 +/- 0.13	1.04 +/- 0.09
body mass	[g]	464.8 +/- 15.2	549.8 +/- 10.9
wing loading	[N/m ²]	33.0 +/- 2.3	96.8 +/- 4.6
aspect ratio		6.89 +/- 0.18	8.27 +/- 0.06
length of ulna	[mm]	106.6 +/- 1.0	62.4 +/- 1.9
thickness of ulna	[mm]	4.7 +/- 0.1	5.4 +/- 0.3
length of radius	[mm]	102.3 +/- 1.1	55.8 +/- 1.6
thickness of radius	[mm]	2.9 +/- 0	3.0 +/- 0.1
bowing ratio of ulna and radius		8.95 +/- 0.44	4.31 +/- 0.12

Three digits and the bones of the hand (Fig. 4C) were the only bony structures forming the leading edge of the wing, whereas the tiny first digit was located distal to the wrist (Fig. 4C). Three small flight feathers, which are collectively referred to as the alula, were supported by this bone. Further distal wing skeletal elements were strongly reduced, but reflected the standard vertebrate forelimb architecture. Carpal (wrist) and metacarpal (hand) bones were fused to the so called carpometacarpus. Bony remnants of the second and third digits formed the most distal portion of the wing (Fig. 4C, note: the third digit is not visible in this wing orientation).

In general, the topographic surface of a bird's wing is formed by feathers that are attached to the skeletal elements of the forelimb and its integument. A basic definition of the two major flight feather groups (primaries and secondaries) is also provided by the skeletal structures of the wing.

In barn owls as well as in pigeons ten primaries were attached to the bones of the hand and fingers (Figs. 4 and 5). The carpometacarpus supported most of the primaries, namely p1-p7. Fourteen secondaries in barn owls, respectively fifteen secondaries in pigeons, were firmly connected to the leading edge of the ulna. Note that barn owls, as all *Strigiformes*, have a so called diastaxic wing [16], which means that the 5th secondary remex is missing leaving a small gap, called diastema. Species with the full set of secondary remiges are said to be eutaxic. *Columbiformes* are both, eutaxic and diastaxic, depending on the species [16]. The investigated specimens of *Columba livia* were eutaxic. No remiges were found at the humerus (Fig. 4C). Ulna and carpometacarpus were connected via a posterior tough

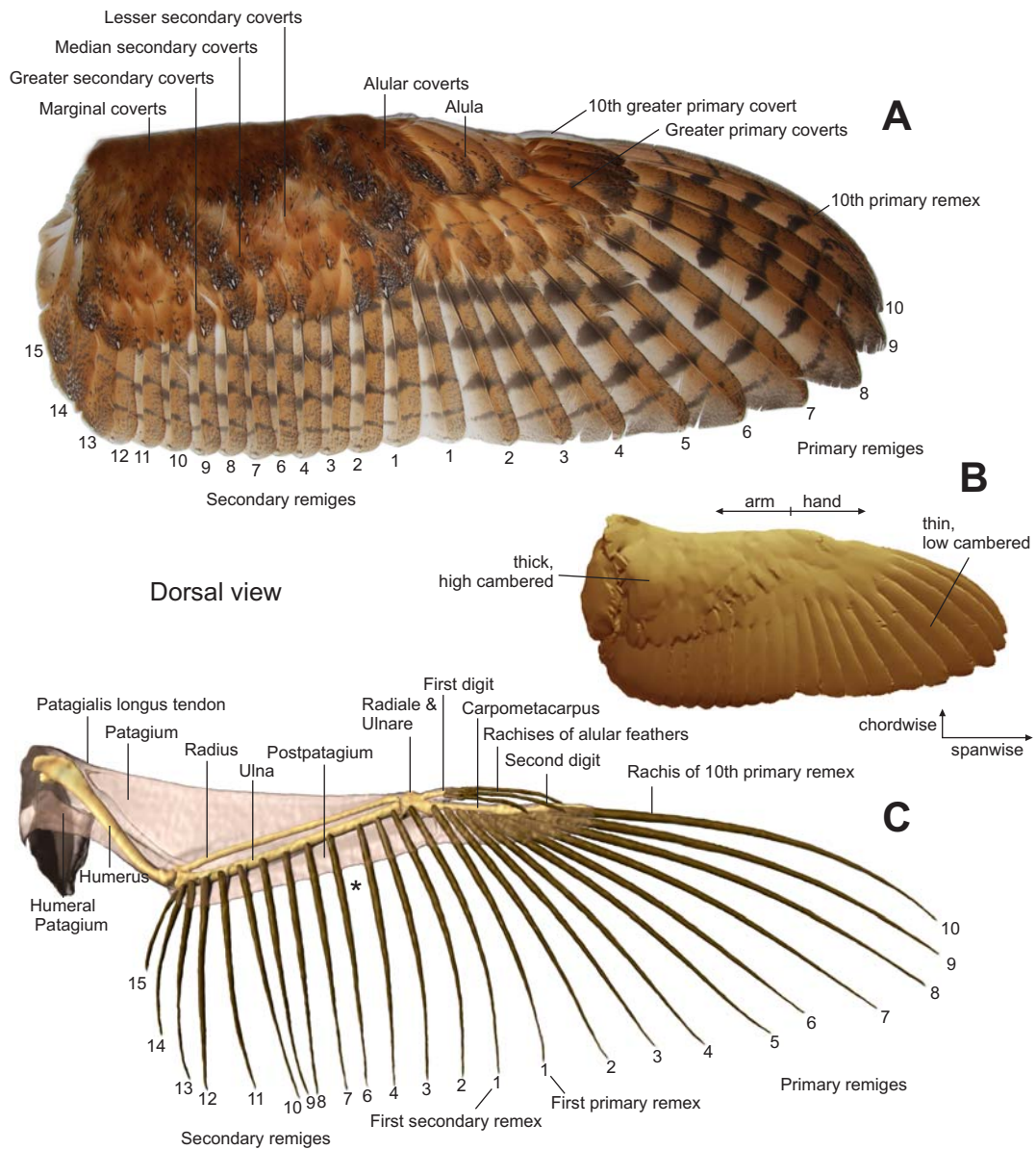


Figure 4: *Anatomy of a barn owl wing - (A) Topography of the dorsal wing (photograph). (B) Surface image of a digitised wing (surface scan). (C) 3D-reconstruction of skeletal elements, skin and rachises of the remiges (CT-scan). Note: A, B and C are the same barn owl wing (A separated, B and C still connected to the bird's body). *The fifth secondary remex is missing leaving a gap, which is called diastema [16].*

bundle of fibres. Muscles and tendons run along the posterior side of the wing supporting the flexion and extension of the wing. Additionally, the postpatagium connected all feather quills of the remiges like rods in a fan, which supported an easier spreading of the flight feathers. The anterior leading edge of the proximal wing was formed by the patagium, patagialis longus muscle and tendons. This tough tissue connected the shoulder area to the carpal bones of the wrist. Additionally, all coverts had their origin here causing upholstery of this wing area (Fig. 4). Posterior regions of the proximal wing were formed by the secondaries. Small muscles at the base of each calamus were found that might be used by the bird to rotate the feathers or to change the angulations between the calamus and the bone. Hereby, the camber of the wing was influenced. At the hand part of the wing the natural curvature of the primaries and their positions relative to each other were responsible for the low camber.

Variations in shape of pigeon wings (Fig. 5) compared to barn owl wings (Fig. 4) were due to differences in the shape of the feathers [4], bones [23] and muscles [23, 24]. Remiges of pigeons were shorter and smaller [4] than those of barn owls leading to a smaller wing area. On the other hand, the coverts covered a higher portion of the wing than those in barn owls. Upholstery in addition to a higher amount of muscle mass and a higher bowing of ulna and radius resulted in a different thickness distribution within the pigeon wing than it was found in the barn owl.

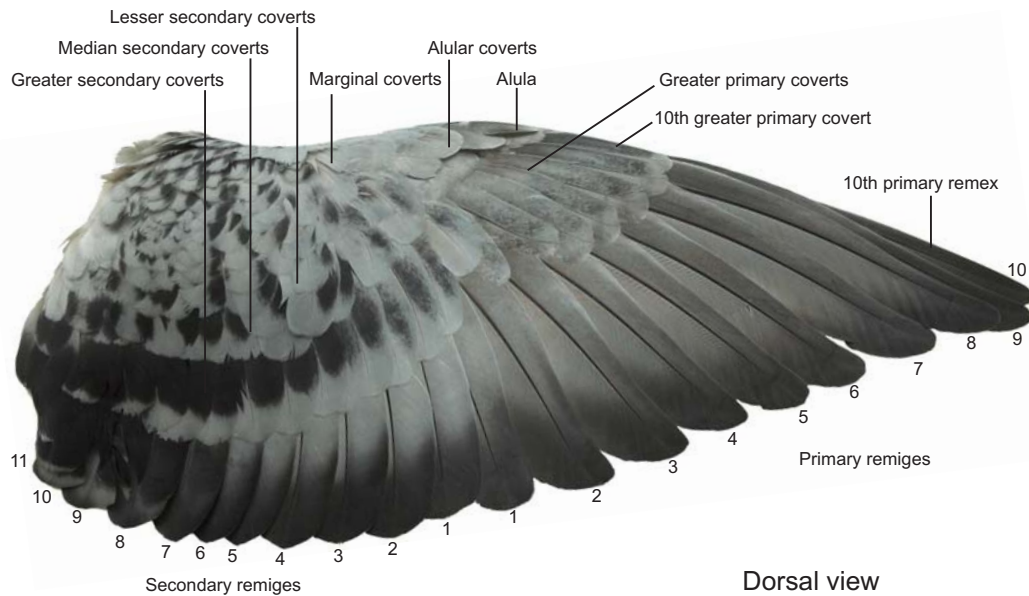


Figure 5: *Topography of a pigeon wing - A dorsal view on separated pigeon wing. Note the different shape of the wing, the feathers and the alula in comparison to the barn owl wing.*

A different appearance and arrangement of the anatomical elements caused different thickness distributions of anterior versus posterior and arm versus hand parts. Bones,

muscles and ligaments were located in the anterior wing region (Fig. 4C). Posterior arm parts and the hand area of the wing consisted of one single layer of wing feathers (remiges), resulting in low thickness. The maximum thickness of areas formed by single feather layers was caused by the thickness and curvature of feather rachises and the overlapping vanes. Thus, two areas, one formed by remiges and one by coverts, and the underlying tissue, were involved in forming thickness and camber. The ratio of these both areas is a rough indication of thickness distribution in the wing. In barn owls the ratio of the area formed by remiges to the area formed by coverts was 1.71 (+/- SD of 0.13) (Fig. 6, Table 1). In pigeons this ratio was 1.04 (+/- SD of 0.09) (Table 1). Since remiges were quite thin, barn owls had a huge portion of thin areas of the wing as well. In pigeons the area formed by remiges was equally sized as the area formed by coverts (Fig. 6) resulting in a relatively small thin part of the wing.

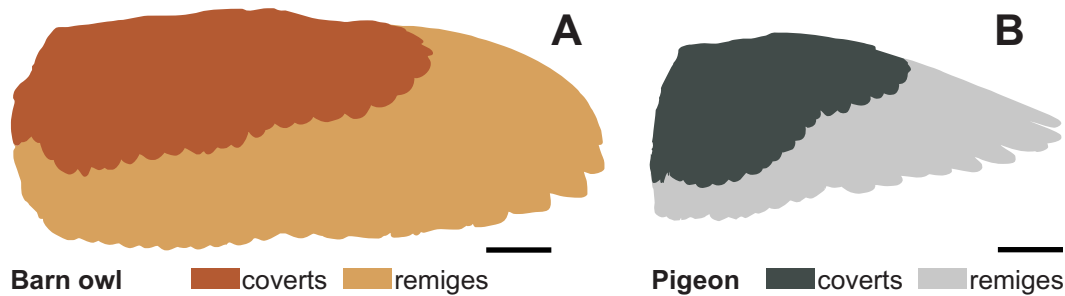


Figure 6: *Wing planform and feather distribution of barn owl and pigeon wings - Wing planform of fully extended wings of the barn owl (left) and the pigeon (right). Dark area - coverts; bright area - remiges. Scale bar represents 50 mm.*

2.3.2 Morphometrics

Span and chord influence the planform (Fig. 6) of a wing. The chord of barn owl wings was constant over most parts of the span. At the wing tip (outermost 30% of span) a round taper shortened the chord. Hence, the fully extended wing appeared elongated with a round tip. The calculated aspect ratio of the owl wing was 6.89 (+/- SD of 0.18) (Table 1). The mean wing area of a single wing of the investigated specimens of *Tyto alba pratincola* was 705.7 cm² (+/- SD of 78.9) (Table 1). With a mean weight of 464.8 g (+/- SD of 15.2) a wing loading of 33.0 N/m² (+/- SD of 2.3) resulted (Table 1). In contrast, the wing of a pigeon was shorter and characterised by a pointed tip, meaning the wings were more triangular shaped in the lateral half. From about 50% of its length, the chord decreased linearly towards the wing tip leading to an aspect ratio of 8.27 (+/- SD of 0.06) (Table 1). The averaged wing area of one single wing of the investigated pigeons was 279.4 cm² (+/- SD of 20.4) (Table 1). Being 16% heavier than barn owls (pigeon: 549.8 g +/- 10.9) the resulting wing loading of pigeons was 96.8 N/m² (+/- SD of 4.6) (Table 1).

2.3.3 Aerodynamic parameters of wing profiles

The overall three-dimensional wing geometry can be approximated by wing planform and spanwise distribution of the local profile parameters such as camber and thickness. Digitised barn owl and pigeon wings were investigated with respect to these parameters. Special attention was directed to the maximum values and their positions in chordwise direction. Data of barn owls will be presented first, followed by data of pigeons and finally a comparison of the two species is given.

2.3.4 Barn owl

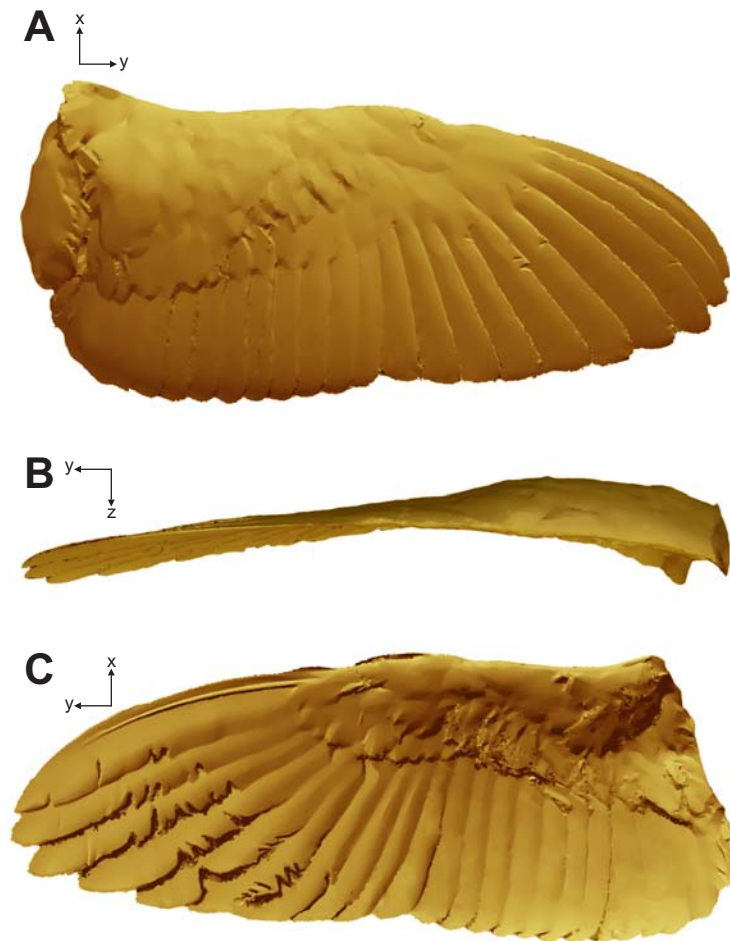


Figure 7: *Surface view of a digitised barn owl wing - (A) dorsal, (B) frontal, (C) ventral.*

Figure 7 shows the digitised surface of a right wing of one barn owl from dorsal, frontal and ventral. Such surfaces were cut into profiles to extract profile parameters. Ten exemplary profiles (every 10% of wing length) are plotted for three barn owl wings in figure 8. Barn owl wings were characterised by a long and broad planform with an almost constant chord (Tables 1, 2) and a rounded wing tip. All investigated wings showed only little intra- and interindividual differences. The arm part of each wing was highly cambered with the maximum thickness located close to the leading edge. While the posterior half of the wing's arm part was thin and low cambered, the distal part of the wing was mainly formed by the primaries (Fig. 4 and 7). Here, thickness and camber were low.

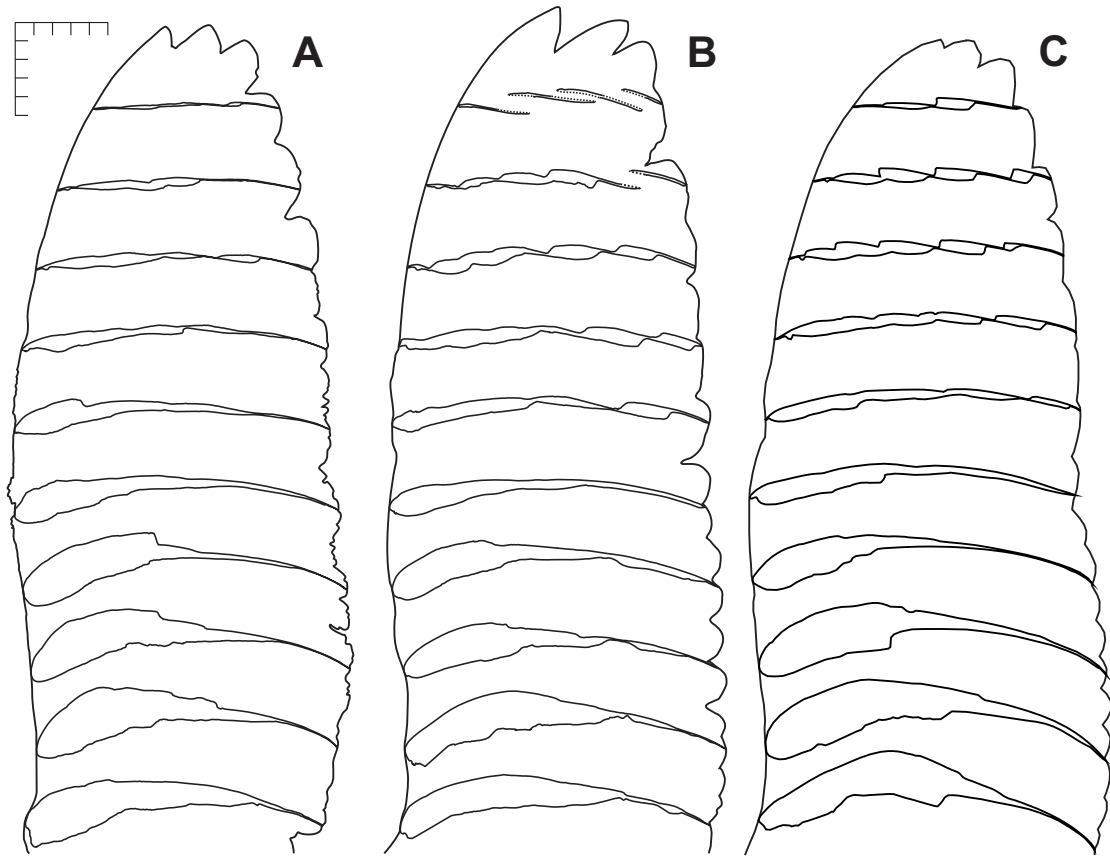


Figure 8: *Wing planforms and profiles of barn owl wings - Wing planforms of three digitised right barn owl wings of three individuals. Ten exemplary profiles are shown for every wing. The dotted lines (distal profiles of wing B) were added to complete single feather profiles. Scale bars represent 50 mm in x- and y-direction.*

Table 2: Mean positions and values of maximum camber (C_{max}) and maximum thickness (t_{max}) of barn owl (*Tyto alba pratincola*) wings normalised by the local chord length. (mean value + SD, $N = 3$).

spanwise position	chord length [mm]	chordwise position of t_{max} [%]	normalised t_{max} [%]	chordwise position of C_{max} [%]	normalised C_{max} [%]
0	160.1 +/- 2.9	17.7 +/- 1.7	15.3 +/- 1.2	48.3 +/- 9.1	11.2 +/- 0.9
5	164.6 +/- 2.5	18.0 +/- 2.9	14.5 +/- 2.1	48.0 +/- 7.9	13.1 +/- 0.9
10	166.4 +/- 0.6	19.7 +/- 1.7	14.7 +/- 2.0	39.0 +/- 0.9	13.0 +/- 0.8
15	170.5 +/- 0.7	17.0 +/- 2.5	13.7 +/- 1.3	36.3 +/- 1.2	12.9 +/- 0.8
20	174.4 +/- 1.0	7.7 +/- 0.3	12.2 +/- 0.9	38.7 +/- 0.1	10.8 +/- 0.5
25	175.1 +/- 2.1	9.7 +/- 0.1	13.3 +/- 1.0	37.7 +/- 1.0	10.9 +/- 0.4
30	178.2 +/- 1.9	7.7 +/- 0.5	12.3 +/- 0.9	41.0 +/- 2.9	9.8 +/- 0.7
35	177.7 +/- 1.2	7.3 +/- 0.7	10.3 +/- 1.1	44.3 +/- 1.2	10.3 +/- 0.6
40	174.4 +/- 3.6	9.0 +/- 0.8	8.9 +/- 0.8	45.7 +/- 2.2	8.2 +/- 0.2
45	169.7 +/- 3.0	9.7 +/- 1.1	8.6 +/- 0.3	48.0 +/- 5.4	6.6 +/- 0.6
50	171.7 +/- 1.0	10.7 +/- 2.0	6.1 +/- 0.5	45.0 +/- 2.6	5.7 +/- 0.6
55	167.0 +/- 0.6	18.0 +/- 0.8	5.0 +/- 0.4	55.7 +/- 3.4	5.7 +/- 0.6
60	164.2 +/- 1.3	18.7 +/- 2.6	4.5 +/- 0.4	62.0 +/- 4.1	5.0 +/- 0.6
65	161.3 +/- 1.2	22.0 +/- 2.8	4.8 +/- 0.5	55.0 +/- 3.7	4.7 +/- 0.7
70	155.2 +/- 1.8	23.7 +/- 0.2	4.8 +/- 0.5	61.7 +/- 9.1	4.2 +/- 0.3
75	148.5 +/- 1.6	23.7 +/- 0.3	4.3 +/- 0.3	65.3 +/- 5.7	4.0 +/- 0.1
80	138.1 +/- 5.7	64.7 +/- 14.6	5.2 +/- 2.6	75.0 +/- 6.3	3.7 +/- 0.2
85	130.5 +/- 5.1	58.0 +/- 14.9	5.1 +/- 1.9	71.7 +/- 4.9	3.6 +/- 0.4

Computer-aided analysis of wing profiles provided precise data of camber and thickness. For each profile, the maximum values and their chordwise position (maximum thickness - t_{max} , maximum camber - C_{max}) were measured. The presented data are normalised with the local chord length. Figure 9 shows the chord- and spanwise distribution of the normalised camber and thickness for three barn owl wings. Values for 19 profiles, i.e., every 5% of length of wing, are depicted.

At the proximal wing the maximum thickness (t_{max}) was located near the leading edge of the wing (about 7.3 - 19.7% in chordwise direction) (Fig. 9, Table 2) in all three cases. In spanwise direction t_{max} decreased from medial to lateral. The highest values for the thickness were found between 0 and 45% length of wing (about 8.6 - 15.3% of local chord length) (Fig. 9, Table 2). In wing tip direction, the thickness decreased towards 5.0% (in average) of chord length (Fig. 9, Table 2).

No life internal structures or external air flow stabilised the wing of the dead animals during the analysis. Thus, camber measurements are prone to errors. However, the following trend in barn owls can be presented: The anterior part of the wing, especially the arm part, consists of many supplementary elements such as bones with joints, muscles, ligaments and feather layers (Fig. 4). Using these elements the bird is able to vary the camber of its wing according to the flight conditions. However, the bird is unable to actively bend a feather.

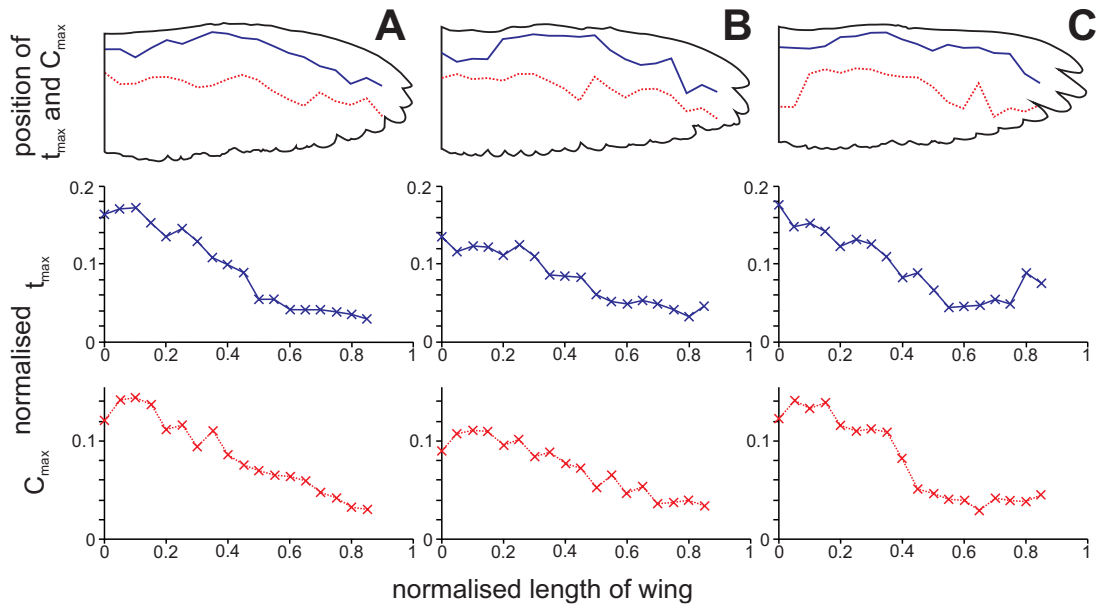


Figure 9: *Thickness and camber distribution of barn owl wings - The position (top row) and values of maximum thickness (middle row; t_{max} ; blue line) and maximum camber (bottom row; C_{max} ; dotted, red line) are shown every 5% of normalised wing length. The values of thickness and camber were normalised by the local chord length. (A) Right wing of individual 1; (B) right and (C) left (mirrored) wing of individual 2.*

Considering the anterior-posterior direction these facts lead to a higher camber in the anterior arm part of the wing (Figs. 7, 8, 9). At the proximal wing the maximum camber was measured to be in the range of 5.7 to 13.1% of the local chord length (Fig. 9, Table 2). At the distal wing the obtained values of maximum camber were in the range of 3.6 to 5.7% of local chord length (Fig. 9, Table 2). The positions of the maximum camber (C_{\max}) were shifted towards the leading edge at the arm part (position of C_{\max} : 36.3 – 48.3% of chord length, Table 2) considering the centre of the chord. Note the different positions of C_{\max} for the hand and the arm part of the wing. At the hand part the positions were located closer to the trailing edge (position of C_{\max} : 55.0 – 71.7% of chord length, Table 2).

In spanwise direction the normalised value of camber was highest close to the body (Fig. 9). Here, strong elements of the forelimb such as bones and muscles were located (Fig. 4). The camber was decreasing from wing root to wing tip (Fig. 9), while it decreased most between 15 and 55% length of wing. At the wing root and beyond 55% length of wing, the camber stayed almost constant, forming two plateau-like phases. As mentioned above, the bird is unable to bend its feathers, but is able to change the position of the feathers relative to each other. Vertical movement in the wing is restricted due to strong ligaments, i.e. motion is mainly performed in the horizontal plane. Due to this fact, the hand part of the wing was thin (4.3 – 5.2% of local chord length) and mostly low cambered (3.6 – 5.7% of local chord length) (Figs. 7, 8, 9, Table 2).

2.3.5 Pigeon

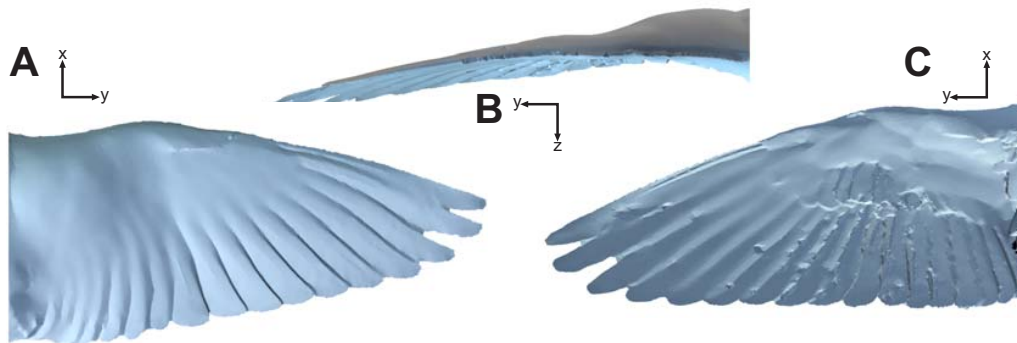


Figure 10: *Surface view of a digitised pigeon wing - (A) dorsal, (B) frontal, (C) ventral.*

A surface reconstruction of a digitised pigeon wing is shown in figure 10. As for the barn owl, the wing orientation is dorsal, frontal and ventral. In the lateral half, the pigeon wing was approximately triangular shaped, which can be seen in a linearly decrease of the chord and thus a pointed tip (Figs. 10, 11). The wing was thick and highly cambered in the anterior arm region (Fig. 11). Thickness decreased from anterior to posterior, but due to a different distribution of remiges and coverts (Figs. 5, 6) not as strong as in the barn owl (compare Fig. 8 with 11). At the distal wing, the thickness and the camber were low and only the overlapping feathers and rachises formed an undulated structure of the profiles in this area (Fig. 11).

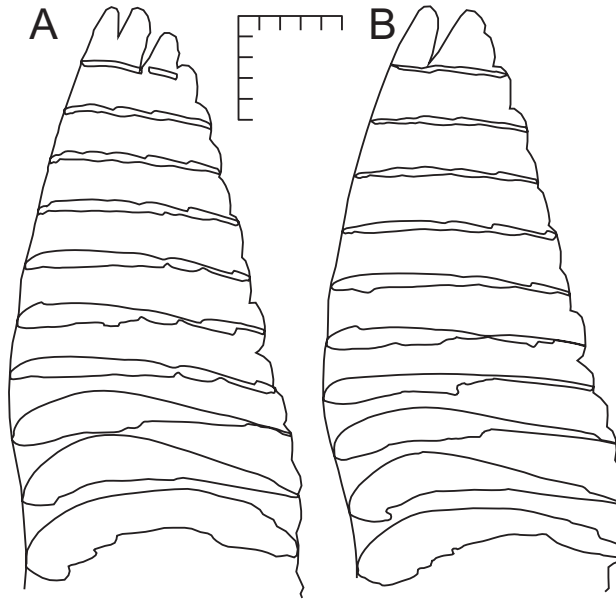


Figure 11: *Wing planform and profiles of pigeon wings - (A) Right and (B) left (mirrored) wing of one individual. Ten exemplary profiles are shown for every wing. Scale bars represent 50 mm in x- and y-direction.*

Maximum thickness (t_{\max}) was located close to the leading edge of the wing in both three-dimensionally investigated wings (Fig. 12). In spanwise direction, the values of t_{\max} decreased rapidly and almost linearly from 24.4/20.8% to 7.4/7.4% (of local chord length) (Fig. 12, Table 3) until reaching 50% length of wing. In the region from 50% length of wing to the wing tip, the maximum thickness stayed almost constant at about 5.6% of chord length (Fig. 12, Table 3).

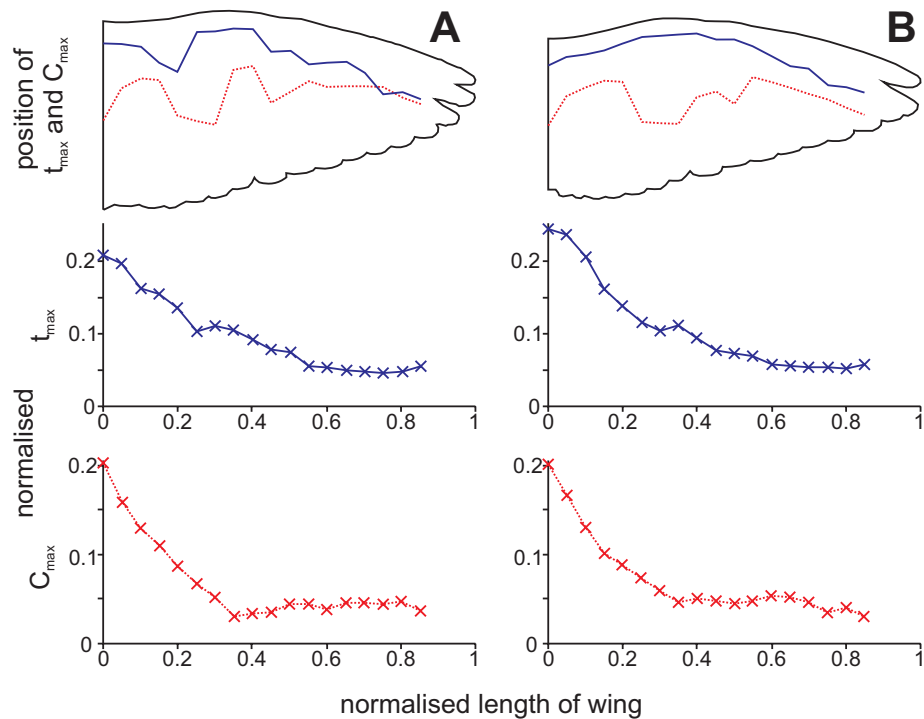


Figure 12: *Thickness and camber distribution of pigeon wings - The position (top) and values of maximum thickness (middle; t_{max} ; blue line) and maximum camber (bottom; C_{max} ; dotted, red line) are shown every 5% of normalised wing length. The values of thickness and camber were normalised with the local chord length. (A) Right (B) and left (mirrored) wing of one individual.*

As in case of the owl wings, no internal structures or external air flow stabilised the pigeon wings. Again, camber measurements are only reliable to a certain degree. Between wing root and 35% length of wing the maximum camber decreased rapidly from 20.3/20.1% to 3.0/4.7% of local chord length (Fig. 12, Table 3). In the more distal wing part (35-90% length of wing) the maximum camber stayed almost constant at about 4.5% of local chord length (Fig. 12, Table 3).

Table 3: *Positions and values of maximum camber (C_{max}) and maximum thickness (t_{max}) of two pigeon wings (*Columba livia*) normalised by the local chord length.*

spanwise position [%]	chord length		chordwise position		normalised		chordwise position		normalised	
	[mm]		of t_{max} [%]		t_{max} [%]		of C_{max} [%]		C_{max} [%]	
	wing 1	wing 2	wing 1	wing 2	wing 1	wing 2	wing 1	wing 2	wing 1	wing 2
0	126.2	129.0	18	12	24.4	20.8	58	53	20.3	20.1
5	127.9	130.7	12	12	23.8	19.6	37	36	15.9	16.7
10	129.4	134.0	12	14	20.6	16.4	32	31	13.0	13.1
15	134.3	133.8	12	23	16.2	15.4	30	32	10.9	10.1
20	134.5	134.7	10	29	14.0	13.6	33	52	8.7	8.8
25	134.2	135.6	9	10	11.4	10.4	59	57	6.7	7.4
30	130.0	129.6	10	11	10.4	11.0	61	61	5.2	6.0
35	126.4	124.5	10	10	11.2	10.6	65	33	3.0	4.7
40	123.4	121.7	9	10	9.4	9.2	50	32	3.4	5.1
45	119.0	116.2	12	22	7.6	7.8	46	52	3.5	4.8
50	114.1	109.7	12	21	7.4	7.4	57	47	4.4	4.4
55	107.4	105.7	15	29	6.8	5.4	38	40	4.4	4.7
60	101.0	99.0	21	26	5.8	5.4	41	43	3.8	5.4
65	95.4	94.6	28	24	5.6	5.0	46	43	4.5	5.3
70	88.2	88.3	29	32	5.4	4.8	52	43	4.6	4.6
75	78.6	81.2	44	49	5.4	4.6	59	42	4.4	3.4
80	74.7	73.4	44	46	5.2	4.8	66	51	4.7	4.1
85	63.5	65.0	51	55	5.8	5.4	80	61	3.6	3.0

2.3.6 Comparison between barn owl and pigeon

Comparisons of the normalised positions and normalised values for camber and thickness between barn owl and pigeon wings showed the differences and similarities in both species (Fig. 13).

In both species, the maximum thickness was located at the leading edge of the wing. A typical shift of the maximum thickness was observed at 15% length of wing in barn owls, and in 25% of wing length in pigeons. From the wrist the location of maximum thickness followed the curvature of the 9th primary remex in barn owls, respectively the 7th/8th primary remex in pigeons (Fig. 13A, B).

The stretch of the location of maximum camber was less wavy in barn owls than in pigeons. At the proximal wing of barn owls the position of the maximum camber was slightly anterior of the midline of the wing. In contrast, at the distal wing the position of maximum camber followed the curvature of the 7th, respectively the 5th primary remex. Thus, in the posterior part it was shifted to the midline of the wing (Fig. 13A). In pigeons, the position of the maximum camber varied around the midline of the wing between 0 and 60% length of wing. Between 60% of the wing and the wing tip the position of maximum camber followed the curvature of the 6th/7th primary remex (Fig. 13B).

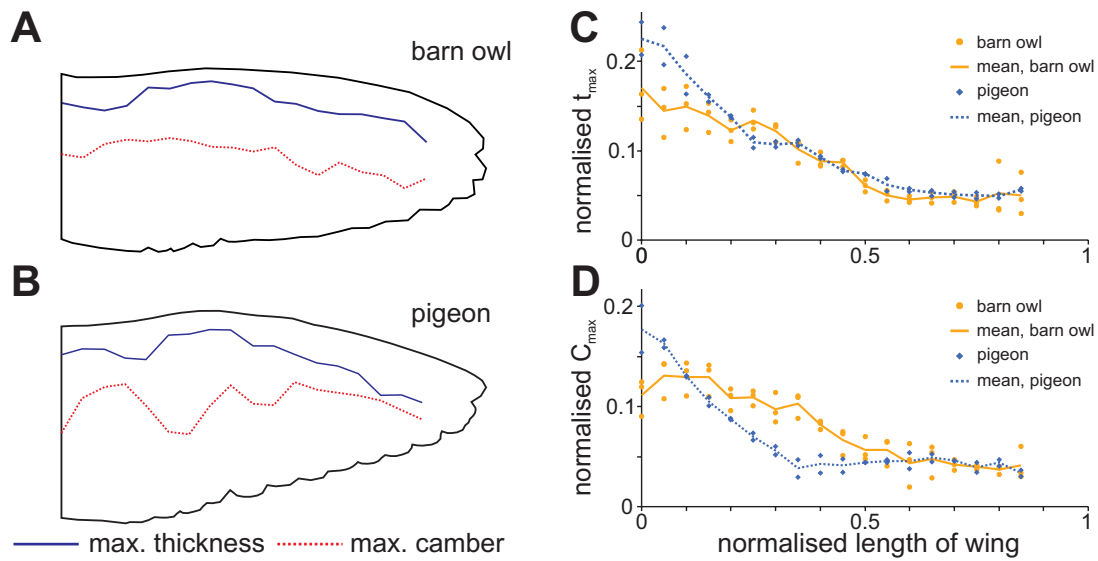


Figure 13: *Thickness and camber distribution of barn owl and pigeon wings - (A+B) Mean position of maximum camber and maximum thickness of mean (A) barn owl and (B) pigeon wings. (C) Distribution of maximum thickness (t_{max}) and (D) maximum camber (C_{max}) of barn owl ($N = 3$) and pigeon ($N = 2$) wings. The lines reflect the mean values for each species. The wing planforms are normalised by the wing length, the values are normalised by the local chord length.*

Regarding the values of maximum thickness and maximum camber almost no differences were found at the distal wing. However, the proximal wing differed distinctly. Pigeon wings were relatively thicker at the wing root, but the normalised thickness decreased fast. In the normalised depiction, barn owl wings were thinner at the proximal wing and the thickness decreased only slightly towards the wrist (Fig. 13C).

Camber measurements were more distinctly different in the two species between 0 and 60% length of wing (Fig. 13D). In barn owls the curve progression of the maximum camber can be divided into three parts. At the base, between 0 and 15% length of wing, C_{max} stayed almost constant at about 13% of local chord length. Furthermore, it decreased to 5% of local chord length between 15 and 60% length of wing. Between 60% of the wing and the tip the maximum camber stayed again constant at about 4% of local chord length (Fig. 13D). In pigeons the normalised camber was higher at the wing root, but then decreased rapidly until reaching 35% of length of wing. From this point on towards the tip the normalised camber had an almost uniform value of about 4.3% of local chord length. While the values of the normalised camber differed between the two species at the proximal wing, camber differed little at the distal wing (Fig. 13D).

2.4 Discussion

Barn owl and pigeon wings were investigated with high-resolution imaging techniques. Anatomical and aerodynamic parameters were obtained from 2D images, 3D surface scans and 3D reconstructions of internal structures such as bones, skin and feather rachises. In the following the methods of a three-dimensional reconstruction will be compared with those used by other authors. Furthermore the anatomical differences between the species will be pointed out, and the aerodynamic properties of the wings will be discussed.

2.4.1 Reconstruction of a three-dimensional wing

Nachtigall and Wieser [61] were the first to establish a measuring method to obtain wing profiles of pigeons. A comb with movable metal brads was used to frame the wing profiles at defined positions. In combination with photogrammetry they were able to reconstruct the dorsal surface of pigeon's wings in low detail [12]. Nachtigall and Klimbingat [59] investigated three different owl species. They provided ten wing profiles of three different wings per species. The authors claim that the wing profiles of owls are characteristic for this taxon. However, the data is quite incomplete since the measured points per profile were restricted to the number of metal brads. Furthermore, quantitative data of thickness and camber distributions is missing.

Nowadays methods such as laser scanning or optical digitising provide data with a higher spatial resolution, which can then be processed and analysed in high detail with appropriate software. Liu et al. [52] digitised wings of different bird species via laser scanning for numerical purpose. They provided algorithms for profile analysis that were adjusted for this study. Unfortunately, Liu et al. investigated wings that were separated and dried. This procedure deformed the wings so that the natural geometry was not conserved, which can be seen by comparing the photographs provided by Liu et al. with pictures of free gliding birds. For this thesis, the whole dead bird was carefully fixed in gliding flight position in order to avoid such problems. Video analysis and photographs of gliding owls and pigeons were used as references. All three-dimensionally investigated wings were still connected to the bird's body. Thus, neither a separation of the wing nor any drying of muscles or tendons caused any changes in the geometry. In this way it was aimed to reproduce more natural wing forms than presented by other authors. However, note that the current data is still based on fixed wings. Possible deviations of the geometry under flight conditions have to be obtained in free gliding experiments and with living animals.

2.4.2 Are barn owl wings adapted to low-speed flight?

Aspect ratio and wing loading belong to the parameters that describe the wing in terms of its aerodynamic characteristics. The aspect ratio is lower in barn owls than in pigeons, indicating a potentially lower flight speed and a higher manoeuvrability. Differences in wing loading between barn owl and pigeon were larger than differences in aspect ratio. Barn owl wings are huge in relation to the body mass resulting in a very low wing loading. This is regarded as an adaptation to low-speed flight. Figure 14 shows aspect ratios and wing loadings of various flying object, especially birds. The two species investigated, barn owls and pigeons, were added to the diagram. Barn owls are perchers that fly close to or within

vegetation. The low aspect ratio contributes to a high induced drag, but on the other hand their low weight and wing loading cause a decrease of the flight costs [63]. Pigeons have a high wing loading and relatively short wings. Since their aspect ratio is still high, pigeons are adapted to fast and rather inexpensive flight. Short wings reduce the profile power, which is expected to be large in fast-speed flight [63].

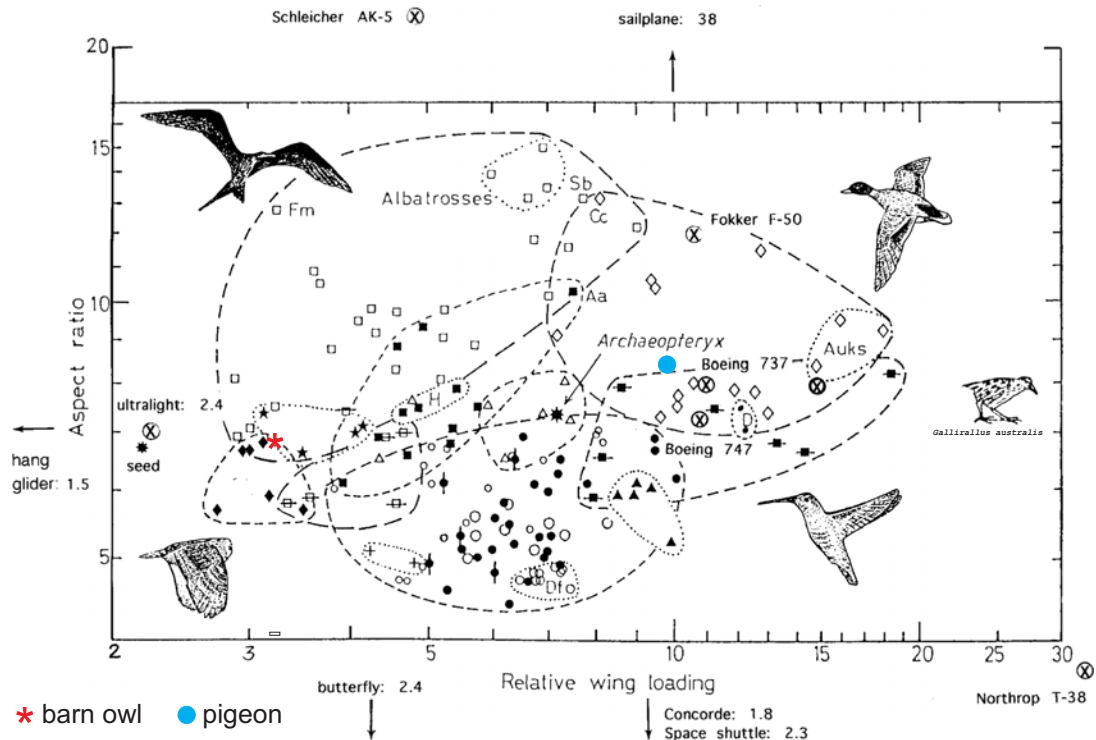


Figure 14: *Index of aspect ratio versus wing loading (kg/m^2) in some birds (barn owl and pigeon were added), airplanes, a butterfly, a hang glider and a maple seed. The number after some objects refer to the aspect ratio. (modified from [63])*

Barn owls fly with speeds of about 2.5 m/s to 7 m/s [56]. The flight is slow compared to the flight of birds with a similar weight such as pigeons [1]. Birds that are able to fly in the flight-speed range of the barn owl are usually lighter and have much higher wing loadings [1]. In low-speed flight wing beat frequency and wing beat amplitude is higher in birds with high wing loadings [88, 90]. Such birds require more flight power for wing movements to produce enough lift while flying slowly [88, 89, 90]. The appearance and bowing of ulna and radius is a good indication whether a bird uses rather steady or unsteady flight [23, 70]. Birds with higher wing loadings, such as pigeons, have to beat their wings with high frequencies in order to produce enough lift. This flight style requires more power. In fast cruise flight, barn owls beat their wings with a maximum frequency of 5.6 Hz. They vary flight speed depending on the illumination (2.5 – 7 m/s) [56]; the darker the environment the slower the owls fly. In contrast, when pigeons fly at low speed (4.9 m/s), they beat their wings with frequencies of 9.6 Hz [9]. Compared to barn owls, the frequency is much higher.

Skeletal elements of the wing reflect the need of higher wing beat frequencies as well. Ulna and radius of pigeons show a high bending while being relatively stronger and thicker than the equivalent bones of barn owls. The skeletal elements of pigeons provide more space for muscle mass within the wing confirming the higher power requirement for low-speed flight such as take off. The higher amount of muscle mass was also seen in a high thickness of the proximal pigeon wing. In pigeons the flight muscle mass represents approximately 30% of the body weight. However, in barn owls the muscle mass used for flight is less pronounced and represents only 10% of the body weight [17]. As a consequence ulna and radius are less bowed and the muscle mass at the wing is less pronounced in barn owls than in pigeons. During hunting, barn owls reduce flight speed, wing beat frequency and amplitude [56] in order to detect their prey and probably to reduce noise emission. The reduced flight speed (2.5 m/s) and wing beat frequency is compensated for by an enlarged wing area. In this way enough lift may be produced at low flight speed. Good manoeuvrability is also linked to low wing loading and low flight speed [63].

One source of the increased wing area in barn owls is the enlarged size of the remiges. A typical barn owl's primary is almost 3 times larger than a pigeon's primary [4]. The ratio of area formed by the remiges to that formed by the coverts was calculated. In pigeons this ratio was almost 1, meaning both areas were equally sized. In barn owls the area formed by remiges is 1.7 times larger than that formed by coverts.

Due to the stronger appearance of muscles and bones and due to the arrangement of the differently shaped remiges and coverts, the hand part of the pigeon wing has a larger normalised thickness and a steeper gradient of the maximum camber than the barn owl wing. In conclusion it seems that the wing geometry of pigeons is adapted to higher flight speeds [71], respectively that of barn owls is adapted to lower flight speeds. To prove this statement a comprehensive morphological study with several different species needs to be done.

2.4.3 Aerodynamic properties of the wing

In general the wing of a bird can be divided into two different parts that have different aerodynamic characteristics: the proximal wing (from shoulder joint to wrist) and the distal wing (from wrist to wing tip). The proximal wing is highly cambered and thickened anteriorly providing lift even at low velocities [80]. It consists mainly of bones, muscles, ligaments and the overlapping remiges and coverts. Klän et al. [41] quantitatively analysed the flow conditions around an owl-based airfoil in wind tunnel experiments. Experiments with airfoils that had a clean surface showed a separation bubble on the dorsal side that decreased at high Reynolds numbers. While the separation bubble was quite huge and the airfoil showed a tendency of flow separation in low Reynolds number experiments [41], the separation bubble was decreased in size and shifted towards the leading edge when the wing model was equipped with a velvet surface. Under these conditions the velocity gradient near the surface was increased and the overall flow was stabilised [41]. As a consequence for the owl, the velvet-like dorsal structure does not only dampen the friction noise [62], but also stabilises the air flow around the wing at low flight speeds. Relatively to the proximal barn owl wing, the pigeon wing is much thicker due to a thicker appearance of bones and muscles. Although the two bird species have a similar weight, pigeons have much smaller

wings. Regarding slow flight speeds, pigeons must beat their wing at higher frequencies in order to produce enough lift [56, 71]. Measurements on the pectoralis mass-specific power output [91, 93] and the pressure maps of a pigeon wing in flight [93] confirm this statement. In wind tunnel experiments, pigeon wings performed best at speeds of about 14-22 m/s [93], which is distinctly higher than the flight speed of barn owls.

Distal bird wings are distinctly different from proximal wings. In barn owls the distal wing is thin and represents a slightly cambered plate. Only a very small part of the leading edge is formed by bony structures (hand and finger bones), associated ligaments and skin. The residual part of the distal wing is mainly built up of remiges and greater primary coverts. Thus, this wing part is very thin and shows less curvature than the proximal wing. Neuhaus et al. [62] performed wind tunnel experiments with wings of tawny owls (*Strix aluco*) and mallard ducks (*Anas platyrhynchos*). These authors found an early separation at the distal wing of the mallard duck. By contrast, in the tawny owl the air current showed a much higher degree of laminar flow around the distal wing. Only after amputation of the leading edge serrations the air flow correlated with that found in mallard ducks. Hence the serrations at the leading edge induced the air flow to stay attached around the wing and thereby producing much lift. Since tawny owls and barn owls have comparable wing geometries and profile characteristics [59] the same effect of the serrations can be expected for barn owls. Due to comparable wing planforms and surface structures, similar effects as of the mallard duck are assumed for pigeons. Although producing lift, the flow separates early producing a well noticeable noise.

2.5 Conclusions

The goal of this study was to investigate the wing anatomy of owls in comparison to pigeons in some detail. Optical measuring methods provide quick and high-resolution data. Natural wing geometries were maintained by careful fixation of the whole birds, which resulted in a better approximation to the wing appearance under natural circumstances.

A comparison of barn owl and pigeon wings demonstrated the specific structures of the wings and plumage and their influence on the flow field. Wing morphology and anatomy suggest that the wings of barn owls are adapted to low-speed flight. Owl wings are bigger in size resulting in low wing loadings that guarantee slow flight with enough lift reserve to carry heavy weight (prey). Furthermore, anatomical parameters confirmed a low wing beat frequency and amplitude. This reduces the required power need and might be a further adaptation since the owl has only little energy reserves. In addition, aerodynamic experiments with wing models demonstrated that the serrations and the velvet-like dorsal surface interact to stabilise the air flow around the wing at low velocities.

Wings of pigeons do not show such obvious specifics of the plumage. Their wing edges are smooth and the surface is structured only by the barb shafts. The wings are suitable for the living conditions and the flight style of pigeons. As a bird that feeds on seeds, it does not necessarily need to have a slow or even silent flight.

3 3D Reconstruction and Investigation of Plumage Specifics of Barn Owls

3.1 Introduction

The aerodynamic performance of a wing depends on its overall three-dimensional geometry, its surface texture and the characteristics of the leading and trailing edges. Members of the taxon *Strigiformes* (owls) developed particularly unique feather structures. Graham [31] was the first to describe serrations at the outer vanes of those feathers that build up the leading edge of the distal wing of owls. Further he mentioned fringed edges of the inner vanes and a velvet-like dorsal surface of each feather of the wing. These structures influence and modify the aerodynamic performance of the wing [35, 41, 62]. Additionally, they are supposed to reduce noise [47, 51, 62]. Owls rely on a slow and silent flight while hunting in twilight and darkness [87], because they mainly use acoustic information to detect prey [87]. Several morphological structures are specialised to detect and localise the prey precisely. Barn owls' eyes are equipped with high quality optics that possibly grant a feasible visual acuity even under dim light conditions [33, 32]. The facial ruff works as an amplifier that directs the sound to the asymmetrically arranged ears [43, 44]. In order to process acoustic information during flight, the owl has to perform a silent flight with stable flow conditions even at low-speed flight (2.5 m/s [56]). The overall wing geometry suggests adaptations to low-speed flight (see chapter 2). Further, the leading [36, 86] and trailing [51, 84] edges and the surface texture [41, 78, 79] influence the flow field over the wing. These specialised structures of owl feathers have been investigated in some detail in the past with respect to either the suppression of noise [31, 47, 51, 62] or the effect on the flow field and thus the flight performance [36, 41, 47, 62, 78, 79]. However, in almost all studies artificial models were investigated by abstracting the natural specimens and applying artificial copies to wing models investigated in wind tunnel experiments. A complete quantitative three-dimensional description of the specialisations of owl's feathers has not been accomplished so far, probably due to the specimen size. In an earlier work [4] the morphometry of feathers of barn owls (*Tyto alba pratincola*) and pigeons (*Columba livia*) were quantitatively characterised. The origin of the feather specialisations was determined in this study, but a three-dimensional description was not provided. Since the feather is a three-dimensional object, and since the specialised structures have a complex shape, there is a need of a three-dimensional description and characterisation in order to investigate the influence of each structure on the flow field and to understand noise suppression.

Three-dimensional specimen scans and surface reconstruction become more and more important in describing the anatomy and morphology of natural structures [5, 11, 37, 52, 96]. However, high-resolution scanning methods are often time-consuming and expensive when analysing the whole object and not only the surface [11]. Modern confocal laser scanning microscopes (CLSM) that are able to produce z-dependent image stacks can be used to investigate small-sized, (semi-)translucent objects. Such microscopes detect fluorescence either by auto-fluorescence or fluorescent staining. Three-dimensional information can be extracted by scanning several layers of the specimen in z-axis [37]. Since feather keratin is auto-fluorescent and slightly translucent, the whole specimens can be scanned with such

microscopes. Thereby, the visualisation of hidden structures becomes possible. Spatial resolution is only limited by the lenses of the microscope. Post processing software for 3D-reconstructions can then be used to visualise the surface of internal structures and to perform measurements of these surfaces. The objective of this study is to provide a quantitative three-dimensional description of the specialisations found in barn owls' flight feathers and to introduce a method of three-dimensional surface reconstruction using confocal laser scanning microscopy that provides high-resolution three-dimensional information.

3.2 Materials and Methods

3.2.1 Confocal laser scanning microscopy and 3D reconstruction

A confocal laser scanning microscope (Leica TCS SP2, Leica Microsystems GmbH, Wetzlar, Germany) was used to scan different feather parts. The auto-fluorescence of feather keratin was excited by applying a diode laser with a wavelength of 405 nm. All specimens were scanned from dorsal to ventral. Since the feather keratin is slightly transparent almost all structures became visible with this method. Spatial resolution depended on the specimen size and the lenses used (for more detail see the relevant subsection). The recorded images were exported as image stacks in TIFF format. Three-dimensional models were assembled from these image stacks using the software Amira (Mercury Computer Systems GmbH, Berlin, Germany). Further analysis and morphometric measurements were done using the software Amira, Photoshop (Adobe Systems, San Jose, California, USA) and MatLab (The MathWorks Inc., Natick, MA USA).

3.2.2 Feather material

Flight feathers (remiges) of barn owls (*Tyto alba pratincola*) were investigated. Moulted feathers of the institute's own colony and feathers of specimens that had been used in other experiments under a permit of the local authorities (Landespräsidium für Natur, Umwelt und Verbraucherschutz Nordrhein Westfalen, Recklinghausen, Germany (LANUV)) were investigated.

3.2.3 Serrations of the barn owl's 10th primary

Outer vanes of barn owls' 10th primaries are equipped with serrations. Single and intact barbs of 4 different 10th primaries and 4 different positions (20%, 40%, 60% and 80% length of vane) were investigated for a three-dimensional characterisation of the serrations. In total 16 serrations from 4 feathers were obtained, which were cut at the rachis and placed with polymer clay (Fimo classic, STAEDTLER Mars GmbH & Co. KG, Nuremberg, Germany) on an object slide, whereas the barb tip pointed upwards. All serrations were scanned with a spatial resolution of 5.86 x 5.86 x 5 µm per voxel. Due to the dimension of the serrations, several scans were needed to cover the whole structure. A surface model was generated after merging the specific scans (Fig. 15).

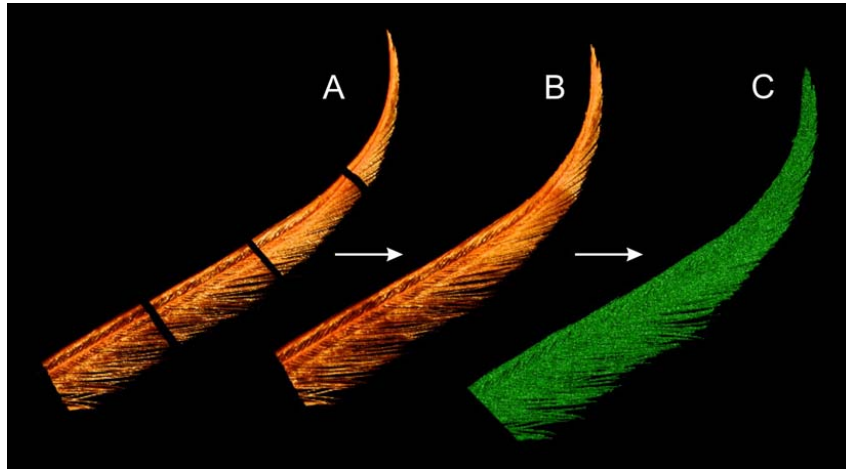


Figure 15: *Three-dimensional reconstruction of a serration. A Single scans of the serration in vortex view (density depiction of the voxel). B Merging of the single scans in one object. C Surface reconstruction (polygon mesh) to a fully three-dimensional object that allows three-dimensional measuring.*

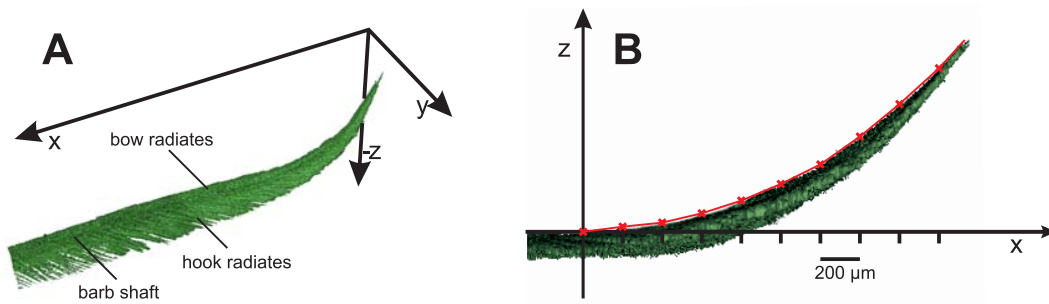


Figure 16: *Curvature measurement at the serrations. A Orientation of the serration. In this depiction the hook and bow radiates that arise from the barb shaft can clearly be seen. B After rotating the serration in a x-z-plane the dorsal curvature was sampled every 200 μm in x-direction.*

Measurements in three dimensions were enabled by the generation of surface models. All surface models were investigated in the same orientation using Amira (Mercury Computer Systems GmbH, Berlin, Germany). The conditions of measurement were kept constant for all serrations by which the results were comparable.

The curvature of the dorsal side of each serration was obtained. To do so, the surface models were oriented in a x-z-plane (Fig. 16A). The z-component was sampled every 200 μm in x-direction (Fig. 16B), which made the comparison of the data points of different serrations possible.

Serrations were not only curved, but the barb tips were tilted towards the feather base. The bended endings were twisted at the serration base resulting in almost no curvature in

y-axis within the serrations (Fig. 16). Thus, the tilt angle of each barb tip was measured. Five distinctive points (Fig. 17) were marked with the option 'landmarks' provided by the software Amira. Landmarks *a* and *b* determined the horizontal orientation of the barb and were rotated until they were exactly horizontal. The landmarks *c* and *d* were placed onto the uppermost dorsal surface of the barb shaft. By fitting these two landmarks in a frontal view, the serrations were prepared for the angle measurements. The landmark *e* was placed at the tip of the barb shaft. The tilt angle of the barb shaft and thus of the serration was measured as the angle between the perpendicular line to the horizontal oriented landmarks *a* and *b* and the connecting line of the landmarks *c* and *e* (Fig. 17).

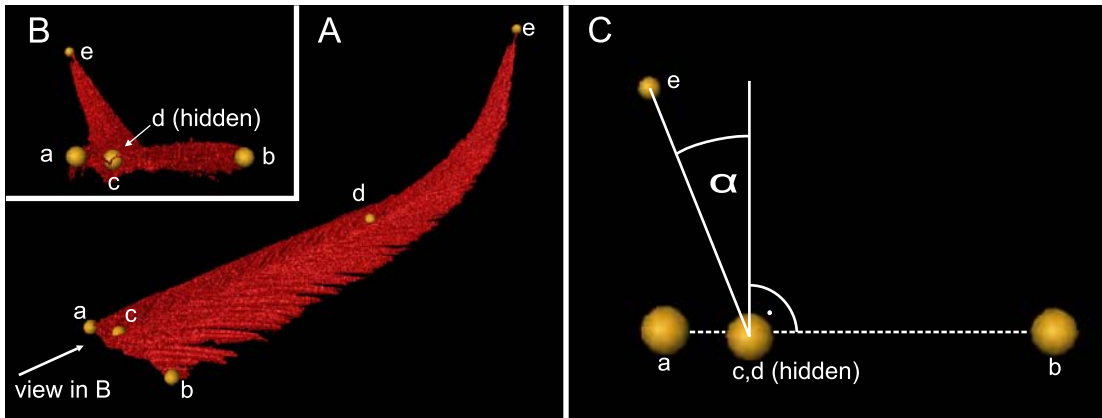


Figure 17: *Tilt angle measurement of the serrations. A* Five landmarks were set to orientate the serration and to measure the tilt angle of the barb tip. *a* and *b* define the horizontal plane. They were placed at the most distal parts of the hook and bow radiates. *c* and *d* were placed onto the dorsal surface of the barb shaft to define the longitudinal axis. *e* was placed at the tip of the serration. *B* The object was rotated until *a* and *b* was exactly horizontal and *c* and *d* fitted perfectly. *C* In this orientation the tilt angle was measured as the angle between the perpendicular line to the horizontal oriented landmarks *a* and *b* and the connecting line of the landmarks *c* and *e*.

Finally, each serration's length was determined. The 3D line measure tool of Amira was applied onto the surface from the beginning of the curvature (on the dorsal side) to the barb's tip (Fig. 18).

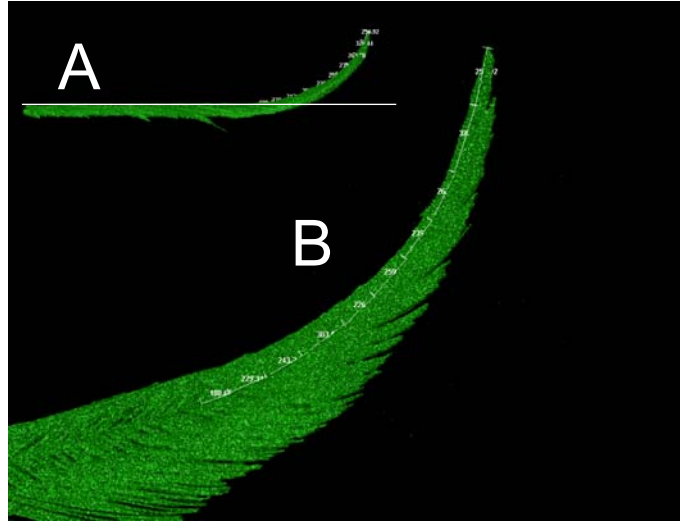


Figure 18: *Length measurement of the serration. A* The measurement of the serration length started at the beginning of the dorsal curvature. *B* The length was measured by sampling the barb shaft from the beginning of the curvature to the tip. The sum of all individual sections represents the serration length.

3.2.4 Fringes of barn owls' remiges

Flight feathers of barn owls form fringes at their inner vanes. Five different remiges (10th primary, p10; 5th primary, p5; 1st primary, p1; 4th secondary, s4; 8th secondary, s8) were investigated with respect to their fringes in order to compare the appearance of fringes at different feather positions. At each of the five feathers three positions (25%, 50% and 75% length of vane) of the inner vane were obtained (Fig. 19A). Vane parts of at least 20 barbs were placed on an object slide to ensure the natural arrangement. The fringes were scanned with a spatial resolution of 5.86 x 5.86 x 2 μm per voxel. The fringe-structure was subdivided into four individual scans due to the length of the structure and the resolution of the microscope. These scans were merged into one three-dimensional reconstruction similar to that of the serrations. The object volume was visualised in a vortex-mode supplied by the software Amira. Lengths of the fringes were measured by applying a line measure tool of Amira (Fig. 19C). At 50% length of the fringes, the number of barbs was counted (Fig. 19B, dotted line) and the density of fringes (barbs + radiates / mm) was calculated. Dorsal snapshots (Fig. 19) were made for visualisation purpose by rotating the reconstructions in the right orientation.

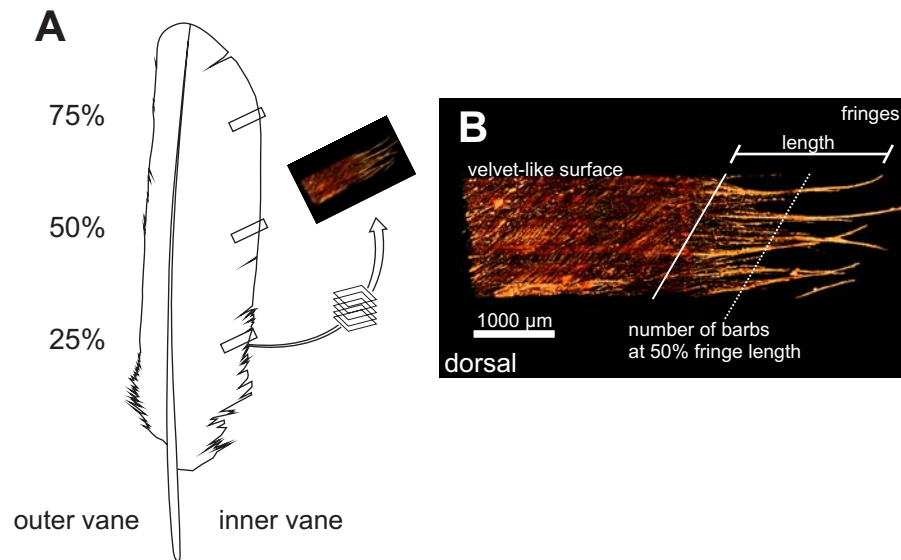


Figure 19: *Measurement of fringes. A* Position of the investigated fringes within a feather. For each position four image stacks were produced along the fringe axis. They were virtually matched to reconstruct a fringe in 3D. *B* The reconstructions were analysed with respect to the length of the fringes and the number of barbs (fringes) per mm.

3.2.5 Velvet-like dorsal surface of barn owls' remiges

Elongations of the hook radiates, so called pennula, form a velvet-like dorsal structure of each barn owl's feather. The surface differs between outer and inner vane. In order to characterise these differences, the velvet-like dorsal surface was analysed at three different positions (25%, 50% and 75% length of vane) at both vanes of the five above mentioned remiges (p10, p5, p1, s4, s8). Again, vane parts of at least 20 barbs were placed on an objective slide to ensure the natural arrangement. Each specimen was scanned with a spatial resolution of $5.86 \times 5.86 \times 2 \mu\text{m}$ per voxel. Scanned structures were investigated with respect to their height (thickness), the density of hairs (pennula per mm^2), the angulations of the pennula to the lower surface and the porosity of the velvet structure (Fig. 20).

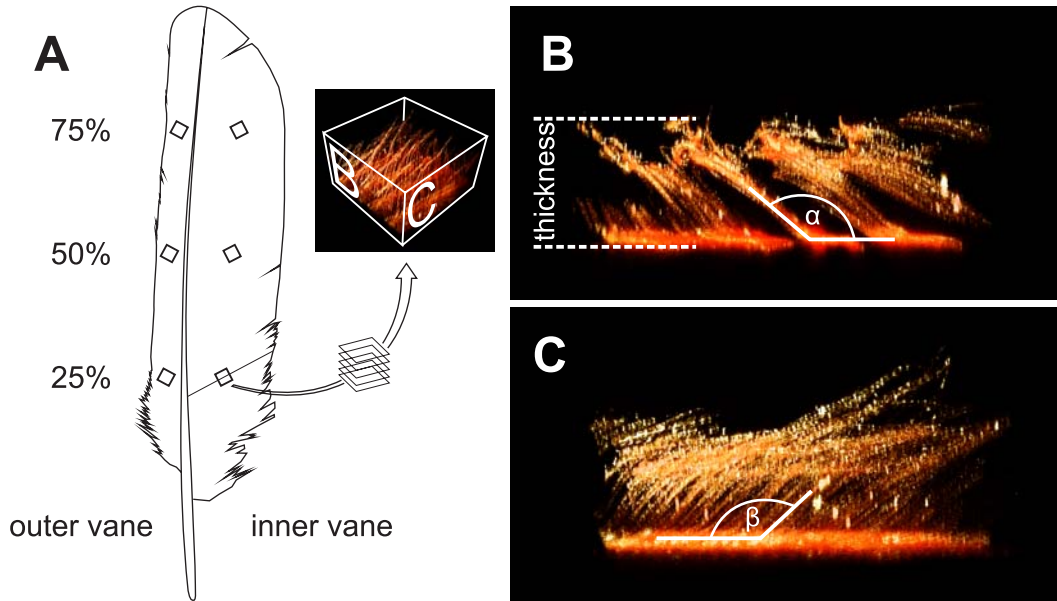


Figure 20: *Measurement of the velvet-like dorsal surface. A Six areas (25%, 50% and 75% of the inner and outer vane) of the dorsal surface were analysed per feather. The resulting image stacks were visualised in a 3D object. Cross-sections (B) and longitudinal sections (C) were analysed. B The thickness of the structure was measured at five different positions of the scan. The angles between barb plane and pennula were measured at four different positions of the scan. C The angles between barb shaft and pennula were measured at four different positions of the scan.*

The velvet-like dorsal surface was analysed with respect to its porosity. A virtual cube of the scanned structure was chosen that lay within the pennula structure. The porosity of the dorsal structure was calculated as the quotient of the air volume and the total volume of the investigated cube.

$$\sigma = \frac{Volume_{air}}{Volume_{total}} \quad (1)$$

While the total volume was calculated by multiplying the number of voxels of the virtual cube with the dimension of one voxel ($68.68 \mu\text{m}^3$), the air volume was calculated by multiplying the number of voxels of the structure (defined by its grey value) with their dimension and subtracting this volume from the total volume of the investigated cube. Grey values of the pennula scans were qualitatively determined with the software Amira and quantitatively measured with the software Matlab. The higher σ gets, the higher is the porosity and thus the ability to dampen noise.

3.3 Results

Confocal laser scanning microscopy (CLSM) is a quick high-resolution imaging technique, which is used to reconstruct three-dimensional images. Specimens are scanned with a laser diode by measuring the emitted light quantitatively. In this way, the specimens are scanned plane by plane. Out-of-focus light is eliminated by a spatial pinhole for specimens that are thicker than the focal plane. Fluorescence increases the image quality dramatically, since more information is available. Therefore, the material or tissue either needs to be dyed with fluorescent stains or alternatively has to be auto-fluorescent. Feather keratin is highly auto-fluorescent. This enabled the visualisation and digitising of the specific feather structures of barn owls using CLSM. Five different remiges (p10, p5, p1, s4, s8) (Fig. 21) were investigated with respect to the fringes of the inner vane and the velvet-like dorsal texture. Four individual 10th primaries were taken to characterise the serrations. In the following the three different feather specialisations of barn owls' remiges are presented and characterised three-dimensionally.



Figure 21: Five different remiges of the barn owl that were analysed with respect to their fringes and the velvet-like dorsal texture. Scale bars represent 5 cm in x- and y-direction.

3.3.1 Serrations

Barbs of the outer vane of the 10th primary remex formed serrations by their tips. Hook and bow radiates decreased in length [4], the barb shaft bent to the dorsal side and tilted towards the feather's base. In this way the barb endings separated and built up a serrated leading edge (Fig. 22).

Figure 23 shows serrations of four 10th primaries of different conditions and ages. While serrations in figure 23A were fully intact and had a pointed tip, those in figure 23B and C were gradually abraded. Finally, the feather in figure 23D has lost its typical serrations.

After losing the bowed serrations, straight serrations have been formed by a loss of hook and bow radiates. In my study preferably fully intact, bowed serrations were investigated and characterised. In order to determine the bending of the serrations, 16 barbs of four different feathers were digitised and analysed.

Figure 24 displays surface reconstructions (polygon meshes) of all investigated serrations. Interestingly, only little differences were found between the curvatures of the barbs in a superposition of all serrations (Fig. 25). However, the length of the serrations and the tilt angle towards the feather's base showed differences. To quantify these findings, the curvature, the length and the tilt angle of the serration was measured and compared between the specimens investigated.

The sampling of the curvature with a given x-value allowed the comparison of the curvature between different serrations. Figure 26 shows the data points of the serrations investigated grouped by their position within the feather.

All data points of the same x-component were analysed statistically in a Levene's test. Statistical differences occurred in a comparison of all serrations (Levene's statistics 9.6385; Degrees of freedom 11, 170; p-value 0). However, for the first ten data points no statistical differences were found when comparing serrations of the same position on a feather (Fig. 27). Therefore, a fitting curve being a polynomial of second order ($z = ax^2 - bx + c$) was generated (Fig. 26) in order to characterise the curvature of a typical serration at this feather position. The constant values c of these polynomial functions were equalised for all fits. However, they are not depicted in figure 26, since the serrations can be placed virtually in space. Although the curvature of serrations of different positions were statistically different, the variations were quite small. This can be seen in the arguments of the polynomial-functions and in the figures 25 and 26.

As mentioned before differences were found in the length and the tilt angle of the serrations. Some serrations ended in an acute tip, others ended with a more rounded tip (Fig. 24). Serrations of distal parts of the feather (80%) had a rounded tip and were shortest (1482 - 1925 μm) in contrast to serrations at basal parts of the feather (20%) (2149 - 2509 μm). Serrations that were located in medial regions of the feather were longest (max. 3045 μm) (Fig. 24, Table 4).

The tilt angle varied strongly between serrations of different positions and different feathers. Tilt angles between 4.6° and 30.8° were measured (Table 4). No clear correlation between the tilt angle and the position investigated was found (Figs. 24 and 25, Table 4).

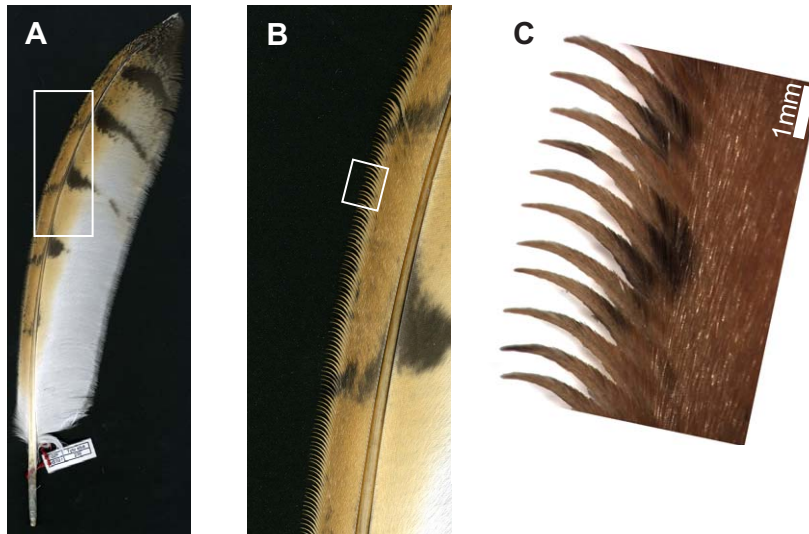


Figure 22: *Serrations of the barn owl's 10th primary in different magnifications. Note also the fringes at the inner vane (left) and the dorsal surface structure.*

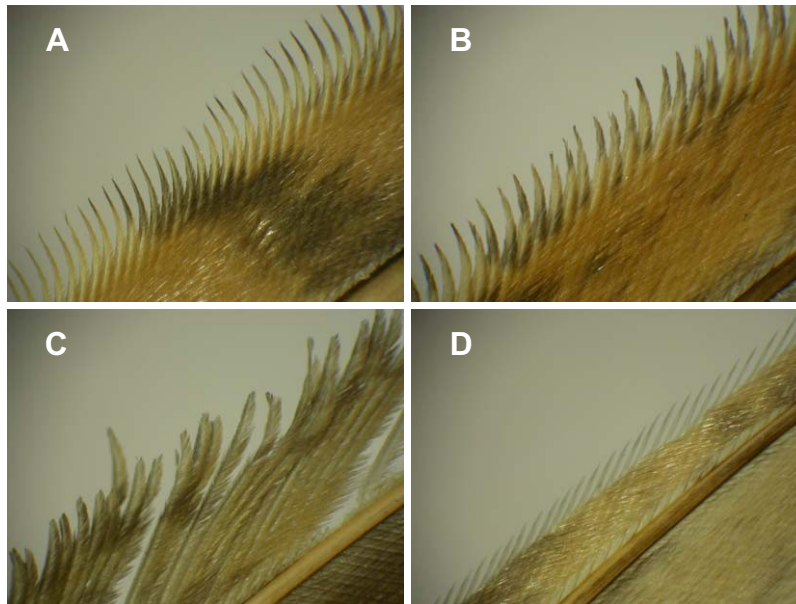


Figure 23: *Serrations of barn owls' 10th primaries in different conditions and ages, diminishing from A to D. A Fully intact serrations with a pointed tip. B Slightly damaged serrations with partially worn out tips. C Mostly damaged serrations with broken endings and rounded tips. D The typical serration structure is no longer visible. Curved parts of the barbs are missing. A loss of hook and bow radiates at more proximal barb parts resulted in a different serration structure.*

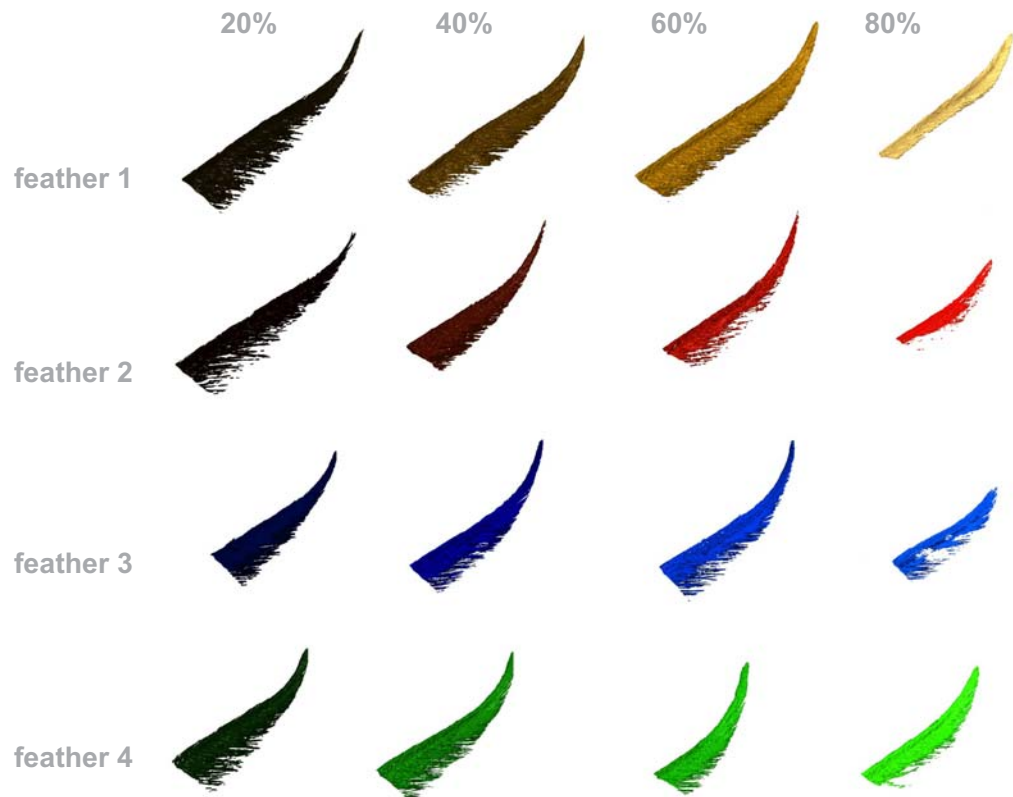


Figure 24: *Surface reconstructions (polygon meshes) of the 16 investigated serrations. The columns reflect the different feathers; the rows depict the different positions of the serrations at the outer vane.*

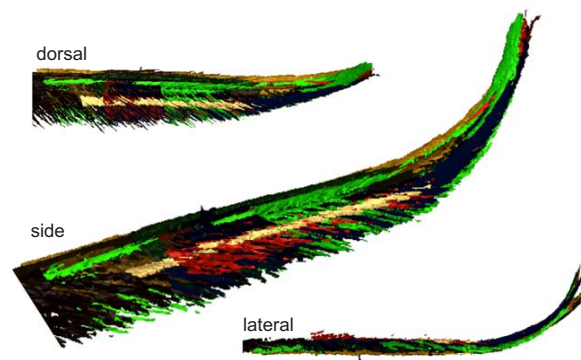


Figure 25: *Superposition of all 16 investigated and reconstructed serrations in three different orientations. Note the similarities in curvature and the differences in length of the barb tips.*

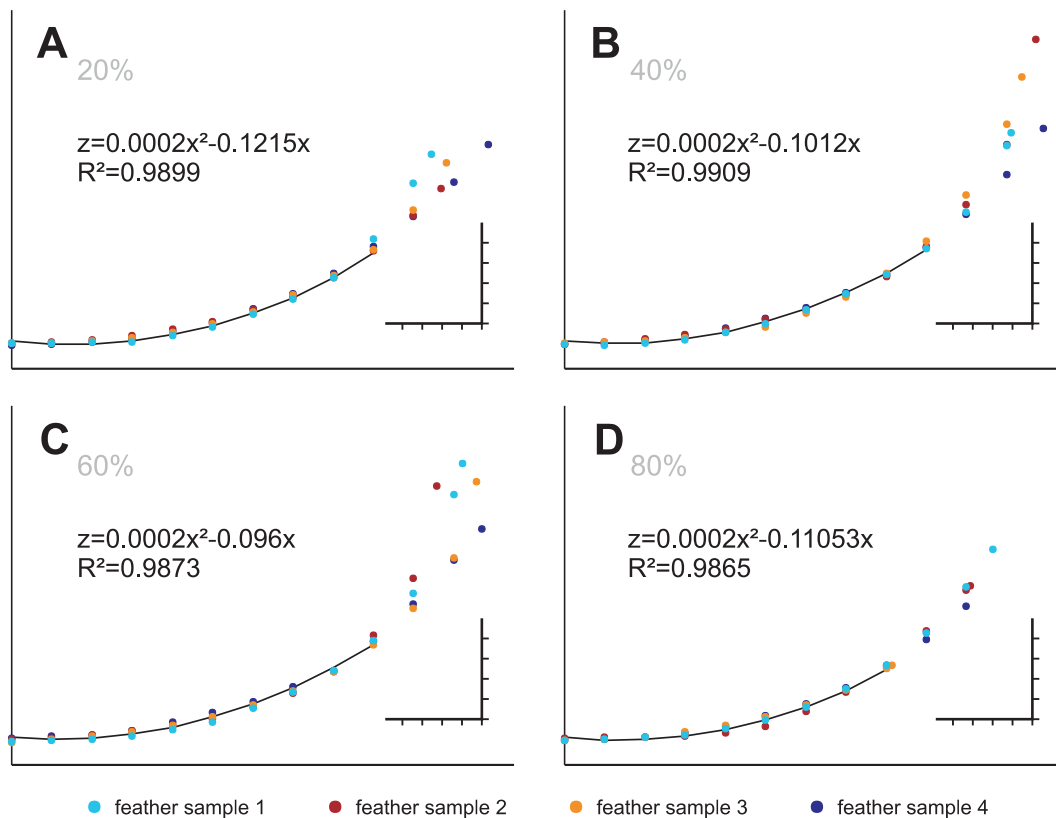


Figure 26: Curvature of serrations of different positions within the feather. **A** 20% **B** 40% **C** 60% **D** 80% length of vane. The black line indicates a fitting curve of the first 10 data points. The formula and its accuracy (R^2) is given in the diagram. Note the differences in length and bending at the serration tips. Scale bars represent 500 μm in x - and y -direction.

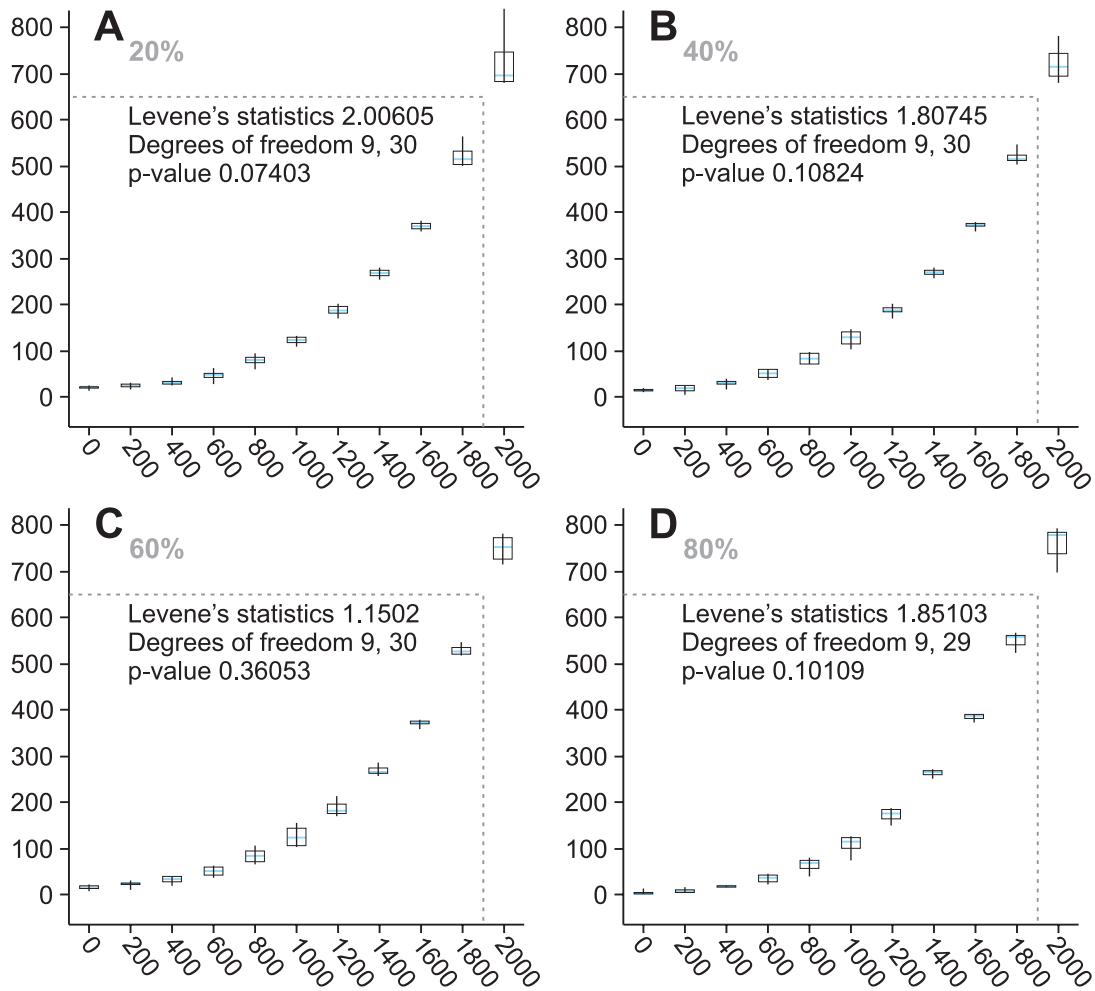


Figure 27: Whisker-Box-Plot and statistical analysis (Levene's test) of the data points of different serrations from the same position (**A** 20% **B** 40% **C** 60% **D** 80%). The results of the Levene's test is given in the diagrams. Data points within the dotted lines show no statistical difference in all cases.

Table 4: Lengths and tilt angles of serrations of barn owls' 10th primaries.

	feather 1		feather 2		feather 3		feather 4	
	length [μm]	tilt angle [°]	length [μm]	tilt angle [°]	length [μm]	tilt angle [°]	length [μm]	tilt angle [°]
20	2509	21,2	2159	9,3	2155	23,5	2149	24,5
40	2474	20,3	3045	12,7	2513	17	2058	28,6
60	2302	30,8	2948	6,2	2704	21,7	2364	23,1
80	1925	4,6	1621	8	1482	28,6	1903	24,9

3.3.2 Fringes

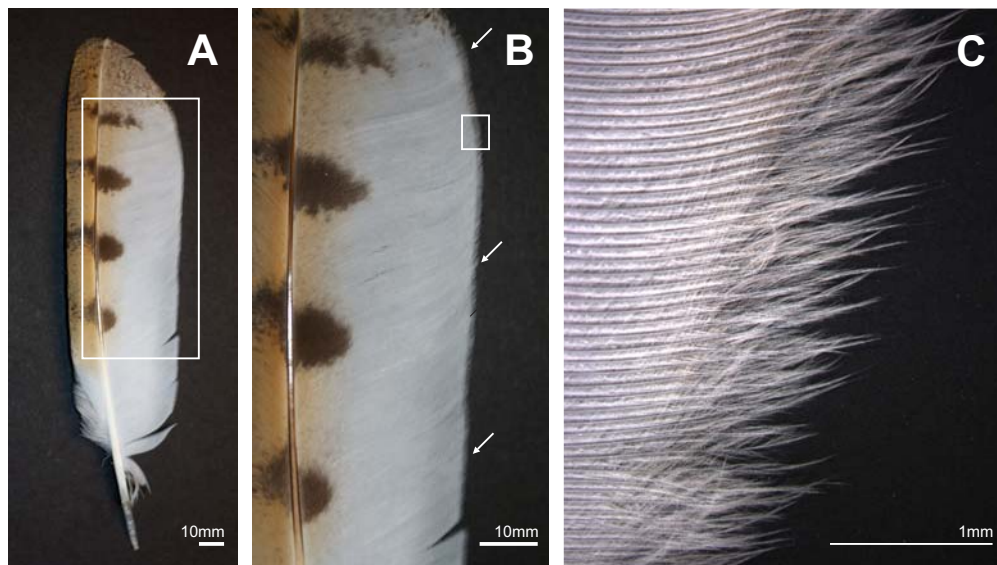


Figure 28: Inner vanes of barn owls' remiges are fringed. This is exemplarily shown for one 5th primary in different magnification. A and B dorsal, C ventral.

Edges of the inner vanes of barn owls' flight feathers were fringed (Fig. 28). Hooklets of the hook radiates were absent in the most distal parts of the barbs, resulting in separated barb endings. Since the radiates were not decreased in length, they supported the fringed structure by aligning with the barb shafts. For this study, three different areas (25%, 50% and 75% length of vane) of five different barn owl feathers (p10, p5, p1, s4, s8) were investigated (Fig. 21). Three-dimensional reconstructions allowed the rotation in high magnification and thus the determination of the exact length and the aligning process of the radiates.

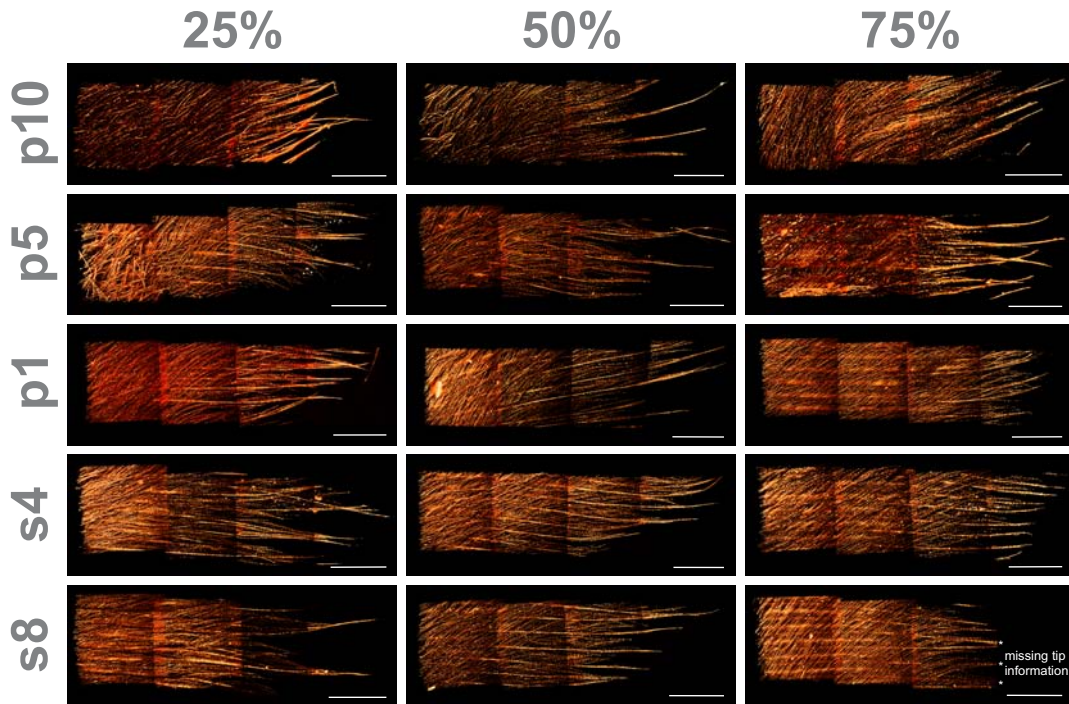


Figure 29: Dorsal view of fringes of five different feathers (10th primary, p10; 5th primary, p5; 1st primary, p1; 4th secondary, s4; and 8th secondary, s8) and three different positions (25%, 50% and 75% length of vane). Each scale bar represent 1000 μm .

Figure 29 shows dorsal views of all fringed areas investigated. Only little differences between fringes of the same position along the vane can be seen. Fringes of distal feather parts tended to be shorter and denser at the tip of the fringe. However, in some cases, e.g. feather p5 at 75% length of vane, the radiates stuck together and formed thicker structures. Although this effect was reversible by manipulation, such areas were scanned without treatment. Age as well as oils or waxes from the uropygeal gland might be the reason for the agglutination.

Table 5 presents values for length and density of the investigated fringes. Fringe length varied between 1.3 and 4 mm. The highest values for the length were found at 50% of the feather's vane length. By contrast, the shortest fringes were found at 75% of vane length in all feathers investigated. Fringes of the 10th primary showed differences in density along the vane. While 4.7 fringes per mm were measured at the feather's base (25% length of vane), only 3.3 fringes per mm were found in central and distal vane parts (50% and 75% length of vane). In the other feathers, 4 barbs per mm were counted in almost all cases. Basal parts of the first primary ($d = 4.7$ b/mm) and distal parts of the fourth secondary ($d = 4.3$ b/mm) were the only exceptions of this finding.

Table 5: Lengths (mean +/- SD, N of fringes investigated = 3-5) and densities of fringes of five different barn owls' remiges at three different positions along the vane.

	25%		50%		75%	
	length [μm]	density [b/mm]	length [μm]	density [b/mm]	length [μm]	density [b/mm]
10 th primary	1890 +/- 121	4,7	3072 +/- 196	3,3	2637 +/- 59	3,3
5 th primary	1903 +/- 119	4,0	2876 +/- 201	4,0	2199 +/- 145	4,0
1 st primary	2351 +/- 97	4,7	3387 +/- 569	4,0	1995 +/- 118	4,0
4 th secondary	2895 +/- 164	4,0	2913 +/- 224	4,0	1442 +/- 49	4,3
8 th secondary	2536 +/- 79	4,0	2658 +/- 107	4,0	1331 +/- 5	4,0

In the fully extended wing, feathers had an imbricate arrangement and large areas of the remiges overlapped. Thereby, barbs of inner vanes of two superjacent feathers were aligned. Since the fringes are formed by the barb endings, they were aligned with barb shafts of the superjacent feather as well. The lower surface of each feather is formed by the barb shafts. The parallel orientation resulted in a grooved structure. Fringes were able to merge into these grooves in a lateral movement of two superjacent feathers. To illustrate this point, figure 30A shows the lower surface of a barn owl's remex with the grooved structure formed by barb shafts. In figure 30B a second remex was placed onto the first remex in its natural arrangement in an extended wing. The black arrows mark the parallel orientation of the fringes and the ventral barb shafts. Note that the parallel orientation of the second remex is less obvious due to the taper of the barb shafts towards their tips. Consequently, the vane is much thinner at the edge.

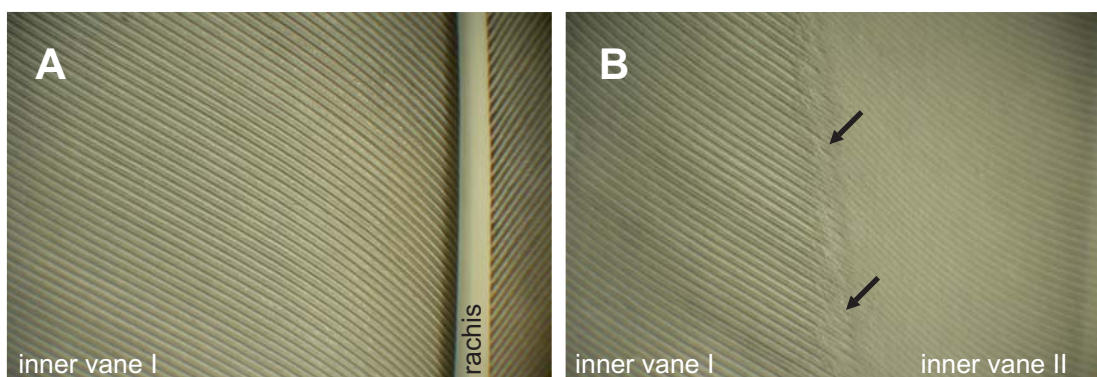


Figure 30: Ventral surfaces of barn owl feathers. **A** Barbs are parallel attached to the rachis and thereby forming a grooved structure. **B** Fringed barb endings of a superjacent feather merge into this grooved structure (black arrows) resulting in a smooth surface without sharp edges.

3.3.3 Velvet-like dorsal surface

Each feather of the barn owl had a velvet-like dorsal surface. Elongations of the hook radiates, called pennula, formed this structure. Five feathers of the wing (p10, p5, p1, s4, s8) (Fig. 21) were investigated and three areas of the outer as well as of the inner vane (25%, 50% and 75% length of vane) were scanned, three-dimensionally visualised and measured. Several differences were found by comparing covered and uncovered areas.

Figure 31 shows all five investigated feathers and the results of the measurements. The dorsal side of each barn owl feather can be divided into a white and a brownish patterned area. White areas were normally covered by the overlaying remex or by coverts (see Fig. 4). During flight, the brownish patterned areas are subjected to the flow field.

The two areas exhibited different morphometric characteristics. The areas that are subjected to the flow field (brown areas) (Fig. 31, A and B of each feather) had a higher density of pennula ($d = 80.0 - 130.7 / \text{mm}^2$), especially at distal feathers (primaries) (Fig. 31). The obtuse angulation ($\alpha = 133.1^\circ - 170.9^\circ$; $\beta = 150.0^\circ - 171.5^\circ$) of the pennula resulted in a low porosity ($\sigma = 0.45 - 0.90$) (Fig. 31). All parameters led to a relatively thin ($t = 80.9 - 130.7\mu\text{m}$) surface texture of the uncovered areas. In covered areas, the density of pennula was lower ($d = 57.8 - 104.4 / \text{mm}^2$), but the structure became thicker ($t = 275.6 - 1072.4\mu\text{m}$) and more porous ($\sigma = 0.75 - 0.93$) due to a more acute angulations of the pennula base ($\alpha = 116.8^\circ - 147.2^\circ$; $\beta = 107.9^\circ - 151.0^\circ$) and due to longer pennula [4]. A further difference was found regarding the orientation and length of the pennula. The surface of areas subjected to the flow field showed a brush-like shape. Each pennulum pointed upwards and ended with its tip in the air (Fig. 32A, B, E). In those areas that are covered by other feathers the pennula bent downwards and even dived back into the surface. In that way tiny loops were formed (Fig. 32C, D, F). Since the pennula were only fixed with one end, the whole structure was soft and pliant.

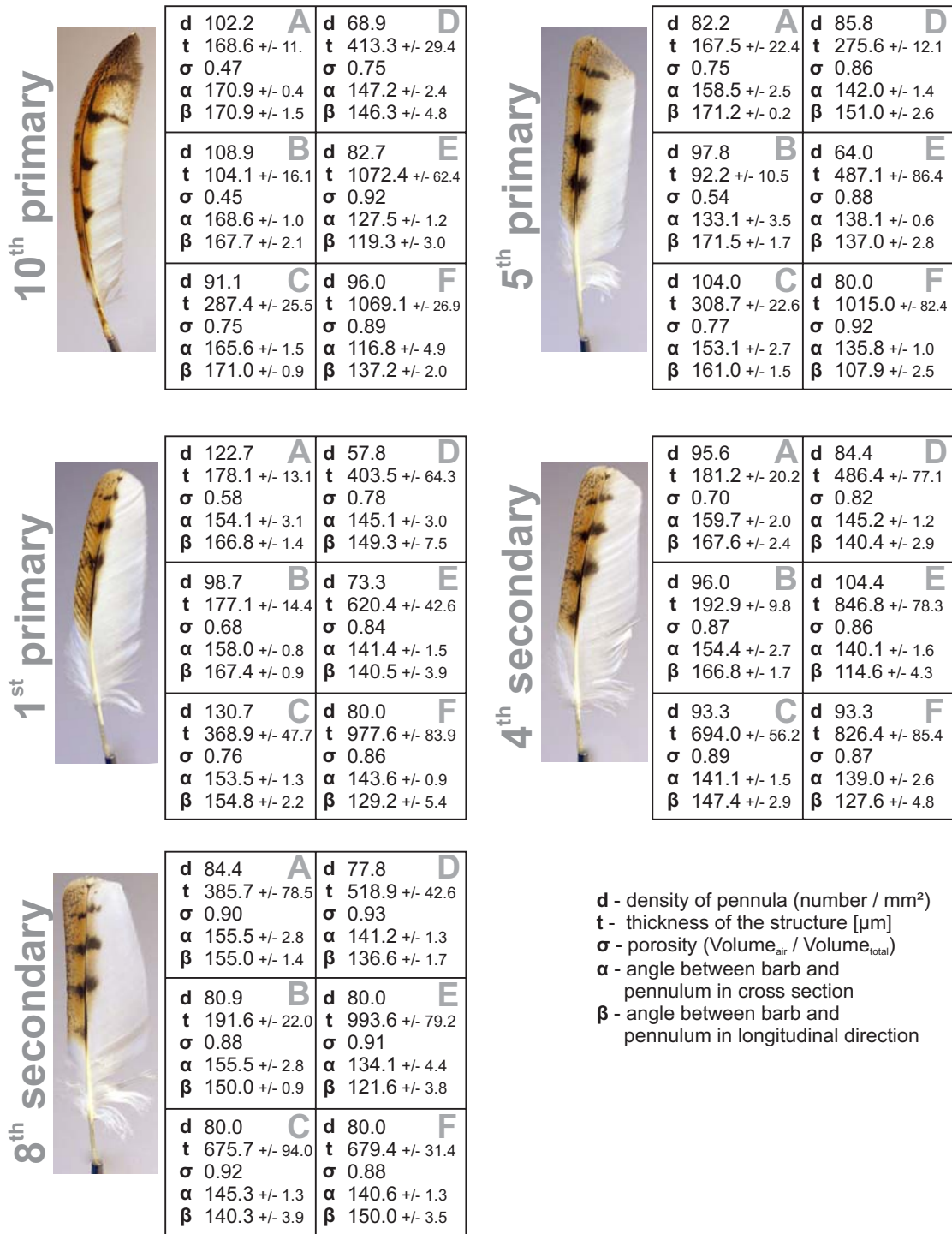


Figure 31: Results of the surface analysis at five different feathers of the barn owl (p10, p5, p1, s4, s8). **A-C** represent the positions 25-75% of the outer vane, **D-F** the relevant areas of the inner vane. A symbol explanation can be found at the right bottom.

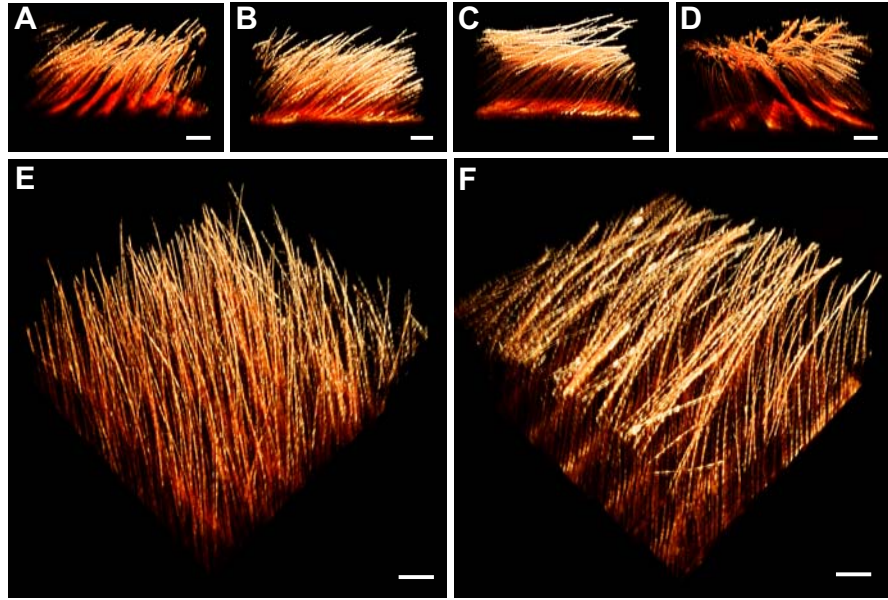


Figure 32: *Typical three-dimensional visualisation of the velvet-like dorsal surface. A transversal, B longitudinal and E isometrical view of the dorsal structure of the **ou-**ter vane; C transversal, D longitudinal and F isometrical view of the dorsal structure of the **inner** vane. Scale bars represent 100 μm each.*

3.4 Discussion

Confocal laser scanning microscopy was used to examine serrations, fringes and surface modifications of remiges three-dimensionally. Each structure was virtually reconstructed and characterised.

I observed an almost uniform serration shape, which is expressed by a constant curvature and length. Only at the feather's tip, serrations become shorter and showed a rounded tip. Fringes were very fluffy and unstable in shape. They were longest in the centre of the vane. The density of fringes was almost constant in the feathers investigated except for the 10th primary. Here, higher densities were found at the feather's base and lower densities were found at the rest of the feather's vane. The surface analysis revealed differences in thickness, porosity and density of pennula between areas that are subjected to the air flow and areas that are covered by other feathers. In the following the three-dimensional shape of each specialisation will be discussed with respect to a possible influence on either sound generation or air flow control. Finally, the method will be briefly discussed by comparing it to other three-dimensional visualisation methods.

3.4.1 Serrations

In barn owls, the leading edge of the distal wing is formed by the 10th primary remex. The outer vane of this feather carries serrations. Barb endings separate and bow to the dorsal side, logically changing their form and function. Even though some publications deal with descriptions of the serrations [4, 31, 36, 51, 56, 62, 87], none provided quantitative three-dimensional information on this filigree and complex structure. The three-dimensional characterisation revealed obviously new facts of the serrations that are discussed in the following.

Even though effects of serrations on the flow field and the acoustics are discussed, contradictory findings have been published. Functionally, serrations might act as a turbulence generator at the leading edge of the wing. In a series of papers from the early 1970^s [2, 36, 62, 85], several wind tunnel experiments were performed in order to investigate the impact of artificial two-dimensional serrations of different length and spacing on the flow field. Arndt and Nagel [2] investigated the effect of serrations on noise reduction. These authors showed that serrations affect the acoustic characteristics. Large vortices that shed from the airfoil investigated, dissipated faster after the model was equipped with serrations. Beyond influencing noise generation, serrations were found to be effective in the reduction of aerodynamic disturbances by enriching the boundary layer energetically. One year later, Schwind and Allen [85] published their results on flow visualisation of an airfoil with and without serrated edges. They tested serrations of different length and spacing. These authors showed that small spacings of the serrations performed best in eliminating the bubble that normally occurs at the leading edge of a wing. Again, this phenomenon was explained by a generation of turbulence on the dorsal surface of the airfoil and thus a creation of a more energetic boundary layer. Unfortunately, the size of the serrations investigated was larger, the geometry of the serrations as well as of the wing models was distinctly different and the air flow velocities were much higher, compared to barn owls.

Neuhaus et al. [62] performed flight experiments with tawny owls (*Strix aluco*) and mallard ducks (*Anas platyrhynchos*) in a more biological approach of understanding the function of serrations. They showed a laminar flow around the intact owl wing in smoke-visualisation experiments with wings of the two species. However, after amputation of the serrations, the air flow around the owl wing resembled the flow conditions found at mallard ducks. Now the air flow around the owl wing separated earlier. After performing acoustical measurements by Neuhaus et al. [62], it was concluded that the sound pressure was not affected in cruise flight conditions without the serrations at the leading edge, but increased during take-off. Finally, a variety of serrations were attached to the leading edge of a stationary airfoil in the study by Hersh et al. [36]. This procedure reduced the noise generated by the airfoils considerably. These authors concluded that the serrations generate chordwise trailing vortices on the suction surface, thereby changing the character of the wake vortex shedding from periodic to broadband, an effect by which the tones are reduced or even eliminated.

The quantitative description of the three-dimensional shape of the serrations found in barn owls might help to produce better artificial serrations for wind tunnel experiments and to get a better understanding of the function of this structure.

Anatomically, each serration is characterised by a few attributes. The curvature is almost constant and could be fitted by a polynomial of second order. The length depended on the position measured. Additionally, the taper of the serration contributes to the characterisation. This value was already determined in an earlier work [4]. The mean width of the serration base is 555 μm . It decreased almost linearly towards the tip, since the width at 50% serration length is 254 μm [4]. For engineering applications a constant shape and curvature of the serrations may be used.

Higher variations in shape of the serrations are found at their tips. Here, curvature as well as length differed significantly. Additionally, the tips of the serrations can be differentiated in pointed and rounded endings. Serrations with a rounded tip are shorter and less bowed. Such serrations are mainly found at distal parts of the feather. The 10th primary of barn owls shows a strong curvature of the rachis in the horizontal plane (Fig. 22) [4]. This causes the serrations to change their orientation with respect to the air flow direction and thus the angle of attack. Higher velocities and constantly changing angles of attack are also expected for this wing part, especially in flapping flight [81]. Additionally, the chord is shorter at the most distal part of the wing and the wing tip vortices shed off in this area. Consequently, the turbulence generators need to be differently shaped in order to influence the air flow regularly, which might be expressed in their length and tip appearance.

The round tips of the serrations may be due to other factors as well. For example, mechanical stress and UV-radiation fatigue keratin molecules [98]. As a consequence, the tips of the serrations show wear effects. The time-dependent loss of keratin molecules may lead to a round tip. This can be tested, when feathers of different age are compared. Serrations of moulted feathers should be distinctly different than serrations of feathers that were just developed. I assume that broken and shortened keratin molecules may result in the lesser bending due to a lesser internal strain, since the intact orientation and cross-linkage of the keratin molecules [3, 68] ensure the curvature of the serration. Although it was aimed to examine preferably intact feathers, the feathers investigated were all of different ages (different age of the bird, different storage time). Since the leading edge of

the wing was exposed to high forces and mechanical stresses, little abrasion and wearing effects were found.

Beside a different length and tip curvature, the tilt angle varies between the serrations investigated. Although the bowing, length and shape of the tip ending are clearly linked to the position of the serration, the tilt angle measured shows no clear correlation to the position of the serration. The orientation of the serrations at the leading edge of the feather is influenced by the attachment of the barbs to the rachis and the curvature of the rachis itself. Nevertheless, the serrations form a regular serrated leading edge in all feathers investigated, independent from the measured tilt angle.

3.4.2 Fringes

Fringes of the trailing edge of barn owl's feathers are very fluffy and unstable in shape. Barb endings separate by a reduction of hooklets of the hook radiates. Hence, connections between the barbs are no longer maintained. Hook and bow radiates do not decrease in length in contrast to the serrations. The radiates are oriented parallel to the barb endings due to a reduction in density and due to missing hooklets. Consequently, they support the barb shafts in forming the fringes. Since the barb shaft does not change its shape, as seen in the serrations, the structure is pliant and the fringes can float freely resulting in a thin, almost two-dimensional structure under non flying, stationary conditions.

The function of fringes is not yet well understood. Only little information is available dealing with flow influencing characteristics of fringed trailing edges. However, turbulent boundary layers being convected past the trailing edge into the wake are known to generate an intense, broadband scattering noise. Herr et al. [35] investigated several brush-type trailing edge extensions in a parametric study with respect to their influence on the scattering noise. Experiments of Herr et al. [35] comprised both acoustical and aerodynamic measurements. A significant noise reduction of 10 dB SPL was reached depending on the fringe configuration used. In conclusion, Herr et al. [35] identified the sound intensity decrease in a reduction of turbulence at the trailing edge supported by the fringes.

Apart from flow interactions, fringes could also be used by barn owls to produce a smooth lower surface of the wing. The parallel orientation of barbs of imbricate feathers facilitates the interaction of two different inner vanes. Barb shafts have a J-shaped cross-sectional geometry. They form a deeply grooved structure by their parallel alignment. Since barbs of two different inner vanes are almost parallel oriented as well, I speculate that fringes of the adjacent feather might merge into these grooves, and thus smoothing the border of two feathers during flight. Additionally, during flight, fringes might be sucked into the grooves due to a lower pressure on the suction (dorsal) side of the wing and due to a different air transmissivity of inner and outer vanes [58]. Müller and Patone [58] investigated air transmissivity of feather vanes. These authors found the transmissivity to be always higher at outer vanes than at inner vanes. Therefore, the inner vane of one feather is pressed towards the superjacent outer vane of the other feather leading to a smooth wing surface during flight. Since barn owl's feathers are highly porous [4, 62], this effect might be even enhanced. Sharp edges are avoided by merging the trailing edges of the remiges with vanes of the surrounding feathers. Consequently, noise sources would be eliminated. Whether

this effect really occurs in free flight has to be investigated in more detail at living barn owls or in wind tunnel experiments.

3.4.3 Velvet-like dorsal surface

The velvet-like dorsal texture of outer as well as inner vanes of barn owls' flight feathers have been characterised. In flight, large areas of the remiges' vanes are covered by adjacent remiges and coverts. The three-dimensional investigation revealed drastic differences between covered and uncovered areas. In uncovered areas, clearly distinguishable by the brownish colouring, the pennula form a brush-like structure (Fig. 33A), meaning their endings are subjected to the air. In covered areas, mainly the white areas of the feather, the velvet-like structure is thicker due to longer pennula [4] and different angulations of the pennula to the barb shafts. The pennula bend at the surface and dive partially back into the structure (Fig. 33B). Additionally, porosity is more increased in covered areas, than in uncovered ones.

The schematic drawing in figure 33 demonstrates the differences between the dorsal surface of the outer and inner vane in a more simple way.

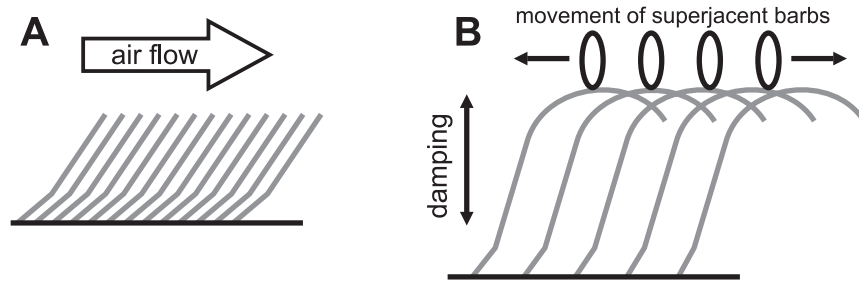


Figure 33: *Schematic drawing of pennula arrangement of the outer (A) and inner (B) vane. A The outer vanes of the remiges are subjected to the flow field. Hence, the pennula tips interact with the air. B The inner vanes are mostly covered by overlying feathers. The length and the curvature of the pennula of the inner vane provide a friction-reductive structure between the barb shafts of the different feathers.*

A modification of surfaces that are subjected to the flow field has a dramatic impact on the air flow conditions. Klän et al. [41] investigated owl-based airfoils with different surface modifications. The clean wing model showed a distinctive separation bubble at the dorsal surface. This bubble increased with higher incident flow. In case the separation bubble would reach the trailing edge of the wing, the flow would separate and the wing would not produce lift any longer. By applying velvet (with similar characteristics of the barn owl's surface) to the dorsal side of the wing, the separation bubble was decreased in size and pushed forwards to the leading edge. Hereby, the flow around the wing was stabilised by the velvet, especially at low velocities [41]. Surface modification can also lead to a reduction of drag. Species living in water developed several mechanisms to reduce drag. Sharks [7],

seals [38] and dolphins [77] influence the boundary layer of the water flow by different surface modifications. Sharks form riblets on their surface that decrease drag [7], seals are discussed to form similar riblet-like structures with their fur [38] and finally dolphins may reduce drag by moving synchronously their skin with small vibrations impinging on its surface [77]. This demonstrates that surface modifications are widely spread to reduce drag, increase flight/swim performance and save energy. Similar effects might be used by the owl to reduce drag and to fly more efficiently.

In contrast, surfaces of the inner vanes of remiges are rarely subjected to the air flow. Here, a different mechanism might act. Considering the flapping flight of birds, feathers rub against each other during beating of the wings or changing wing planform [20, 49, 60, 81]. Since the barbs are arranged in a parallel orientation, rubbing produces a well noticeable noise one can hear, for instance by scaring pigeons in a park. Owls may have solved this problem by forming a friction-reducing surface [31, 62]. The pennula form small loops over which the superjacent barbs can glide without being too noisy. Additionally, the soft structure is highly porous catching and eliminating rising noise. Porous surfaces are well known to reduce friction noise, for instance foams are well suitable to control noise radiation and damping noise [29], and porous road surfaces significantly reduce traffic noise [30]. Such effects might be expected at owl feathers as well.

3.4.4 Confocal laser scanning microscopy in comparison to other volume based methods

In general, three-dimensional reconstruction methods are divided into surface based and volume based methods. The presented CLSM-method is volume based, meaning internal information of the structure investigated are measured. Surface based methods measure only three-dimensional information of the surface of an object. Apart from confocal laser scanning microscopy, several other three-dimensional visualisation methods were tested to reconstruct feather details. In the following these methods are briefly introduced and disadvantages for the purpose of this study will be mentioned.

Wings of barn owls and pigeons were digitised with modern photogrammetry (ATOS, GOM Optical Measuring Techniques, Brunswick, Germany) (see chapter 2). The same method and equipment was used to scan one 10th primary of the barn owl. Due to the relatively low spatial resolution of 100 μm , tiny structures, especially the serrations, were not able to digitise. However, for larger objects, such as the wings, the resolution was sufficient.

Histological slices provide three-dimensional information as well. Objects are embedded in a sliceable substance (Paraffin waxes, Epoxy- or Polyester-resins) and then cut with a suitable apparatus. Afterwards, the slices are digitally photographed and aligned in the right distance with an adequate software. Structures of the sliced specimen can now be reconstructed via surface modelling. In order to reconstruct single barbs and barb arrangements, several slicing methods, such as microtome (R. Jung microtome, Heidelberg, Germany) with C-knives, vibratome (752M Vibroslice, Camden Instruments, Lafayette, USA) with razor blades (Gillette, Proctor and Gamble, Schwabach am Taunus, Germany), semi-thin sectioning (Reichert OmU3, C. Reichert AG, Vienna, Austria) with glass knives, and several different embedding materials, such as different paraffin waxes and Polyester

resins (XOR-Giessharz, hobby-time, Glorex, Füllinsdorf, Germany), were tested. A surface model was manually constructed using the software Amira and Maya (Autodesk GmbH, Munich, Germany). This method offered moderate results that were only hampered by the alignment and the relative distance of the single slices. However, this method is only feasible for larger structures, or structures with a known shape like rachises or barbs. Smaller structures, such as radiates, could not be reconstructed.

Modern three-dimensional microscopes allow high-resolution (up to 1 nm) investigations of small objects. For this thesis it was aimed to digitise surface textures of feathers using a 3D laser microscope (Keyance VK-9710K, Keyance Corporation, Osaka, Japan). The Surface was digitised in z-axis with a scanning laser and optical lenses. Suitable software calculated and reconstructed the surface. However, hidden structures or the back side of the object could not be visualised. In order to measure the object as a whole, it needs to be rotated and the gained surfaces have to be merged afterwards. This procedure is time consuming and provides many problems since the alignment needs to be done manually - infeasible for the quantitative characterisation presented here.

Besides CLSM, different volume based methods were tested. Computed tomography is a medical imaging method, which was used to get an inside view of feathers, respectively the wing (see chapter 2). Around a single axis of rotation, image stacks of the object were gained using X-ray. Each image contained information of the density distribution of the relevant slice expressed in a grey value of the voxel (pixel in 3D). Internal and external structures were visualised by filtering specific grey values. Since the computed tomograph used (Somatom Sensation 16, Siemens, Erlangen, Germany) was designed for the investigation of humans, the spatial resolution was limited to $0.75 \times 0.75 \times 0.5$ mm per voxel, which is much larger than the filigree structures of feathers. Consequently, the spatial resolution of this tomograph was too low. Better results are gained with micro computed tomography, which works in the same manner as the medical CT, but with much higher spatial resolution. I have used a micro CT (Viva CT 40, SCANCO Medical AG, Brüttisellen, Switzerland) in order to scan feathers. Unfortunately, the contrast between feather keratin and air was low. Staining of the feather, using iodine solution or gold sputtering, improved this problem slightly. In a low spatial resolution of $10 \mu\text{m}$, visualisation of covert feathers was possible. However, the interpolation process during analysis eliminated all information of the pictures leading to black slices when scanning with higher resolutions, which would be needed to measure the filigree structures.

3.5 Conclusions

Confocal laser scanning microscopy (CLSM) is a well-suitable method to investigate the feather anatomy. By exciting the auto-fluorescence of feather keratin, surfaces can be visualised and three-dimensionally reconstructed. Even hidden structures become visible due to the translucency of barn owls' feathers. Finally, the high spatial resolution and the reconstruction of a specimen allows a much better measuring of tiny structures.

Owl feathers have unique surface and edge modifications that were investigated and characterised using CLSM and adequate software. Serrations at the leading edge of the wing may serve as a turbulence generator to keep the air flow attached to the distal wing. Their curvature seems to be highly conserved, but also affected by wearing effects. Fringes at the trailing edges of the feathers (inner vanes) are fluffy structured and not restricted to any orientation. Since they are present throughout the inner vane, they might have at least two functional roles. On the one hand, fringes could support the convection of the turbulent boundary layers past the trailing edge of the wing, on the other hand, fringes could merge with the superjacent vane of a neighbouring feather and thereby creating a smooth lower wing surface without noisy edges. The velvet-like dorsal surface can anatomically be divided in two different appearances. Hence, it might have two different functions as well. First, the surface of the outer vane has a brush-like shape, while the pennula tips pointed upwards. They are supposed to interact with the flow field by enriching the boundary layer energetically and thus influencing the separation bubble on the suction side. Second, the surface of the inner vane is much thicker and more porous. Furthermore, the pennula tips bend at the surface and dive partially back into the structure and thereby forming small loops. Friction that occurs between feathers during flapping of the wings might be reduced by this formation, since parallel oriented barbs of different vanes do not have contact. Consequently, friction noise might be reduced. Additionally, a higher porosity might dampen occurring noise.

4 Material Properties of Barn Owls' and Pigeons' Feathers

4.1 Introduction

Feathers of flying birds have to withstand aerodynamic forces during flight [22], since they interact with the air flow, especially remiges and rectrices [10, 20, 22]. The air flow over the wings is influenced by flight feathers, which is achieved by either active control, e.g. erection of the alula [59], or by passive effects, such as lifting the coverts in critical flight manoeuvres [20].

Members of the taxon *Strigiformes* (owls) have evolved feather specialisations for a slow and silent flight. Whether their feather material (keratin) underwent an adaptation in stiffness as well is yet unknown. This study shall provide an estimation of the Young's modulus of rachis keratin of barn owls (*Tyto alba pratincola*) and of pigeons (*Columba livia*), a bird species with a similar body weight, but lacking the specialisations of the barn owl described in chapter 3. Furthermore, geometrical data of the rachises of the two species are provided.

In general, a bird's feather is composed of a hollow, central shaft and two laterally attached vanes. The shaft can be subdivided into the calamus and the rachis. The rachis is filled with a foam-like structure, formed by medullary cells, which protects the outer region of the rachis (cortex) against buckling [15]. Feathers are anchored into the bird's skin with their calamus, the most proximal part of the shaft. Each calamus is supported by muscles, tendons and in the case of remiges and rectrices, by bones [16, 72]. Vanes are formed by barbs that are connected via hook and bow radiates in a parallel orientation. This construction results in vanes that are light, flexible and resistant to damage. In case a feather vane fails and splits, it can be easily reconnected by the bird with its beak. Aerodynamic forces acting onto the vanes of flight feathers are redirected towards the skeleton elements by the rachises [22]. Since feathers are dead structures, their bending properties can only be influenced once - while being developed. Two parameters are mainly responsible for the degree of flexibility in feathers: the elastic modulus (Young's modulus, E) of the material (keratin) and its geometry, more precisely the second moment of area (I) of the rachises. A control of the dorso-ventral bending behaviour of the rachises can be achieved by an adaptation of E , I or both [14].

Until now, little is known about the material properties of feather keratin. Some publications report Young's moduli [13, 14, 15, 19, 21, 28, 54, 73], but due to different methodological approaches and investigated species they are hardly comparable. The few published values of E vary between 0.045 and 10 GPa [54, 73]. Bonser et al. [14] were the first to start a comprehensive study of different bird species having the goal to determine the Young's modulus of feather keratin. These authors performed tensile tests of small rachises parts of eight different bird species, including the tawny owl (*Strix aluco*, 2.76 GPa) and the pigeon (*Columba livia*, 2.42 GPa). The Young's moduli varied around 2.5 GPa for all species investigated, except for the grey heron (*Ardea cinerea*, 1.78 GPa). Sartori [83] measured the Young's modulus of keratin from barbs of barn owl's feathers in tensile tests (*Tyto alba*, barbs: 2.56 GPa). His results are consistent with those of Bonser et al. [14]. It seems that the Young's modulus varies within a limited range, at least if measured in

tensile tests. Furthermore, studies by Rutschke et al. [82] suggested that flexural stiffness is influenced by the geometry of the rachises. These authors already concluded that the control of the feather's bending behaviour is influenced by several cross-sectional shapes of the rachis' cortex that have evolved adaptively in different bird species. They claimed that the geometry has a larger influence than the material property.

In general, the geometry and the profile of a beam influence the bending behaviour. Hollow beams are known to be flexible and at the same time robust against loads [40]. However, such structures tend to buckle in case the load exceeds a critical value. Filling the beam with a foam, as it is done for example in beams of sailplanes, prevent buckling to a certain degree. Variations in the profiles and the applications of bottom booms are further options to influence the bending behaviour [40]. In flight feathers, various adaptations have been evolved depending on the requirements concerning force resistance and lift production. Purslow and Vincent [73] tested the role of the variation in the second moment of area along the rachis length of pigeon primaries by determining the bending behaviour. These authors claimed that the flexural stiffness is largely controlled by the geometry of cortical regions and their specialisations such as cortical ridges and braces.

Although several publications (as cited above) provide data on either the Young's modulus of rachis keratin or the second moment of area, no author measured both values for one specimen at the same time, as it is presented in this study.

4.2 Materials and Methods

4.2.1 Two-point bending test

The rachis can be technically approximated as a cantilever beam structure. Therefore, the Young's moduli of feather keratin from barn owls' and pigeons' rachises can be determined in two-point bending tests. Feather rachises of 4th primaries of 7 barn owls and 7 pigeons were taken from fixed wings. In total 7 remiges per bird species were investigated. Fourth primaries were chosen, because these rachises showed almost no curvature in the horizontal plane of distal parts (Fig. 34), which would cause torsion in bending tests.

The bending specimens were prepared by removing the lateral vanes with a scissor 1 mm besides the central shaft. This effectively prevented damaging the shaft. On the other hand, small remnants of the barbs remained at the shaft. This, however, did not influence the measurements, since the barbs were oriented in bending direction and thus did not support the bending resistance. After removing both vanes, straight rachises parts of at least 50 mm were taken and fixed with superglue in an Aluminium block (Fig. 34). A hole drilled in the Aluminium block was chosen to be almost as thick as the particular rachis in order to minimise the influence of the embedding material. The test length (l) of all specimens was set to 30 mm. A micro-manipulator (Märzhäuser MM33, Wetzlar, Germany) was used to deflect the rachis specimens. Forces that were exerted while pushing the rachises onto a digital-scale (Mettler Toledo XS 205, Mettler Toledo AG, Greifensee, Switzerland) were measured (Fig. 35). The deflection distance $w(x)$ (see Fig. 35) was set to 4 mm for the feather specimens 1-5 of the two species and to 1 mm for the feather specimens I-IV.

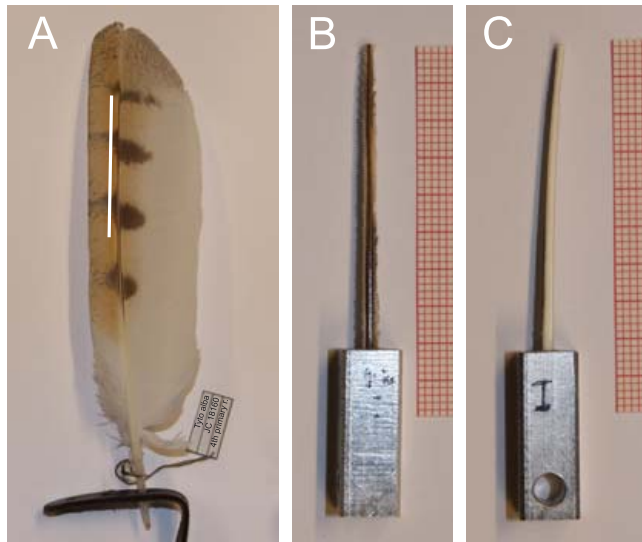


Figure 34: **A** 4th primary of a barn owl. The distal part of the rachis shows almost no curvature in the horizontal plane. **B** and **C** laterally uncurved rachis parts of at least 50 mm were placed in an Aluminium block in order to perform two-point bending tests. **B** dorsal, **C** lateral. Scale: millimetre paper.

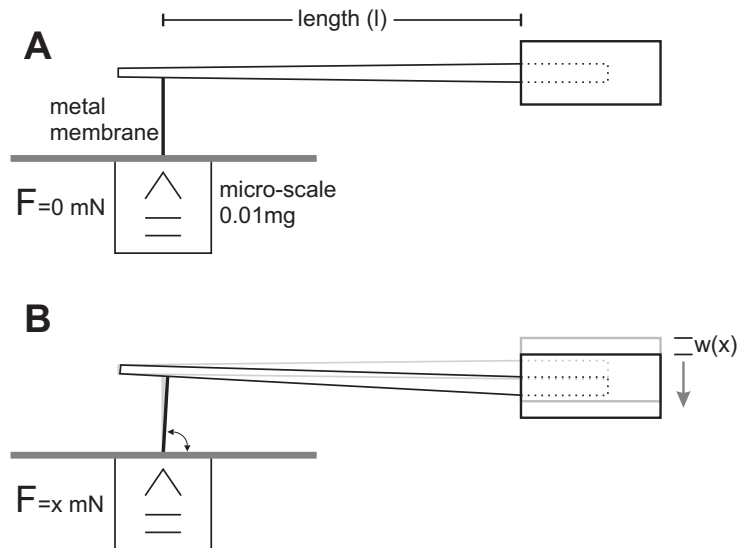


Figure 35: Schematic drawing of the measurement setup of the two-point bending test. **A** A test specimen (rachis part) is fixed in an Aluminium block that in turn is mounted at a micromanipulator (not shown). The rachis is positioned at a defined length l above a micro-scale. **B** Rising forces F are measured with the micro-scale after displacing the rachis for a defined way $w(x)$. To deflect longitudinal forces, a metal membrane is flexibly fixed on the scale.

The micro-manipulator did only perform movements in vertical direction. Hence, the test specimens would get out of place at the contact point of the digital-scale after deflection. To prevent slipping, a metal membrane (blunt razor blade) was flexibly fixed at the contact point onto the micro-scale in order to deflect longitudinal forces while changing the angle between the scale and the rachis base (Fig. 35B).

Hysteresis effects of the material were observed (see results). Because of this hysteresis, a time interval of at least 24 hours was set between the individual material-characterising measurements for each specimen in order to let the material recover over night. The bending tests were repeated 8 times for each rachis part. All experiments were performed under almost constant conditions (23.2° C +/- 0.5, 27.6% humidity +/- 1.0) to avoid an influence of temperature and humidity on the results.

4.2.2 Determination of the second moment of area

Subsequent to the bending tests, each rachis part was embedded in a single-use injection device (5 ml) with epoxy resin (Epon). After polymerisation, each rachis was cut at defined positions using a turning lathe in order to measure area size and second moment of area (I) of the cross-sections.

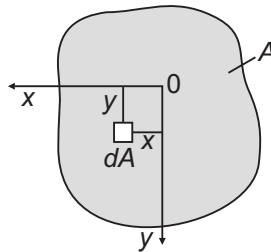


Figure 36: *Geometrical background for equation 2.*

For an area A with a coordinate system of a x - and y -axis and an origin of ordinates of any desired point (Fig. 36), the second moment of area (I) about the x -axis is defined as:

$$I_x = \int y^2 \, dA \quad (2)$$

where I_x is the second moment of area about the x -axis, y is the perpendicular distance from the axis x to the element dA and dA is an elemental area.

In my study I used a different approach to calculate I provided by Baron et al. [6]. Their approximation of the second moment of area uses finite pixel information of pictures of beam cross-sections for the calculations. The second moment of area is given by the equation:

$$I = \sum_{i=0}^{\text{all "black" pixels}} y_i^2 \Delta A \quad (3)$$

In this equation y_i represents the distance of the i th pixel from the neutral axis and ΔA is the area of one pixel [6].

The longitudinal distribution of the second moment of area was characterised by the function $I(x)$. A polynomial of second order ($I(x) = ax^2 + bx + c$) was fitted onto the data of I of the supporting points (slices of each specimen). Four supporting points were chosen to calculate the longitudinal distribution of the second moment of area for those specimens that have been used to determine the Young's modulus. The number of slices was limited by the facilities of the turning lathe. However, the four supporting points were sufficient to calculate a polynomial fit with an accuracy of at least $R^2 = 0.992 \pm 0.016$. Nine cross-sections (every 10% of rachis length) were made for those feather rachises that were used to investigate the distribution of the second moment of area of one fourth primary of the two species. The surfaces of the designated cuts were polished with abrasive paper (800-2000 grain size) and photographed with a digital camera (Nikon Coolpix 4500, Nikon Corp., Tokio, Japan) mounted on a stereo-microscope (Nikon SMZ 10A, Nikon Corp., Tokio, Japan). The cortices of the rachises were marked black (0) and the surroundings white (255) using Photoshop CS (Adobe Photoshop CS, Adobe Systems, San Jose, California, USA). This procedure enabled the measurement of the area (counting the pixels with a given size) and the calculation of the second moment of area. The neutral axis, the line that passes through the centroid of mass of the cross-section [6], had to be found for the determination of the second moment of area. The centroid was found by taking the average of the positions of all black pixels, as the pixels are of uniform size and density. Since the rachis was bend dorso-ventrally and no torsion was observed, the neutral axis was horizontal.

4.2.3 Calculation of the Young's modulus

The Young's modulus was calculated by applying the formula for the curvature of a beam ($w''(x)$), which can be solved with values of the Young's modulus (E), the second moment of area (I) and the bending moment ($M_b(x) = F(x - l)$). The equation for the curvature of a beam is given as:

$$w''(x) = \frac{-M_b(x)}{EI} \quad (4)$$

Since $w(x)$ is known (deflection of the rachis, $w(30) = 4 \text{ mm}$) the right part of the equation needs to be integrated twice.

$$w(x) = -\frac{F}{E} \iint \frac{(x - l)}{ax^2 + bx + c} dx^2 \quad (5)$$

Afterwards equation 5 has to be solved for E.

$$E = - \frac{F \iint \frac{(x-l)}{ax^2+bx+c} dx^2}{w(x)} \quad (6)$$

For a better integration, the term $(x-l)/(ax^2+bx+c)$ was substituted by a polynomial of 6th order ($g(x) = a_n x^n + \dots + a_1 x + a_0$). The argument a_0 of the first and second integration equals zero ($a_0 = 0$), since $w'(0)$ and $w(0)$ equals zero as well. By insertion of the measured parameters for $w(30)$, $M_b(30)$ and I , the Young's modulus was determined for each rachis part.

4.2.4 Nanoindentation

Nanoindentation is a well-suited method to characterise the properties, e.g. the Young's modulus, of micro- and nanostructured materials. This method was performed at rachises parts of barn owls and pigeons in order to substantiate the findings of the two-point bending tests with a second, independent method. The tests were performed in close cooperation with Dr. Jens Emmerlich from the Institute of Material Chemistry of the RWTH Aachen University.

Two small rachis parts (from 10% and 70% of vane length) each of two 4th primaries of the barn owl and the pigeon were investigated. In total 8 samples were tested. Keratin specimens were taken from feathers that had already been used in the bending tests.

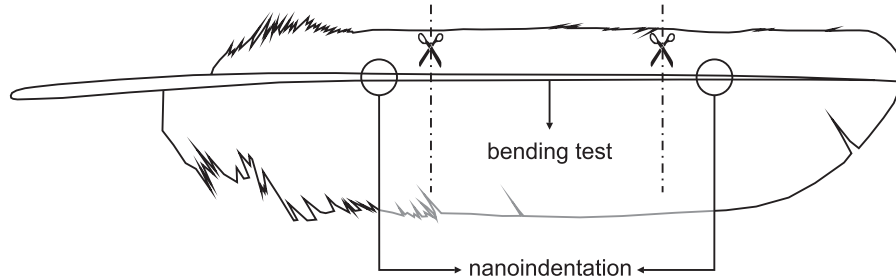


Figure 37: *Sampling area of nanoindentation and bending-test specimens. Uncurved rachis parts of at least 50 mm were taken for bending tests. Adjacent rachis parts of the distal and proximal dorsal rachis were further prepared for nanoindentation.*

Figure 37 shows the sampling areas of the nanoindentation specimens that lie close to the bending-test specimen. Small dorsal parts of the rachis were taken and embedded in Polyester-resin (XOR-Giessharz, hobby-time, Glorex, Füllinsdorf, Germany) that polymerises under room temperature and normal light condition to avoid an influence of temperature and UV-light on the material properties. Afterwards, they were cut transversely with an ultra-microtome (Reichert OmU3 ultra-microtome, C. Reichert AG, Vienna, Austria) and a glass knife with a tip angle of 45°. This procedure provided suitable smooth surfaces. Mechanical properties of the feather keratin were investigated using a depth-sensing nanoindenter (TriboIndenterTM, Hysitron Inc., Minneapolis, USA). A so called Berkovich indenter was used for the measurements. The tip of this indenter resembled a pyramid with

three faces, a tip angle of 142° and a tip diameter of 150 nm. The indenter was calibrated using a fused silica standard prior to the experiments. In the measurements, the applied force (F) and the displacement (h) of the indenter were recorded simultaneously. Each specimen was measured 20 times at different positions (array of 4 x 5 indents). Since a Berkovich indenter was used, the resulting load-displacement curves were then evaluated according to the Oliver and Pharr method [65]. In this method, the slope dF/dh of the initial unloading part of the load-displacement curve (Fig. 38) was used to extract the reduced modulus E_r as given in the following equation:

$$\frac{dF}{dh} = \frac{2}{\sqrt{\pi}} E_r \sqrt{A(h_c)} \quad (7)$$

with $A(h_c)$ as the contact area under the peak load.

In a further step the following formula was used to calculate the Young's modulus (E):

$$\frac{1}{E_r} = \frac{(1 - \nu_i^2)}{E_i} + \frac{(1 - \nu^2)}{E} \quad (8)$$

with E_i being the Young's modulus and ν_i being the Poisson's ratio of the indenter; ν represents the Poisson's ratio of the keratin. Since the Poisson's ratio has not been determined for feather keratin so far, it was estimated by applying the Poisson's ratio of bovine claw horn being 0.4 [27].

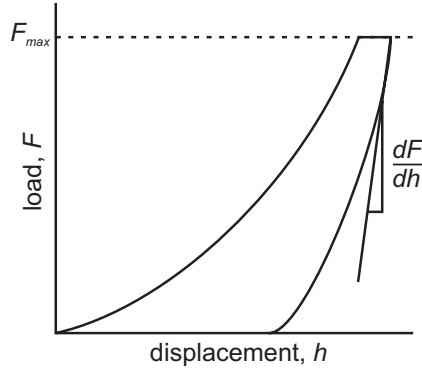


Figure 38: *Schematic drawing of the load-displacement-curve of a nanoindentation test.*

4.3 Results

Seven 4th primaries of barn owls and pigeons were investigated to determine the Young's modulus of their feather keratin with two independent methods. Furthermore, cross-sectional shape, area and the second moment of area along the rachis length were measured. In the following, the material properties are presented first, followed by the geometries of the investigated feathers.

4.3.1 Young's modulus of barn owl's and pigeon's feather keratin

Two-point bending tests were performed to determine the Young's modulus of barn owls' and pigeons' feather keratin. A hysteresis effect of the keratin was found in preliminary experiments. This effect shall be exemplarily demonstrated in one long-time experiment. In this test one rachis of the barn owl was deflected for a given time and the decreasing weight, respectively force, was measured in regular time intervals. The hysteresis curve is depicted in figure 39. While the measured force decreased continuously and very fast in the first hour, the curve flattened as time passed. After 2.5 hours no further changes were measured. In an additional test it took 6 hours until the material was completely restored after the bending force was removed. In order to avoid artifacts due to the hysteresis, each specimen was only examined once every day in the bending experiments in order to let the material recover over night.

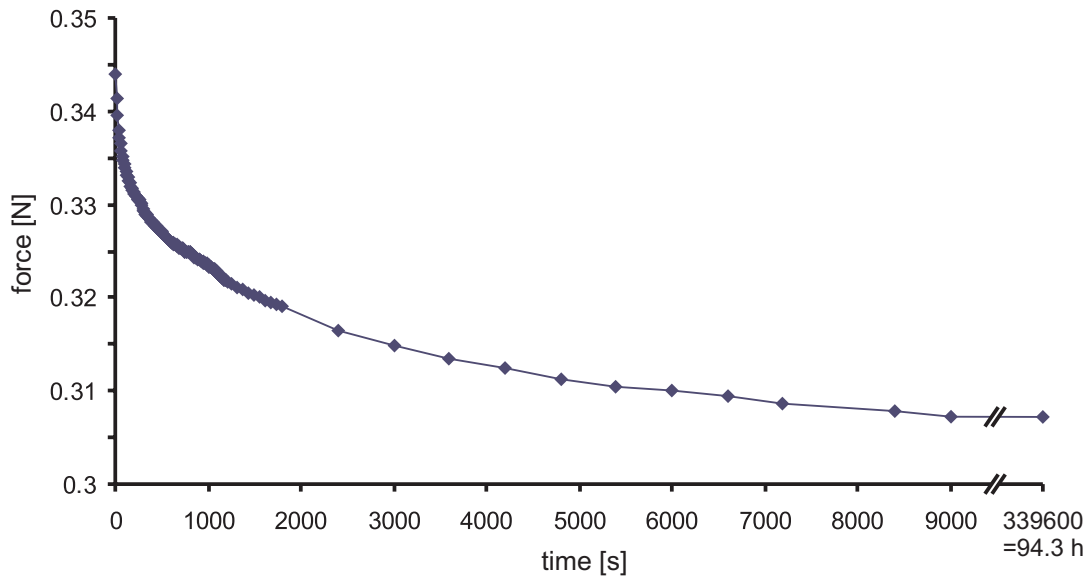


Figure 39: *Hysteresis effect of feather keratin - The time-dependent force decrease was measured at one 4th primary of the barn owl with a given deflection of 4 mm.*

In total seven 4th primaries of the two species were investigated and the Young's modulus of their feather keratin was calculated. The Student's t-test revealed a statistical signifi-

cant difference between the Young’s moduli of keratin from barn owls and pigeons (barn owl 6.49 GPa +/- 0.23 (mean +/- SD), N = 7; pigeon 7.80 GPa +/- 0.75 (mean +/- SD), N = 7; $t = 4.4321$; $p = 0.0008$; $df = 12$) (Fig. 40, Table 6).

Two feathers of the two species were further investigated in nanoindentation experiments. Rachis parts that lay proximal and distal to the bending test samples were investigated and the relevant reduced Young’s moduli (E_r) were calculated (Table 6). By assuming a Poisson’s ratio of 0.4 [27], the Young’s moduli (E) of the specimens were determined. Figure 40 shows the results of the bending and nanoindentation tests. Although the results of the bending test fitted well to those of the nanoindentation tests, the E values of the nanoindentation test depended on the position along the rachis measured. The following opposing trends were observed for the two species. In barn owls the Young’s modulus tended to decrease towards the distal rachis. In feather specimen I the E -modulus decreased from 6.81 GPa (basal) to 6.39 GPa (apical), while it decreased from 7.19 GPa (basal) to 6.62 GPa (apical) in feather specimen II (Fig. 40). In contrast, values of the E -modulus of the pigeon’s keratin showed a tendency for an increase in stiffness towards the feather’s tip. Here, the Young’s modulus increased from 7.12 GPa to 7.77 GPa in feather specimen III, while it increased from 6.90 GPa (basal) to 7.31 GPa (apical) in feather specimen IV (Fig. 40).

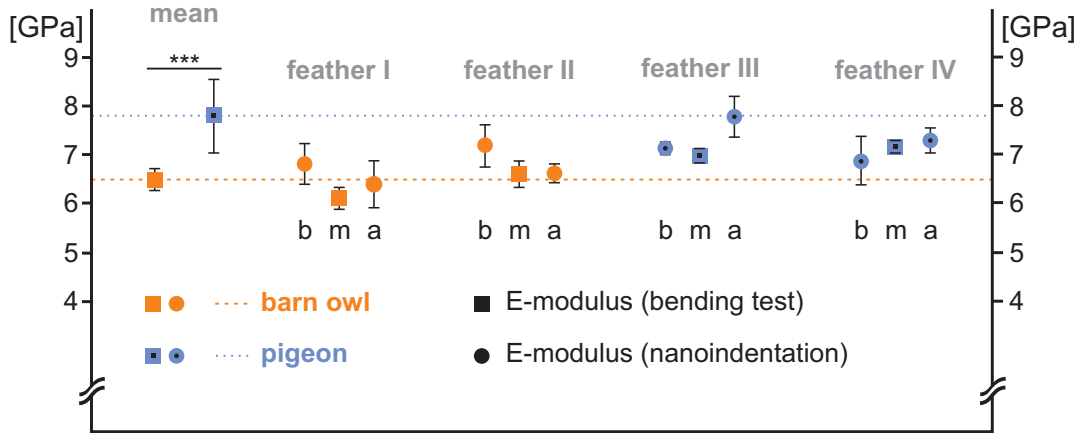


Figure 40: Young’s modulus of feather keratin of barn owls and pigeons measured with two-point bending tests and nanoindentation. Mean data of the bending tests on the left contains the results of 7 feathers each ($N=7$). The values are statistically significantly different (Student’s t -test, $p = 0.0008$). Material properties of four individual feathers are depicted on the right (\mathbf{b} = basal, \mathbf{m} = medial, \mathbf{a} = apical). The error bars of the individual specimens, feather I-IV, correspond to the accuracy of the particular measurements.

Table 6: *Young's modulus of feather keratin from barn owls and pigeons, measured with two independent methods (two-point bending tests and nanoindentation). Mean values of the bending tests arise from 8 repeated bending experiments. Mean values of the nanoindentation arise from 20 separate indents per specimen. Basal and apical refer to the sampling area of the nanoindentation specimens.*

two-point bending

<i>barn owl</i>	E-modulus [GPa] SD		<i>pigeon</i>	E-modulus [GPa] SD	
feather specimen 1	6.75	0.04	feather specimen 1	8.15	0.09
feather specimen 2	6.69	0.03	feather specimen 2	7.21	0.08
feather specimen 3	6.54	0.03	feather specimen 3	8.59	0.06
feather specimen 4	6.36	0.05	feather specimen 4	8.70	0.07
feather specimen 5	6.32	0.09	feather specimen 5	7.98	0.07
feather specimen I	6.11	0.22	feather specimen III	6.96	0.14
feather specimen II	6.63	0.28	feather specimen IV	7.17	0.13
mean 6.49 +/- 0.23			mean 7.80 +/- 0.75		

nanoindentation

<i>barn owl</i>	reduced E-modulus [GPa] SD		<i>pigeon</i>	reduced E-modulus [GPa] SD	
feather specimen I basal	8.06	0.50	feather specimen III basal	8.42	0.18
feather specimen I apical	7.56	0.57	feather specimen III apical	9.18	0.49
feather specimen II basal	8.50	0.52	feather specimen IV basal	8.15	0.58
feather specimen II apical	7.83	0.24	feather specimen IV apical	8.64	0.30
mean 7.99 +/- 0.40			mean 8.40 +/- 0.24		

<i>barn owl</i>	E-modulus ($\nu = 0.4$) [GPa] SD		<i>pigeon</i>	E-modulus ($\nu = 0.4$) [GPa] SD	
feather specimen I basal	6.81	0.42	feather specimen III basal	7.12	0.15
feather specimen I apical	6.39	0.49	feather specimen III apical	7.77	0.42
feather specimen II basal	7.19	0.45	feather specimen IV basal	6.90	0.50
feather specimen II apical	6.62	0.21	feather specimen IV apical	7.31	0.26
mean 6.76 +/- 0.34			mean 7.11 +/- 0.21		

4.3.2 Geometry of the rachis of barn owls' and pigeons' 4th primaries

The bending behaviour of the rachis is not only affected by the material property but also by the geometry. Both feather shafts of the species investigated had some geometrical features in common, but differed in some anatomical aspects as well. Figure 41 depicts two representative 4th primaries of the barn owl and the pigeon. Each feather shaft can be divided into the calamus and the rachis. Inserted into the bird's skin, the calamus of the feathers was a hollow and round, respectively elliptic structure. The inner sidewalls of the calamus next to the vanes were covered by a foam-like structure, termed the *substantia fibrosa*. The *substantia fibrosa* consisted of air-filled compartments of varying size. The cortex (outer region) of the rachis had a more or less rectangular shape. The hollow cortex was filled with a foam-like structure as well, termed the *substantia medullaris*, which was a similar structure as the *substantia fibrosa*. Dorsal and ventral parts of the cortex were thicker compared to the sidewalls where the vanes emerged (Fig. 41). In barn owls, the

dorsal cortex had a mean thickness of 161 μm (+/- SD of 44), the ventral cortex of 193 μm (+/- SD of 68) and the sidewalls of 45 μm (+/- SD of 10). In pigeons, similar results were obtained with the dorsal cortex being 141 μm (+/- SD of 35), the ventral cortex being 151 μm (+/- SD of 54) and the sidewalls being 34 μm (+/- SD of 6) thick.

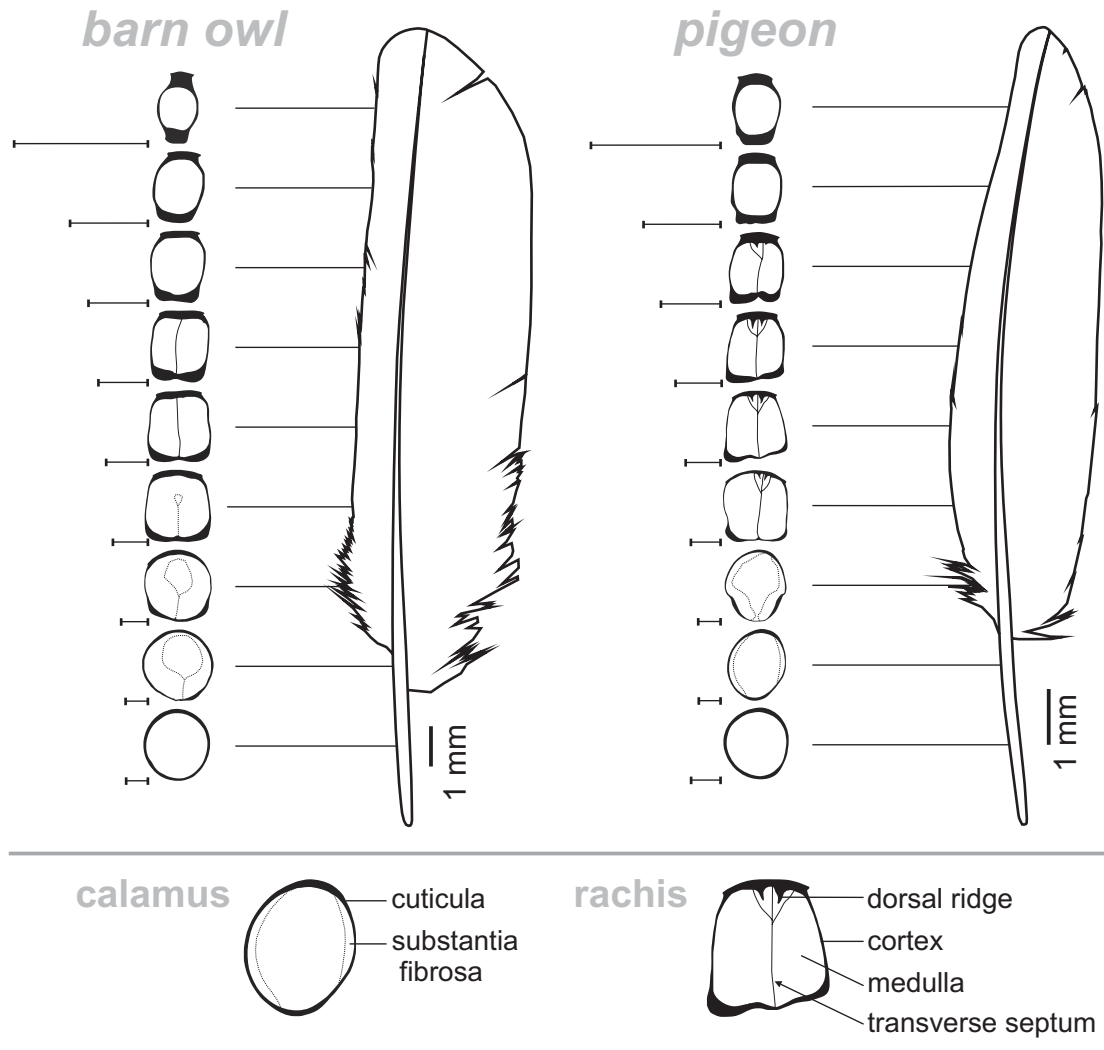


Figure 41: *General cross-sectional shape of the shaft of a 4th primary of the barn owl (left) and the pigeon (right). The feathers are normalised by their length for better comparison. Elements of the shaft are named at exemplary cross-sections (bottom). Scale bars represent 1 mm each.*

Although the pigeon's 4th primary was shorter in length than the barn owl's 4th primary (pigeon's 4th primary: 142 mm; barn owl's 4th primary: 198 mm), their calami were equally sized (calamus of pigeon's 4th primary: 33 mm; calamus of barn owl's 4th primary: 33.5 mm)

(Fig. 41). However, the calami of the two species differed in their cortex shape. Cross-sections of the pigeon's calami had an elliptic shape, while cross-sections of the barn owl's calami were almost round (Fig. 41).

Changes in the cross-sectional area and in the second moment of area along the whole rachis length were measured for one 4th primary of the barn owl and the pigeon. The cross-sectional shape of the cortex differed between the two species in some detail. In the barn owl, the cortex was smooth on the inner as well as on the outer contour (Fig. 41 top left). The only exception was a small spine or ridge observed at the inner ventral side between 30% and 50% of the rachis length. A membranous structure, termed the transversal septum, emerged from this spine. The transversal septum spanned between the dorsal and ventral side of the cortex and ended within the medulla or at the smooth inner cortex respectively (Fig. 41).

A similar spine was found at the ventral cortex of the pigeon's feather that also supported a transversal septum. However, the transversal septum of the pigeon's remex had a richer structural appearance with several branches. It emerged at the ventral spine and ended between dorsal spines at the inner dorsal cortex. These dorsal spines formed two longitudinal ridges on the inner dorsal cortex between 40-70% (Fig. 41 top right). The ridges run along the inner cortex and faded out towards the feather's tip. Such ridges were totally absent in all barn owl feathers investigated.

Figures 42C and D show changes of the cross-sectional area of the two feathers every 10% of their length. Between 20% and 90% of length, the cross-sectional area of the pigeon's feather decreased almost linearly ($a_p = -0.0085x + 1.1433$) from 0.9 to 0.06 mm² (Fig. 42A, Table 7).

Cross-sectional areas of the barn owl's remex were larger than those of the pigeon's remex regarding the position within the feather in mm. The values decreased almost linearly ($a_{bo} = -0.008x + 1.3984$), but somewhat slower than values of the cross-sectional area, especially at the feather's tip. In relation to the normalised length of the feather, the area size differed between the two species only in the proximal half of the feather's length. Here, the barn owl feather had always larger cross-sectional areas than pigeon feathers. In the distal half of the feather, the cross-sectional areas were almost of equal size in the normalised view (Fig. 42C, Table 7).

A similar relation as shown for the cross-sectional area was found for the second moment of area (I). This value was always higher in the barn owl, regarding the length of the feather in mm (Fig. 42B). In the two species I decreased almost linearly (1.2256 to 0.4804 mm⁴ in the barn owl; 1.2238 to 0.5447 mm⁴ in the pigeon) in the proximal half of the feather, while it showed and asymptotic behaviour in the lateral half.

As for the cross-sectional area, the values of I of the feathers of the two species were almost alike to each other by plotting them against the percental length of the feather. Only at 40-50% the values differed little (Fig. 42D).

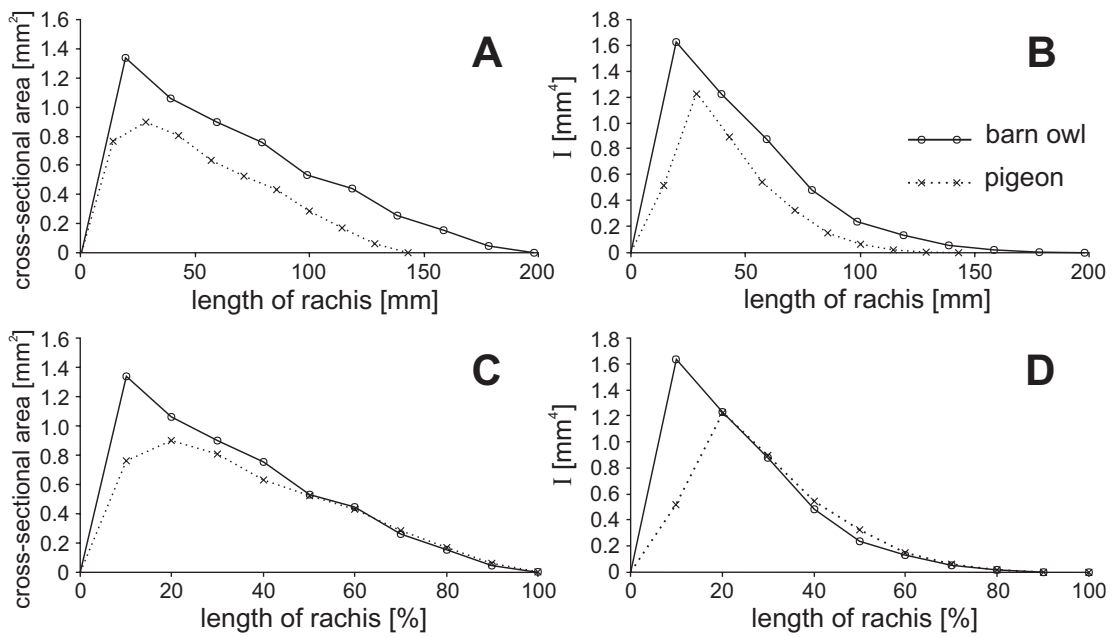


Figure 42: Changes of cross-sectional area (*A + C*) and second moment of area (*B + D*) of a 4th primary of a barn owl and a pigeon against the length of rachis in mm in *A* and *B* and in a normalised depiction in *C* and *D*.

Finally, table 7 summarises the values of the second moment of area (I) and the measured forces (F) of those specimens that were used in the bending tests. The second moment of area decreased towards the tip in all rachis parts investigated. The relevant forces, which were measured in the bending tests, are shown on the left. Remember that feather specimens 1-5 of the two species were displaced 4 mm and feather specimens I-IV were displaced 1 mm.

Table 7: *Presents the measured force (F) exerted on the balance (at 4 mm displacement for feather specimens 1-5 of each species and at 1 mm displacement for feather specimens I-IV) and the second moment of area (I) of the four supporting points of the relevant 4th primaries of barn owls and pigeons*

<i>barn owl</i>	F [mN]	I_0 [mm ⁴]	I_{10} [mm ⁴]	I_{20} [mm ⁴]	I_{30} [mm ⁴]
feather specimen 1	354.3 +/- 2.1	0.1466	0.1183	0.0735	0.0419
feather specimen 2	366.5 +/- 1.7	0.1628	0.1177	0.0774	0.0475
feather specimen 3	313.9 +/- 1.7	0.1487	0.1100	0.0554	0.0316
feather specimen 4	278.6 +/- 2.3	0.1282	0.1011	0.0541	0.0242
feather specimen 5	235.0 +/- 3.6	0.0995	0.0928	0.0437	0.0237
feather specimen I	391.0 +/- 7.1	0.2153	0.0142	0.0878	0.0620
feather specimen II	588.0 +/- 6.2	0.2639	0.1932	0.1276	0.0770

<i>pigeon</i>	F [mN]	I_0 [mm ⁴]	I_{10} [mm ⁴]	I_{20} [mm ⁴]	I_{30} [mm ⁴]
feather specimen 1	152.0 +/- 1.7	0.0748	0.0420	0.0168	0.0049
feather specimen 2	126.4 +/- 1.5	0.0670	0.0400	0.0161	0.0040
feather specimen 3	125.3 +/- 0.9	0.0650	0.0322	0.0129	0.0037
feather specimen 4	165.8 +/- 1.3	0.0796	0.0406	0.0186	0.0067
feather specimen 5	134.1 +/- 1.2	0.0644	0.0375	0.0154	0.0033
feather specimen III	528.3 +/- 5.2	0.3153	0.1721	0.0891	0.0360
feather specimen IV	399.8 +/- 4.3	0.2334	0.1487	0.0875	0.0384

Note that in the two-point bending tests, each rachis was deflected and the transmitted forces were measured (Table 7). Since attention was focused on rachis parts that are only curved in dorso-ventral direction, the specimens were not taken from exactly the same location. Thus, different forces were measured due to a different distribution of the second moment of area for each specimen (Table 7). Therefore, the values of I and F are only meaningful when evaluated in combination.

4.4 Discussion

Young's moduli of feather keratin from 4th primaries of barn owls (*Tyto alba pratincola*) and pigeons (*Columba livia*) were determined in two-point bending tests and nanoindentation tests. Young's moduli of barn owls' and pigeons' feather keratin obtained in the two-point bending tests are statistically significantly different. The control data of the nanoindentation tests confirm the measurements of the two-point bending tests. In the following, I shall first review the methods used, and then discuss the data on the Young's modulus of rachis keratin and the geometry of feather shafts.

4.4.1 A critical view on the methods used

The Young's modulus of feather keratin of barn owls and pigeons was investigated with two individual methods that provided similar results. However, the results are only good approximations to the real values, because assumptions had to be made in both cases that will be critically discussed in the following.

The two-point bending test is a well established method to determine mechanical and material properties. Normally, a solid beam with a constant cross-section is formed out of the material and further analysed with machine-aided setups. However, biological structures look different. Feather rachises for instance have a solid 'hollow' cortex that is filled with a foam-like structure (medulla). Purslow et al. [73] measured the mechanical influence of the medulla. They performed bending tests and used rachises with and without the medulla. Purslow et al. removed the medullary foam manually. Test specimens of 5 cm length were taken and measured in lateral and dorso-ventral deflection. The loss of the medulla resulted in a loss of dorso-ventral stiffness of 16.1% and a loss of lateral stiffness of 7.8%. However, it remained unclear to what extent the removal of the foam-like structure damaged the cortices of the rachises investigated. As shown above, pigeon rachises developed dorsal ridges and a well pronounced transversal septum that influence the dorso-ventral stiffness. These devices might have been damaged by the removal of the medulla in the studies of Purslow et al. [73]. In my study the medulla was not taken into account, since it was suggested that this structure does not affect the bending behaviour at low deflections of 1-4 mm. Furthermore, the removal of the medulla could cause uncontrolled damages of the inner cortex that might have a greater impact on the bending behaviour than the medulla itself.

A second source of error might be the varying profiles of feather rachises and the tube-like construction of the rachises. Changes of the second moment of area were approximated by a polynomial of second order in the calculations. Although the fitting curves had a mean coefficient of determination of $R^2 = 0.992 \pm 0.016$, the error propagation started here, because a second fit for the term $(x - l)/(ax^2 + bx + c)$ was made for better integration. Here, the mean coefficient of determination was $R^2 = 0.9998 \pm 0.0005$.

Nanoindentation is a well-suited method to investigate material properties of microstructured materials. The tip of the Berkovich indenter used had a tip diameter of 150 nm. Hence a precise specimen preparation is indispensable, since little surface asperities result

in different contact points. Best results for a smooth surface were gained by cutting the surface with a glass knife and an automated semi-thin slicer. However, each surface was slightly structured. The larger error bars of the (reduced) Young's modulus measured in nanoindentation tests might be a result of this surface structure, because the load-displacement curve varies in dependence of the contact point of the indenter tip. More precisely, higher initial forces are measured when the tip gets contact on top of a buckle, respectively low initial forces are measured when the tip indents between two buckles.

Furthermore, the Poisson's ratio is needed to calculate the Young's modulus. Since the exact value of feather keratin is unknown, it was suggested by applying the Poisson's ratio of a different keratin composition - bovine claws [27]. Thus, the Young's moduli are still approximations to the real values.

4.4.2 Young's modulus of feather keratin and the geometry of the feather shaft

In a global view, keratin of barn owls' feathers is more elastic (≈ 6.6 GPa) than that of pigeon's feathers (≈ 7.5 GPa). However, longitudinal variations along the rachis were found in nanoindentation tests. In pigeons, the Young's modulus increased towards the feather's tip. These results are in agreement with observations of Macload [54] on contour feathers of various bird species and with results of Bonser et al. [14], which measured the Young's modulus along the rachis of a mute swan's (*Cygnus olor*) primary feather. In both studies, an increase in stiffness towards the feather's tip was measured. In contrast, the data presented here suggest that longitudinal variations in the Young's modulus are different in barn owls. In this species, the Young's modulus decreased towards the feather's tip resulting in higher elasticity in distal rachis parts.

It is discussed whether the differences in flexural stiffness among flight feathers are more likely to be due to changes in geometry [73] or to changes in the material of the shaft [82]. The authors of the latter study already claimed that the geometry of the shaft has a larger influence on the feather's bending behaviour than the material property. The results of my study suggest that both the geometry and the material properties are responsible for the bending behaviour as outlined in the following.

The geometry of the rachises differed between the two bird species investigated. The cortex of the barn owl's rachises was regular shaped and the transversal septum was little pronounced, while the cortex of the pigeon's rachises comprised small ridges on the inner dorsal side. Additionally, the transversal septum was distinctly developed in pigeon feathers and showed several branches. These differences in geometry result in different bending behaviour under load and might be the result of the different requirements of the flight apparatus of the two bird species.

Barn owls fly slowly over vegetation while searching for prey [56, 87]. The slow flight is enabled by a large wing area due to large feathers [4], which in turn results in low wing loading (see Chapter 2). Consequently, mechanical loadings in dorso-ventral as well as lateral direction are low as well. However, high lift is not always an advantage. During hunting, barn owls perform flight manoeuvres by acceleration and deceleration with tight turning radii [17, 56, 62, 87]. In these situations the lift produced by the wings has to be controlled

dynamically. If the forces acting on the feathers exceed a critical value, the angle of attack would change rapidly by the torsion of the feathers [81], thereby changing the profile of the wing and thus the lift. Such behaviour can be seen in landing owls. This bending-torsion effect can be actively initiated, whereas the actual torsion is a passive movement of the feather shaft [20, 59, 81]. The bending-torsion linkage is mainly provided by the geometry, more precisely by the cross-sectional shape of the shaft. As mentioned before, dorsal and ventral parts of the rachis' cortex are thickened in relation to the sidewalls, and the transversal septum that spans between the dorsal and ventral cortex is only little pronounced in barn owls. These facts lead to a beam structure, which is easy to bend and twist.

Pigeons are fast and persistent flying birds [1, 71]. Their wing area is much smaller than that of barn owls (see Chapter 2), e.g. due to smaller and narrower feathers [4]. Since pigeons have the same body weight as barn owls, their wing loading is much higher. Therefore, pigeons have to beat their wings with high frequencies in order to become airborne [9, 10, 88], which in turn results in high forces acting on the feathers. Consequently, higher dorso-ventral as well as lateral forces are expected in pigeons than in barn owls. Pigeon feathers are medium sized and narrow with a stiff appearance. The dorsal and ventral sidewalls of the shaft are thickened as it was found in barn owls. In contrast to barn owls, cortex profiles of pigeons' feathers are structured. Small ridges run along the dorsal and ventral inner cortex. Additionally, the transversal septum is well pronounced and shows several branches. Such devices stiffen the feathers in dorso-ventral and rotatory directions, but do not strongly influence lateral movements. Bending stiffness in lateral direction seems to be controlled by the increased anterior ventral cortex. Such thickening might act on the lateral bending behaviour, since this structure is located near the leading edge of the feather and thus has to withstand high aerodynamic forces induced by the drag of the fast air flow.

This study shows differences of the Young's modulus and the geometry of barn owls' and pigeons' primary feathers. Therefore, the data presented here is in line with the statement of Bonser et al. [14], who claimed that adaptations in flexural stiffness are due to two parameters, the material property (E) and the geometry of the shaft (I).

In summary, barn owls' feather shafts have profiles that are easier to bend in lateral and dorso-ventral direction than pigeons' feather shafts. The thicker dorsal and ventral sidewalls contribute mainly to this behaviour. Apart from the different thickness of the sidewalls, both bird species differ in the appearance of structures that inhibit torsional movements of the shaft, such as ridges or the transversal septum. These structures are only little pronounced in barn owls' rachises. In contrast, pigeons' rachises comprise several cortical ridges and a well pronounced transversal septum. The Young's modulus of barn owls' feather keratin is lower than that of pigeons' feather keratin. Furthermore, variations in the elastic modulus along the rachis length differ between the two species. In barn owls, the Young's modulus tends to decrease from the feather's base towards the tip, while it increases towards the feather's tip in pigeons. These facts lead to differently flexible feathers that seem to be perfectly adapted to the relevant birds' flight styles. The high flexibility of the barn owls' feathers could also contribute to the noise damping during flight, since the vanes and the specialised structures are easier to deflect by the air flow and thus can follow occurring turbulence.

4.5 Conclusions

Two independent methodological approaches were used to determine the Young's modulus of feather keratin of barn owls' and pigeons' primary feathers. The Young's modulus was lower in barn owl than in pigeon feathers. However, it was argued here that this finding alone is not sufficient to explain the different bending behaviour of the feathers. The influence of the geometry has an additional impact. Nonetheless, the measured values of the material properties can now be used to manufacture artificial applications for wing models used in wind tunnel experiment. The utilisation of materials with similar properties might help to understand aerodynamic effects used by birds.

5 General Discussion

In this thesis I have characterised wings and feathers of barn owls (*Tyto alba*) and pigeons (*Columba livia*) with anatomical, morphometrical and biomechanical methods. One goal of this work was to provide aerodynamic parameters characterising the silent flight of barn owls compared with the noisy flight of pigeons. The understanding of the mechanisms underlying silent flight could help to reduce noise produced by airplanes and wind farms.

Interestingly, it does not matter which text book on ornithology one considers, the content with respect to owl flight is mainly the same: “Owls fly silently due to their feather specialisations.” No further explanations are given. Until now only few publications deal with the investigation of the owl’s flight [17, 31, 36, 39, 51, 56, 62, 87]. Nevertheless, what is surprisingly lacking from the existing literature is a comprehensive characterisation of the flight apparatus of owls that provide possible explanations of the mechanisms underlying silent flight. In my thesis I provide quantitative data of one biological role model for studying silent flight, the barn owl (*Tyto alba*). For comparison most of the experiments were also performed with a bird species having a comparable body weight, the pigeon (*Columba livia*). The results are generally discussed in the following with respect to five selected topics: wings, feathers, material properties, hunting strategy and ecological niche.

5.1 Wings

I have investigated wings of barn owls and pigeons two- and three-dimensionally with non-invasive modern imaging techniques. The great variety of methods (photogrammetry, laser-scanning, computed tomography, digital photography) used allowed the investigation of aerodynamic relevant parameters with high spatial resolution. Artifacts due to drying or the severance of muscles and tendons were avoided by taking recently dead birds. Furthermore, the wings remained attached to the bird’s body. In my study only camber measurements could be prone to errors, since the muscles were relaxed and did not actively influence the wing geometry any longer. Wing planform, area size and the thickness distribution of the wings investigated are not affected by the death of the bird. The wing planform was manually determined and the thickness distribution is formed by the appearance of bones, the amount of muscle mass and the arrangement of the feathers. The death of the bird will not change these values.

Two-dimensional parameters of the wings of barn owls and pigeons provide distinctive differences. Wings of barn owls are 2.5 times larger in area size than pigeons’ wings. Since the two bird species have a similar body weight (approximately 500 g), the resulting wing loading ((body weight x gravitational force) / body weight) is much lower in barn owls as well (barn owl: 33.0 N/m²; pigeon: 96.8 N/m²). The larger wing size of barn owls is a result of larger feathers [4], since barn owls and pigeons have the same number of remiges (= 24). In general, lower wing loadings are associated with lower flight speeds, improved manoeuvrability, improved gliding performance and reduced agility [8, 39, 80]. Indeed, barn owls fly slowly searching for prey. Their flight style alternates between flapping flight with low amplitude and frequency and gliding phases. By contrast, higher wing loadings reflect

higher flight speeds, higher agility, but only a moderate glide performance [8, 74]. Birds with high wing loadings, such as pigeons, have to beat their wings at higher frequencies in order to become airborne [9]. Furthermore, a high velocity is needed to perform a stable gliding flight in these birds [71].

The aspect ratio is a measure of the wing shape. It is defined as (wing span)² divided by the wing area, respectively as the mean wing span divided by the mean wing chord. A low aspect ratio, as it is found in barn owls (*Tyto alba pratincola*: AR = 6.89 +/- 0.18), facilitate take-off and flight in wooded and cluttered environments. Pigeons have higher aspect ratios (*Columba livia*: AR = 8.27 +/- 0.06). Such values are linked to greater aerodynamic efficiency and are more related to flapping than gliding flight [8, 74].

Two-dimensional parameters, such as wing area, wing span and aspect ratio, alone are not sufficient to describe a wing and its aerodynamic performance. Parameters such as camber and thickness distribution have to be regarded as well. The three-dimensional investigation leads to a division of the bird's wing into a proximal (from shoulder joint to wrist) and a distal wing (from wrist to wing tip). The proximal wing of barn owls is highly cambered and anteriorly thickened. The posterior part of the proximal wing is formed by a single layer of remiges, and thus it is extremely thin. In wind tunnel experiments highly cambered, anteriorly thickened wing profiles show a quite large separation bubble on the suction side that increases with increasing angle of attack [41]. Nevertheless, these profiles are known to produce much lift even at low velocities [80]. By an adaptation of the surface and the edges of the wing, the air flow can be stabilised [41, 86]. Such devices are found at owl's feathers [31] and are discussed in the next subdivision (5.2). The barn owls' distal wing resembles a slightly cambered plate. It is built up of remiges and greater primary coverts. Only a very small part of the leading edge is formed by bony structures, associated ligaments and skin. Consequently, the distal wing is very thin and shows less curvature than the proximal wing. The aerodynamic performance of the distal wing of birds is still not well understood. Neuhaus et al. [62] provided some data of distal wings of tawny owls (*Strix aluco*) and mallard ducks (*Anas platyrhynchos*) investigated in wind tunnel experiments. Smoke was used to visualise the air flow conditions around the wings. While the air flow separated early in the wing of the mallard duck, it stayed attached to the wing of the tawny owl. The leading edge of the distal wing of the tawny owl is equipped with serrations similar to that of barn owls. After amputation of the serrations the air flow resembled that found in mallard ducks. Hence, the air flow is influenced by the serrations in such a way that it is forced to stay attached around the distal wing and thereby producing a high amount of lift [80].

Pigeon's wings are smaller than barn owl wings. The wing shape differs from that of barn owls as well. [12, 61, 71]. Profiles of the proximal wing are thicker than the corresponding profiles of barn owls, which is a result of the smaller remiges [4] and the larger areas covered by covert feathers. The distal wing tapers towards the tip. Consequently, the lift producing area becomes smaller towards the wing tip [80]. As a result of the high wing loading and the high aspect ratio, pigeons have to beat their wings with high amplitudes and frequencies [88, 93]. The clap-and-fling mechanisms, which is known from insects to produce additional lift [57], has also been reported in this bird [60]. The presented data on

the wing configuration is consistent with the reported flight style of pigeons [9, 71, 88, 93], since the proximal wing produces a high amount of lift by its camber and thickness distribution [80] and the distal, tapered wing reduces drag as well as the inertia of the wing tip [81]. The high amount of active wing beating during flight correlates with a high amount of muscle mass and the appearance of the supporting skeleton elements. Ulna and radius support muscles that are responsible for movements within the wing. In pigeons the flight muscle mass represents approximately 30% of the body weight [17]. By contrast, in barn owls the muscle mass used for flight is less pronounced and represents only 10% of the body weight [17]. Here, ulna and radius are lesser bowed and relatively thinner than pigeons, which is a further indication of different flight styles of the two bird species investigated.

In conclusion, barn owl's wings are well suitable for a slow flight. Since, the air flow tends to separate in critical flight manoeuvres, specialisations of the plumage that compensate negative effects of the barn owl wing come into play.

5.2 Feathers

Flight feathers of barn owls exhibit specialisations on the surface and edges. The outer vane of the 10th primary remex carries serrations. Edges of the inner vanes of all feathers are fringed, and the dorsal surface has a velvet-like texture. These specialisations have already been described by Graham in 1934 [31]. Although some authors provided descriptions or even morphometric characterisations [4, 31, 51, 62], only a three-dimensional investigation of the specialisations reveals some possible functional aspects of these structures. I have established a method to digitise these tiny structures at high spatial resolution using confocal laser scanning microscopy. The reconstruction of 3D models enabled the comparison between structures of different feathers and feather parts.

Pigeon's feathers do not have any obvious surface or edge modification apart from a grooved texture [4]. The upper and lower surface is grooved due to the parallel aligned barb shafts. The edges are sharp and unstructured. Feathers of pigeons are small and narrow compared to barn owls' feathers [4]. Since pigeons lack specialisations similar to that found in barn owls, the following discussion refer only to the barn owl's plumage specifics.

5.2.1 Serrations

Functionally, serrations at the leading edge might act as a turbulence generator [2, 35, 62, 85]. As mentioned before, the distal wing of barn owls resembles a slightly cambered plate. Wind tunnel experiments showed that the airflow tends to separate at such devices [62]. Turbulence generators at the leading edge, such as the serrations, might enrich the boundary layer energetically leading to a stable air flow around the distal wing [2, 62, 86]. Beyond influencing the boundary layer, serrations were found to be effective in the reduction of noise. Arndt and Nagel [2] showed that serrations affect the acoustic characteristics. Large vortices that shed from the investigated airfoil dissipated faster after the model was equipped with serrations. Consequently, the wing model was quieter. In barn owls, the

curvature of the serrations seems to be constant throughout the outer vane. However, length and tip shape differs. While long serrations with sharp tips were found at the basal vane, serrations of distal vane parts were shorter and had a rounded tip. On the one hand, distal serrations may be differently shaped, since the angle of attack and the velocity change constantly during flight, especially during flapping flight. Furthermore, the distal chord is shorter. Thus, the air flow needs to be differently influenced. On the other hand, shorter serrations with a round tip within the vane might be due to wear effects caused by UV-exposure, material abrasion and fatigue. These factors could shorten the serrations as time passes.

5.2.2 Velvet-like dorsal texture

During flight, feathers rub against each other caused either by the beating of the wings or by unstable flow conditions and thus passive deflections of the feathers [9, 20, 71]. The parallel orientation of the barbs forms a grooved structure that produces a well noticeable sound by rubbing. In pigeons this noise is discussed to warn other members of the flock in situations of danger and escape [81]. Such friction noise would disturb the barn owl during hunting, because the owl would mask noise emitted by prey and would scare its prey away before being successful in striking. In barn owls, barb shafts of imbricate feathers do not contact each other. Elongations of the hook radiates, the pennula, form a velvet-like dorsal structure. The three-dimensional reconstruction revealed a surface texture of bent pennula that enables a smooth gliding of the barb shafts. The porosity of the velvet-like dorsal structure is increased in areas that are covered by other feather (remiges and coverts). I claim that this structure reduces or inhibits friction noise between superjacent feathers. Furthermore, noise is dampened at the point of production by the porosity of the structure. Porous surfaces are well known to reduce friction noise, for instance foams are well suitable to control noise radiation and damping noise [29].

The velvet-like surface was also found in areas that are subjected to the flow field. Here, a different mechanism might act. Klän et al. [41] measured the air flow over an owl-based airfoil in wind tunnel experiments. The air flow tended to separate at low velocities and high angles of attack. This phenomenon was compensated by applying velvet to the suction side of the wing model. The separation bubble on the dorsal side was decreased in size and slightly pushed towards the leading edge of the wing. Hereby, the velvety surface stabilised the air flow at low velocities. I suggest that a similar effect can be expected for the barn owl, since the texture of the velvet used in the artificial model and the pennula of the real owl wing are comparable.

The two different functions of the pennula can also be seen in their shape. While pennula of uncovered areas had a brush-like shape with the pennula tips ending in the air flow, those pennula of covered areas were bent downwards at the surface. Furthermore, the porosity was higher in these areas as well resulting in a better noise suppression.

5.2.3 Fringes

Each feather is surrounded by a fringed structure formed by barb endings. The fringes are very fluffy and unstable in shape. Their function is not yet clear. In the following I will provide at least two possible functional explanations for this structure. On the one hand, fringes at the trailing edge of the wing decrease the intensity of noise. Turbulent boundary layers being convected past the trailing edge into the wake are known to generate an intense, broadband scattering noise [35]. Herr et al. [35] performed wind tunnel experiments with wing models that were equipped with varying fringes. The noise reduction potential of several design concepts was determined in this parametric study on brush-type trailing edge extensions. Depending on the configuration, Herr et al. could reduce noise up to 10 dB SPL. One explanation for the noise reduction is that the fringes support the convergence of the different air flows of the upper and lower boundary layer at the trailing edge.

However, fringes are also found at feather parts that do not form the trailing edge of the wing. A possible explanation for the existence of fringes at the whole inner vanes of remiges could be found in the orientation of distal barb parts of imbricate feathers. Barbs of inner vanes of adjacent feathers are more or less aligned in the fully extended wing, e.g. in gliding flight. Since the lower surface of the feather is not covered by any structure, the barb shafts form a deeply grooved structure comparable to that of pigeon's feathers [4]. I hypothesise that fringes merge into these grooves due to their size and orientation during flight. Moreover, fringes could be sucked into the grooves during flight due to a lower pressure on the upper wing surface [80] and due to the air transmissivity of the feathers [58]. Fringes could fuse adjacent feather vanes leading to a smooth lower wing surface without sharp and noisy edges. To test this hypothesis, more experiments, especially in wind tunnels, are necessary.

5.3 Material properties and geometry of the feather shafts

The Young's modulus is a measure of the elasticity of a material. Typical values are 0.01 GPa for rubber, 2-4 GPa for Nylon, 200 GPa for steel and 1220 GPa for diamonds. Hence, high values of the Young's modulus are associated with stiff materials and *vice versa*. The Young's modulus is used for instance to calculate the bending behaviour of a beam structure made of an isotropic elastic material under tensile and compressive loads.

I have determined the Young's modulus of feather keratin of barn owls' and pigeons' rachises (4th primaries) in two-point bending tests. Additionally, a different methodological approach, nanoindentation, was used to verify the results. Both methods provided similar results, albeit with small differences. Barn owl's feather keratin has a Young's modulus of 6.6 GPa. It is 12% weaker than pigeon's feather keratin with 7.5 GPa. However, differences in geometry of the shaft contribute to a different bending behaviour as well.

Pigeons are fast flying birds. Their feathers have to withstand high aerodynamic forces, since wing loading and drag is high [9, 22, 24, 73, 93]. Furthermore, pigeons have to beat their wings at high frequencies in order to become airborne [9, 24, 88]. Consequently, dorso-ventral as well as lateral forces acting on the feathers are high. The bending behaviour of

the feather is controlled by dorsal ridges and a well pronounced transversal septum that spans between the dorsal and ventral cortex. Such devices stiffen the feathers in dorso-ventral direction efficiently while being light and material-saving. Lateral movement is controlled by a thickened anterior ventral edge of the shaft. In addition to the shaft, the vanes contribute to the stiffness of a feather. Pigeons' barbs comprise more hooklets of the hook radiates than barn owls' barbs leading to a strongly connected and thus more rigid vane [4, 26]. Whether the Young's modulus of rachises and barbs differs has to be tested in further experiments even though the bending of barbs is somehow more difficult to measure. In summary, flight feathers of the pigeon are configured to form a wing that fits well to the high forces acting on the wing.

Feathers of barn owls are much larger than those of pigeons [4]. In normal cruise flight, low aerodynamic forces are expected for barn owls' flight feathers, since the wings of this bird are characterised by low wing loadings [39]. Moreover, the flight speed of owls is low as well [17, 56, 87]. As shown above, the construction of the barn owl's wing provides high lift that enables the owl to fly slowly searching for prey. However, high lift is not always an advantage for barn owls. In landing manoeuvres, especially when striking prey, owls need to decelerate quickly. In such situations, barn owls spread their wings and tails for maximum drag [81]. Beating of the wings is further used to control the landing [20]. In order to reduce the lift-producing area of the wing during the upstroke, the owl rotates its wing feathers to let the air flow between the feathers. This effect is actively initiated by a wrist-posture change and a rotation of the calami, whereas the torsion of the feather shafts is a passive movement ensured by the geometry of the shaft and its material property. Cortices of barn owls' feather shafts do not have internal ridges that control the bending. The transversal septum is only little developed and does not branch as the transversal septum of pigeons' remiges. Hence, dorso-ventral bending behaviour is less restricted compared to pigeon feathers [73]. The vanes of barn owls' feathers appear soft and pliant. Hook radiates comprise only a few hooklets. Furthermore, the number of radiates is lower in barn owls compared to pigeons [4]. Consequently, less components are involved in forming the vane and thus, lateral movement of the barn owl's feathers is also less restricted by the vanes. In summary, these attributes of barn owls' feathers result in a structure that is easy to bend and twist. Hereby, feathers protect themselves against failure by bending and deflecting forces in case the loading exceeds a critical value [20, 81].

5.4 Hunting strategy of barn owls

Barn owls are medium sized nocturnal birds of prey hunting for small mammals and birds, sometimes insects and frogs [56]. Since visual information is limited in twilight, barn owls have evolved a precise sound localisation system to detect and localise prey using acoustic information [32, 34, 42, 43, 44, 46, 94, 97]. While rustling through leaves or squeaking, mice emit noise which may be detected by the owl. Barn owls use at least two different hunting strategies depending on the environment, respectively the weather condition [56]. First, barn owls fly slowly in low height over vegetation searching for prey. The head is pointed downwards scanning the ground for noise emitted by prey [87]. The specialised wing and feather structures that are presented above enable the slow and silent flight. Flying

slowly improves the detection of prey, while the silent flight does not disturb the hearing system during localisation. Second, barn owls sit on a perch and observe the surrounding. This strategy is seen in more wooded environments, where free flight is restricted by the vegetation [56]. Perching is also chosen in bad weather conditions such as rain or snow. Such conditions are critical for barn owls, because the prey is also less active during rain. Furthermore rain complicates the flight by wetting the feathers. This effect is even enhanced by the filigree structures and the porosity of the plumage. Consequently, wings and feathers become heavier, the flight costs increase and coincidentally the noise suppressing devices lose their functions. Additionally, rain on the extended wings might produce an intense noise, which may irritate the owl.

Nevertheless, when prey is detected, barn owls dive quickly downwards striking the prey [56, 87]. Thereby, critical flight manoeuvres have to be performed by acceleration, deceleration and quick flight-direction changes. The flow stabilising devices and the high lift configuration of the wings enable these critical flight manoeuvres without failure. Furthermore, the bending behaviour of the feathers guarantees lift control. In case the forces acting on the wing exceed a critical value, the feathers bend and twist and thereby deflect the forces [20, 81]. Once the owl is on ground and the prey is subdued, the large wings prevent the owl from sinking into the vegetation, respectively they screen the prey from competing conspecifics [56]. In environments with poor vegetation, barn owls use their wings for shielding in order to hinder the prey from escape. The weaker material and the bending capabilities of the feathers prevent damage and failure of the plumage. In case the owl was successful in striking, the prey is transported to the nesting place of the owl [87]. The large wing area and the resulting low wing loading provide enough lift reserves for the transport.

5.5 Ecological niche

Barn owls have an almost global distribution [87]. The urbanisation and the increase in agriculture has led to an increase in food resources by the storage of grain and as a consequence thereof to an increase in rodent population. Furthermore, nesting places in barns and churches were incidentally created. Hence the population size of barn owls grew as well [56]. However, nowadays silos and gated buildings decreased the number of prey and nesting places. Consequently, the populations of predators such as the barn owl are also decreasing, although alternative nesting boxes are being created.

Barn owls are highly adapted and specialised to hunt for small mammals in open habitat and low light conditions [44, 56, 87]. The presented data on wing and feather specialisations represents only a few adaptations of barn owls for occupying such ecological niche. A slow and noiseless flight and the co-evolved precise sound localisation system are the basic requirements to detect prey by hearing in low light conditions. Although other predators such as kestrels, buzzards, cats and weasels prey for small mammals, none of these hunt in the same way as barn owls.

In Central Europe 50-80% of the barn owls' prey are voles and mice [56]. These mammals are active during twilight. In times of large vole populations, different owl species inhabit the same ecological niche and do not mind the interspecific competition [56]. However, in

times of low prey populations, the survival of each individual is influenced by the ability to change diet. Thereby, the activity patterns of barn owls, respectively owls in general, change in dependence on the prey. Nevertheless, owls will catch prey that fits to their relevant weight class. In each case owls have to balance between prospect of success, risk of injury, transport and hunting costs. Large owls such as the eagle owl (*Bubo bubo*) are able to conquer different habitats and to hunt for larger prey than the smallest owl, the Eurasian pygmy owl (*Glaucidium passerinum*). Interestingly, the body weight of owls has a larger influence on the biotope than on prey choice [56]. Mainly all European owls prey for small rodents, however smaller owls are able to hunt in vegetation whereas larger owls are restricted to open habitats.

5.6 Conclusions

Wings and feathers of barn owls and pigeons were characterised by anatomical, morphometrical and biomechanical parameters. Specialisations that might lead to a silent flight of the barn owl were presented and discussed. Although the mechanisms underlying noise reduction are not yet clarified, this thesis provides data that may now be used as a basis for the construction of a new three-dimensional wing models and applications, which allow even more veridical measurements of the flow around the barn owl wing than it was possible so far. Ideally, such a wing model comprises the wing planform with the specific profile characteristics, the flexibility of the real feathers and the surface and edge modifications similar to that of barn owls.

6 Summary

Wings and feathers of barn owls (*Tyto alba*) were investigated with anatomical, morphometrical and biomechanical methods in order to specify noise reduction and noise suppressing structures evolved by the owl. Pigeons (*Columba livia*) with a similar body weight were taken as a reference species.

Barn owls' wings are 2.5 times larger in area size than wings of pigeons, resulting in a much lower wing loading. Furthermore, barn owls' wings are characterised by a high camber and a high thickness in anterior proximal wing regions and by a low camber and a low thickness in distal and posterior proximal wing regions. Such a wing configuration enables the barn owl to fly slowly, which in turn might reduce flight noise.

Pigeons' wings are smaller, less cambered and show a different thickness distribution. Since their wings do not produce as much lift as wings of the barn owl, pigeons have to beat their wings at high frequencies in order to fly slowly, e.g. during take-off. In general, pigeons beat their wings more often than barn owls to produce more lift. The increased wing beat frequency is also reflected by the increased amount of muscle mass and the appearance of the supporting bones.

Barn owls' wings are equipped with several surface and edge modifications that are responsible for either flow control or noise suppression or both. A new three-dimensional measuring method was established in order to reconstruct and investigate the filigree structures with high spatial resolution.

Bending and shape of the serrations of the barn owl's 10th primary remex was found to be more or less constant throughout the vane. Only length and tip shape differences were found that might be due to wearing effects or different angles of attack of the wing tip during flapping flight. Functionally, serrations might act as turbulence generators. Each feather of the wing is covered with a velvet-like dorsal surface formed by elongations of the hook radiates, the pennula. The structure of the pennula differed between covered and uncovered feather areas. In covered areas, the porosity of the pennula-structure was high and the pennula formed a friction reductive surface. The surface that is subjected to the air flow was characterised by a brush-like shape. The pennula tips ended in the air flow. At the same time the porosity was lower. Such a structure in combination with the wing geometry of barn owls stabilises the air flow, especially at low flight speed. Finally, the edges of the inner vanes of all flight feathers were fringed. On the one hand, fringes might merge the different fast air flows of the upper and lower wing side at the trailing edge of the wing, on the other hand, they might fuse superjacent vanes by gliding between the grooves formed by the ventral barb shafts. Thereby, a smooth lower wing surface might be formed without sharp and thus noisy edges.

Biomechanical measurements with two independent methods (two-point bending tests and nanoindentation tests) were performed to determine the Young's modulus of barn owls' and pigeons' feather keratin. While barn owls' feather keratin has a Young's modulus of 6.6 GPa, the Young's modulus of pigeons' keratin is 7.5 GPa and thus by 12% higher. However, this difference could not explain the different bending behaviours of feathers of the two species. The geometry of the shafts had a large influence as well, which is expressed by several adaptations of the shaft's cortex.

The results of this thesis may now be used for follow-up analysis of the mechanisms underlying noise reduction in a more veridical way.

7 Zusammenfassung

Flügel und Federn von Schleiereulen (*Tyto alba*) wurden mit anatomischen, morphometrischen und biomechanischen Methoden untersucht um geräuschreduzierende und geräuschunterdrückende Strukturen, die von der Eule im Laufe der Evolution entwickelt wurden, zu bestimmen. Tauben (*Columba livia*) wurden als Referenz für diese Studie gewählt.

Schleiereulenflügel haben eine 2,5-mal größere Flügelfläche als Taubenflügel. Da Schleiereulen und Tauben in etwa gleich schwer sind, ist folglich die Flächenbelastung bei Schleiereulen deutlich geringer. Schleiereulenflügel zeichnen sich durch eine hohe Wölbung und eine deutliche Dicke in anterior-proximalen Flügelregionen und durch eine geringe Wölbung und geringe Dicke in distalen und posterior-proximalen Flügelregionen aus. Eine solche Flügelkonfiguration ermöglicht es der Schleiereule langsam zu fliegen, wodurch Fluggeräusche reduziert werden.

Taubenflügel sind kleiner, weniger gewölbt und zeigen eine andere Dickenverteilung. Sie erzeugen weniger Auftrieb als die Flügel der Schleiereule. Wenn Tauben in zu Eulen vergleichbaren Geschwindigkeitsbereichen fliegen, zum Beispiel beim Starten, so müssen sie mit deutlich erhöhter Frequenz mit ihren Flügeln schlagen. Um zusätzlichen Auftrieb zu erzeugen schlagen Tauben öfter mit ihren Flügeln als Schleiereulen. Diese erhöhte Flügelschlagfrequenz spiegelt sich auch in einem unterschiedlichen Muskelvolumen und in einem unterschiedlichen Knochenbau wieder.

Schleiereulenflügel weisen einige Oberflächen- und Kantenmodifikationen auf, die entweder für eine Strömungsbeeinflussung, eine Geräuschreduktion oder beides verantwortlich gemacht werden. Eine neue drei-dimensionale Messmethode, die die Konfokale Laserscanningmikroskopie nutzt, wurde etabliert, um diese filigranen Federstrukturen mit sehr hoher Auflösung zu rekonstruieren und zu untersuchen.

Die Außenfahne der zehnten Handschwungfeder der Schleiereule weist eine Hakenkammstruktur auf, die durch die Enden der Federrami gebildet werden. Es zeigte sich, dass entlang der Federfahne sowohl die Verbiegung als auch die Form mehr oder weniger konstant sind. Kleine Unterschiede in der Länge und der Spitzenform könnten auf verschiedene Anströmwinkel zurückgeführt werden, oder sie könnten die Resultate von Abnutzungserscheinungen sein. Funktionell wird die Hakenkammstruktur als Turbulenzgenerator angesehen. Die Oberfläche jeder Schleiereulenfeder ist samtig weich. Diese samtartige Struktur wird von Verlängerungen der Hakenstrahlen, den so genannten Pennula, gebildet. Interessanterweise unterscheidet sich die samtige Struktur zwischen bedeckten und nicht bedeckten Federflächen. In den Flächen die bedeckt sind ist die Porosität der Oberflächenstruktur erhöht und die Pennula bilden eine reibungsreduzierende Oberfläche. Dadurch werden auch Reibungsgeräusche zwischen den Federn verringert. Die Oberfläche, die dem Luftstrom ausgesetzt ist, ist durch eine bürstenartige Struktur charakterisiert. Die Spitzen der Pennula enden in der Luftströmung und die Porosität ist geringer, verglichen mit der inneren Fahne. Derartige Strukturen an Eulenflügelprofilen stabilisieren die Umströmung, besonders bei geringen Fluggeschwindigkeiten. Schlussendlich sind alle Federn von einem Fransensaum umrandet. Einerseits sorgen die Fransen an der Flügelhinterkante dafür, dass die verschieden schnellen Luftströmungen sanft ineinander geführt werden, andererseits könnten die Fransen übereinander liegende Federfahnen miteinander verbinden, indem die Fransen in die durch die Federrami gebildeten Furchen hineingleiten. Hierdurch könnte eine glatte Flügelunterseite

ohne scharfe und dadurch laute Kanten gebildet werden.

Biomechanische Messungen mit zwei unabhängigen Methoden (Biegebalkentests und Nanoindentation) wurden genutzt, um den E-Modul von Federkeratin der Schleiereule und der Taube zu bestimmen. Schleiereulen haben einen E-Modul von 6,6 GPa, Tauben hingegen haben mit 7,5 GPa einen 12% höheren E-Modul. Darüber hinaus zeigten sich Anpassungen der Kielgeometrien an verschiedene Biegeverhalten der beiden untersuchten Vogelarten.

Die Ergebnisse der vorliegenden Arbeit können nun genutzt werden, um die Mechanismen der Geräuschreduktion mit einer höheren Genauigkeit zu untersuchen, als es bisher möglich war.

References

- [1] Alerstam, T., M. Rosen, J. Bäckman, P. Ericson, and O. Hellgren: 2007, 'Flight speeds among bird species: Allometric and phylogenetic effects'. *PLOS Biology* **8**, 1656–1662.
- [2] Arndt, R. and T. Nagel: 1972, 'Effect of leading edge serrations on noise radiation from a model rotor'. *AIAA Paper* **1972-655**.
- [3] Astnury, W. and E. Beighton: 1961, 'Structure of feather keratin'. *Nature* **191**, 171 – 173.
- [4] Bachmann, T., S. Klän, W. Baumgartner, M. Klaas, W. Schröder, and H. Wagner: 2007, 'Morphometric characterisation of wing feathers of the barn owl (*Tyto alba pratincola*) and the pigeon (*Columba livia*)'. *Frontiers in Zoology* **4**, 23.
- [5] Baier, D., S. Gatesy, and J. F. Jenkins: 2007, 'A critical ligamentous mechanism in the evolution of avian flight'. *Nature* **445**, 307–310.
- [6] Baron, P., R. Fisher, A. Sherlock, F. Mill, and A. Tuson: 1997, *Evolutionary computing*, Chapt. A voxel based approach to evolutionary shape optimisation., pp. 251–261. Springer Berlin / Heidelberg.
- [7] Bechert, D., M. Bartenwerfer, G. Hoppe, and W.-E. Reif: 1986, 'Drag reduction mechanisms derived from shark skin'. *AIAA Paper* **2**, 1044–1068.
- [8] Benton, M.: 2000, *Vertebrate Palaeontology*. Blackwell Science Ltd.
- [9] Berg, A. and A. Biewener: 2006, 'Kinematics and power requirement of ascending and descending flight in the pigeon (*Columba livia*)'. *Journal of Experimental Biology* **211**, 1120–1130.
- [10] Berg, C. and J. M. V. Rayner: 1995, 'The moment of inertia of bird wings and the inertial power requirement for flapping flight'. *Journal of Experimental Biology* **198**, 1655 – 64.
- [11] Betz, O., U. Wegst, D. Weide, M. Heethoff, L. Helfen, W. Lee, and P. Cloetsens: 2007, 'Imaging applications of synchrotron X-ray phase-contrast microtomography in biological morphology and biomaterials science. I. General aspects of the technique and its advantages in the analysis of millimetre-sized arthropod structure'. *Journal of Microscience* **227**, 51–71.
- [12] Biesel, W., H. Butz, and W. Nachtigall: 1985, *Biona Report 3*, Chapt. Erste Messungen der Flügelgeometrie bei frei gleitfliegenden Haustauben (*Columba livia* var. *Domestica*) unter Benutzung neu ausgearbeiteter Windkanaltechnik und der Stereophotogrammetrie., pp. 139–160. Gustav Fischer, Stuttgart und New York.
- [13] Bonser, R.: 1995, 'Melanin and the abrasion resistance of feathers'. *Cooper Ornithological Society* **97**, 590–591.

- [14] Bonser, R. H. and P. Purslow: 1995, 'The Young's modulus of feather keratin'. *Journal of Experimental Biology* **198**, 1029 – 1033.
- [15] Bonser, R. H. C.: 2001, 'The mechanical performance of medullary foam from feathers'. *Journal of Materials Science Letters* **20**, 941 – 942.
- [16] Boswick, K. and M. Brady: 2002, 'Phylogenetic analysis of wing feather taxis in birds: Macroevolutionary patterns of genetic drift?'. *The Auk* **119**(4), 943–954.
- [17] Brand, T. and C. Seebaß: 1994, *Die Schleiereule*. Aula Verlag.
- [18] Busching, W.-D.: 1997, *Handbuch der Gefederkunde europäischer Vögel*. AULA-Verlag Wiesbaden.
- [19] Cameron, G., T. Wess, and R. Bonser: 2003, 'Young's modulus varies with differential orientation of keratin in feathers'. *Journal of Structural Biology* **143**, 118 – 123.
- [20] Carruthers, A. C., A. L. R. Thomas, and G. K. Taylor: 2007, 'Automatic aeroelastic devices in the wings of a steppe eagle *Aquila nipalensis*'. *Journal of Experimental Biology* **210**, 4136 –4149.
- [21] Censhaw, D.: 1980, 'Design and materials of feather shafts: very light, rigid structures'. *Symposium of the Society for Experimental Biology* **43**, 485–486.
- [22] Corning, W. R. and A. A. Biewener: 1998, 'In vivo strains in pigeon flight feather shafts: implications for structural design'. *Journal of Experimental Biology* **201**, 3057 – 3065.
- [23] Dial, K.: 1992, 'Avian forelimb muscles and nonsteady flight: Can birds fly without using the muscles in their wings?'. *The Auk* **109**(4), 874–885.
- [24] Dial, K. and A. Biewener: 1993, 'Pectoralis muscle force and power output during different modes of flight in pigeons (*Columba livia*)'. *Journal of Experimental Biology* **176**, 31–54.
- [25] Dyson, M., G. Klump, and B. Gauger: 1998, 'Absolute hearing thresholds and critical masking ratios on the European barn owl: a comparison with other owls'. *Journal of Comparative Physiology A* **182**, 695–702.
- [26] Ennos, A. R., J. R. E. Hickson, and A. Roberts: 1995, 'Functional morphology of the vanes of the flight feathers of the pigeon *Columbia livia*'. *Journal of Experimental Biology* **198**, 1219 – 1228.
- [27] Franck, A., G. Cocquyt, P. Simoens, and N. De Belie: 2006, 'Biomechanical properties of bovine claw horn'. *Biosystems Engineering* **4**, 459–467.
- [28] Fraser, R. and T. Macrae: 1980, 'Molecular structure and mechanical properties of keratins'. *Symposia of the Society for Experimental Biology* **32**, 211 – 246.

- [29] Gentury, C., C. Guigou, and C. Fuller: 1997, ‘Smart foam for applications on passive-active noise radiation control’. *Journal of the Acoustical Society of America* **101**(4), 1771–1778.
- [30] Golebiewski, R., R. Makarewicz, M. Nowak, and A. Preis: 2003, ‘Traffic noise reduction due to porous road surfaces’. *Applied Acoustics* **64**, 481–494.
- [31] Graham, R.: 1934, ‘The silent flight of owls’. *Journal Royal Aerodynamic Society* **38**, 837–843.
- [32] Harmening, W., P. Nikolay, J. Orłowski, and H. Wagner: 2009, ‘Spatial contrast sensitivity and grating acuity of barn owls’. *Journal of Vision* **9**(7), 1–12.
- [33] Harmening, W., M. Vobig, P. Walter, and H. Wagner: 2007, ‘Ocular aberrations in barn owl eyes’. *Visual Research* **47**(23), 2934–2942.
- [34] Hausmann, L., v. M. Campenhausen, F. Endler, M. Singheiser, and H. Wagner: 2009, ‘Improvements of sound localization abilities by the facial ruff of the barn owl (*Tyto alba*) as demonstrated by virtual ruff removal’. *PLoS ONE* **4**(11), e7721.
- [35] Herr, M. and W. Dobrzynski: 2005, ‘Experimental investigations in low-noise trailing-edge design’. *AIAA Journal* **43**(6).
- [36] Hersh, A., P. Sodermann, and R. Hayden: 1974, ‘Investigation of acoustic effects of leading-edge serrations on airfoils’. *Journal of Aircraft* **11**:4, 197–202.
- [37] Heuer, C. and R. Loesel: 2009, ‘Three-dimensional reconstruction of mushroom body neuropils in the polychaete species *Nereis diversicolor* and *Harmothoe areolata* (Phylodocida, Annelida)’. *Zoomorphology* **128**(3), 219–226.
- [38] Itoh, M., S. Tamano, R. Iguchi, K. Yokota, N. Akino, R. Hino, and S. Kubo: 2006, ‘Turbulent drag reduction by the seal fur surface’. *Physics of Fluids* **18**(065102).
- [39] Johnson, D.: 1997, *Biology and conservation of owls of the Northern Hemisphere*, Chapt. Wing loading in 15 species of North American owls, pp. 553–561. 2nd International symposium. Gen Tech Rep.
- [40] Klein, B.: 2009, *Leichtbau - Konstruktion*. Vieweg + Teubner Verlag, Wiesbaden.
- [41] Klän, S., T. Bachmann, M. Klaas, H. Wagner, and W. Schröder: 2008, ‘Experimental analysis of the flow field over a novel owl based airfoil’. *Experiments in Fluids* **46**, 975–989.
- [42] Knudsen, E.: 1981, ‘The hearing of the barn owl’. *Scientific American* **245**(6), 113–125.
- [43] Koch, U. and H. Wagner: 2002, ‘Morphometry of auricular feathers of barn owls (*Tyto alba*)’. *European Journal of Morphology* **40**, 15–21.
- [44] Konishi, M.: 1973, ‘How the owl tracks its prey’. *American Scientific* **61**, 414–424.

- [45] Konishi, M.: 2003, ‘Coding of auditory space’. *Annual Review of Neuroscience* **26**, 31–55.
- [46] Konishi, M., T. Takahashi, H. Wagner, W. Sullivan, and C. Carr: 1988, *Auditory function - Neurobiological Bases of Hearing*, Chapt. Neurophysiological and anatomical substrates of sound localization in the owl, pp. 721–745. John Wiley Sons Inc. New York.
- [47] Kroeger, R., H. Gruschka, and T. Helvey: 1971, ‘Low speed aerodynamics for ultra-quiet flight’. *AFFDL* **71-75**, 1–55.
- [48] Kubke, M., D. Massoglia, and C. Carr: 2004, ‘Bigger brains or bigger nuclei? Regulating the size of auditory structures in birds’. *Brain, Behaviour and Evolution* **63**, 169–180.
- [49] Lentink, D., U. K. Müller, E. J. Stamhuis, R. de Kat, W. van Gestel, L. L. M. Veldhuis, P. Henningsson, A. Hedenström, J. J. Videler, and J. L. van Leeuwen: 2007, ‘How swifts control their glide performance with morphing wings’. *Nature* **446**, 1082 – 1085.
- [50] Lilienthal, O.: 1889, *Der Vogelflug als Grundlage der Fliegekunst*. Gaertner Verlagshandlung, Berlin.
- [51] Lilley, G.: 1998, ‘A study of the silent flight of the owl’. *AIAA Paper* pp. 98–2340.
- [52] Liu, T., K. Kuykendoll, R. Rhews, and S. Jones: 2006, ‘Avian wings’. *AIAA Paper* **44**, 954–963.
- [53] Lockwood, R., J. Swaddle, and J. Rayner: 1998, ‘Avian wingtip shape reconsidered: wingtip shape indices and morphological adaptations to migration’. *Journal of Avian Biology* **29**, 273–292.
- [54] Macload, G.: 1980, ‘Mechanical properties of contour feathers’. *Journal of Experimental Biology* **87**, 65–71.
- [55] Mayr, G., B. Pohl, and S. Peters: 2005, ‘A well-preserved *Archaeopteryx* specimen with theropod features’. *Science* **310**, 1483–1486.
- [56] Mebs, T. and W. Scherzinger: 2000, *Die Eulen Europas*. Franckh-Kosmos Verlag.
- [57] Miller, L. and C. Peskin: 2009, ‘Flexible clap and fling in tiny insect flight’. *Journal of Experimental Biology* **212**, 3076–3090.
- [58] Müller, W. and G. Patone: 1998, ‘Air transmissivity of feathers’. *Journal of Experimental Biology* **201**, 2591 – 2599.
- [59] Nachtigall, W. and A. Klimbingat: 1985, *Biona Report 3*, Chapt. Messung der Flügelgeometrie mit der Profilkamm-Methode und geometrische Flügelkennzeichnung einheimischer Eulen, pp. 45–86. Gustav Fischer, Stuttgart und New York.
- [60] Nachtigall, W. and H.-J. Rothe: 1982, ‘Nachweis eines "clap-and-fling-Mechanismus" bei einer im Windkanal fliegenden Haustaube’. *Journal of Ornithology* **4**, 439–443.

- [61] Nachtigall, W. and J. Wieser: 1966, ‘Profilmessungen an Taubenflügeln’. *Zentralblatt für vergleichende Physiologie* **52**, 333–346.
- [62] Neuhaus, W., H. Bretting, and B. Schweizer: 1973, ‘Morphologische und funktionelle Untersuchungen über den lautlosen Flug der Eule (*Strix aluco*) im Vergleich zum Flug der Ente (*Anas platyrhynchos*)’. *Biologisches Zentralblatt* **92**, 495–512.
- [63] Norberg, U.: 2002, ‘Structure, form, and function of flight in engineering and the living world’. *Journal of Morphology* **252**, 52–81.
- [64] Oehme, H.: 1970, ‘Die Flügelprofile von Star und Türkentaube’. *Forma et Functional Ecology* **2**, 266–287.
- [65] Oliver, W. and G. Pharr: 1992, ‘Measurement of hardness and elastic modulus by instrumented indentation: Advances in understanding and refinements to methodology’. *Journal of Material Research* **7**, 1564.
- [66] Padian, K. and L. Chiappe: 1998a, ‘The origin and early evolution of birds’. *Biological Reviews* **73**, 1–42.
- [67] Padian, K. and L. Chiappe: 1998b, ‘The origin of birds and their flight’. *Scientific American* **278**, 38–47.
- [68] Pauling, L. and R. Corey: 1951, ‘The structure of feather rachis keratin’. *PNAS* **37**, 256–261.
- [69] Payne, R.: 1971, ‘Acoustic location of prey by barn owls (*Tyto alba*)’. *Journal of Experimental Biology* **54**, 535–573.
- [70] Pennycuik, C.: 1967, ‘The strength of the pigeon’s wing bones in relation to their function’. *Journal of Experimental Biology* **46**, 219–233.
- [71] Pennycuik, C.: 1968, ‘A wind-tunnel study of gliding flight in the pigeon *Columba livia*’. *Journal of Experimental Biology* **49**, 509–526.
- [72] Proctor, N. and P. Lynch: 1993, *Manual of ornithology*. Yale University Press New Haven and London.
- [73] Purslow, P. P. and J. F. V. Vincent: 1978, ‘Mechanical properties of primary feathers from the pigeon’. *Journal of Experimental Biology* **72**, 251 – 260.
- [74] Rayner, J.: 1988, ‘The evolution of vertebrate flight’. *Biological Journal of the Linnean Society* **34**, 269–287.
- [75] Rayner, J.: 1999, ‘Estimating power curves of flying vertebrates’. *Journal of Experimental Biology* **202**, 3449–3461.
- [76] Rayner, J., P. Viscardi, S. Ward, and J. Speakman: 2001, ‘Aerodynamics and energetics of intermittent flight in birds’. *American Zoologist* **41**, 188–204.

- [77] Ridgway, S. and D. Carder: 1993, 'Features of dolphin skin with potential hydrodynamic importance'. *Engineering in Medicine and Biology Magazine* **12**, 83–88.
- [78] Roberts, S. and M. Yaras: 2005, 'Boundary-layer transition affected by surface roughness and free-stream turbulence'. *Journal of Fluids Engineering-Transaction of the ASME* **127**, 449–457.
- [79] Roberts, S. and M. Yaras: 2006, 'Effects of surface-roughness geometry on separation-bubble transition'. *Journal of turbomachinery-transactions of the ASME* **128**, 349–356.
- [80] Roskam, J. and C.-T. Lan: 1997, *Airplane aerodynamics and performance*. Lawrence: Design, analysis and research cooperation.
- [81] Rüppell, G.: 1980, *Vogelflug*. Rowohlt Taschenbuch Verlag GmbH.
- [82] Rutschke, E.: 1966, 'Untersuchungen über die Feinstruktur des Schaftes der Vogelfeder'. *Zool. Jb. Abt. Syst.* **93**, 223–288.
- [83] Sartori, J.: 2008, 'Barbs of barn owl's feathers as components of acoustically optimised airfoils: A study based on mechanical characterisation and FE-Modelling'. *Bachelor-thesis, Hochschule Bremen*.
- [84] Schröder, A., M. Herr, T. Lauke, and U. Dierksheide: 2006, *New results in numerical and experimental fluid mechanics V*, Chapt. A study on trailing edge noise sources using high-speed particle image velocimetry, pp. 373–380. Springer Berlin / Heidelberg.
- [85] Schwind, R. and H. Allen: 1973, 'The effects of leading edge serrations on reducing flow unsteadiness about airfoils'. *AAIA Paper* **1973-89**.
- [86] Soderman, P.: 1972, 'Aerodynamic effects of leading-edge serrations on a two-dimensional airfoil'. *NASA Technical Memorandum* **X-2643**.
- [87] Taylor, I.: 1994, *Barn Owls: predator-prey relationships and conservation*. Cambridge University Press.
- [88] Tobalske, B. and K. Dial: 1996, 'Flight kinematics of black-billed magpies and pigeons over a wide range of speeds'. *Journal of Experimental Biology* **199**, 263–280.
- [89] Tobalske, B. and K. Dial: 2000, 'Effects of body size on take-off flight performance in the phasianidae (*Aves*)'. *Journal of Experimental Biology* **203**, 3319–3323.
- [90] Tobalske, B., W. Peacock, and K. Dial: 1999, 'Kinematics of flap-bounding flight in the zebra finch over a wide range of speeds'. *Journal of Experimental Biology* **202**, 1725–1739.
- [91] Tobalske, T.: 2007, 'Biomechanics of bird flight'. *Journal of Experimental Biology* **201**, 3135–3146.
- [92] Tucker, V. and G. Parrot: 1970, 'Aerodynamic of gliding flight in a falcon and other birds'. *Journal of Experimental Biology* **52**, 345–376.

- [93] Usherwood, J., T. Hedrick, C. McGowan, and A. Biewener: 2005, 'Dynamic pressure maps for wings and tails of pigeons in slow, flapping flight, and their energetic implications'. *Journal of Experimental Biology* **208**, 355–369.
- [94] v Campenhausen, M. and H. Wagner: 2006, 'Influence of the facial ruff on the sound-receiving characteristics of the barn owl's ears'. *Journal of Comparative Physiology A* **192**, 1073–82.
- [95] Veasey, J., N. Metcalfe, and D. Houston: 1998, 'A reassessment of the effect of body mass upon flight speed and predation risk in birds'. *Animal Behaviour* **56**, 883–889.
- [96] Veselka, N., D. McErlain, D. Holdsworth, J. Eger, R. Chhem, M. Mason, K. Brain, P. Faure, and M. Fenton: 2010, 'A bony connection signals laryngeal echolocation in bats'. *Nature Letters* **463**, 939–942.
- [97] Wagner, H.: 2004, 'A comparison of neural computations underlying stereo vision and sound localization'. *Journal of Physiology Paris* **98**, 135–145.
- [98] Weber, T., J. Borgudd, A. Hedenström, K. Persson, and G. Sandberg: 2005, 'Resistance of flight feathers to mechanical fatigue covaries with moult strategy in two warbler species'. *Biology Letters* **1**, 27 – 30.
- [99] Willot, J.: 2001, *Handbook of Mouse Auditory Research*. CRC Press.

Danksagung

An erster Stelle möchte ich mich bei Prof. Dr. Hermann Wagner für die wissenschaftliche Betreuung dieser Arbeit bedanken. In jeglichen Fragestellungen, wissenschaftlich wie privat, stand er mir stets konstruktiv zur Seite. Dabei hat er mich bei der Entwicklung meiner eigenen Forschungsrichtung gefördert und mir zugleich viel Freiraum für eigene Ideen gegeben. Ich freue mich auf weitere zukünftige Projekte mit ihm.

Prof. Dr. Werner Baumgartner danke ich für die Erstellung des Zweitgutachtens und für die vielen Antworten auf meine biomechanischen und technischen Fragen. Seine oft unkonventionellen Methoden waren stets eine Bereicherung meiner Forschung.

Mein besonderer Dank gilt meinem Freund und Kollegen Stephan Klän. Worte allein können meinen Dank an ihn nicht beschreiben.

Weiterhin möchte ich denjenigen Personen danken, die mich und meine Arbeit durch ihr geteiltes Wissen und tatkräftige Unterstützung gefördert haben. David Stadler möchte ich für die vielen Vorexperimente für die Etablierung der Biegebalkenversuche danken. Jens Emmerlich danke ich für die Durchführung der Nanoindentationsversuche und deren Interpretation. Agnes Weth und Sandra Brill danke ich für die Hilfe bei methodischen und statistischen Fragen. Bei Helga Gaube möchte ich mich ganz herzlich für das schnelle und gründliche Korrekturlesen meiner Arbeit bedanken.

Ich möchte arbeitsgruppenübergreifend allen Freunden und Mitgliedern des Instituts für Biologie II danken. Durch die zahlreichen wissenschaftlichen Diskussionen und privaten Veranstaltungen haben sie zu dem Erfolg dieser Arbeit beigetragen. Ich werde die schöne Zeit im Institut sehr vermissen.

Ich danke zudem der Deutschen Forschungsgemeinschaft für die Ermöglichung meiner Forschung und allen Mitgliedern des Schwerpunktprogramms 1207 für die zahlreichen Diskussionen und interdisziplinären Kooperationen.

Ich danke meinen Freunden und engsten Vertrauten für ihre Unterstützung in allen Lebenslagen.

Ich danke meiner Familie dafür, dass sie mich immer bedingungslos unterstützt und zu mir steht. Mein ganz besonderer Dank gilt hierbei meiner Mutter Marianne Bachmann, meinen Geschwistern Annika und Christian, meinen Schwiegereltern Marlies und Walter Schönherr und meiner Schwägerin Caroline. Es ist schön, eine solch starke Familie hinter sich zu wissen.

Mein herzlichster Dank gilt meiner Liebsten, Nadine, für ein erfülltes und glückliches Leben.

Curriculum vitae

Persönliche Daten

Name Thomas Willem Bachmann
Geburtsdatum 01. Dezember 1980 in Bonn
Anschrift Boxgraben 110, 52064 Aachen

Schulische und wissenschaftliche Ausbildung

1987 - 1991 Katholische Grundschule Mehlem in Bonn
1991 - 2000 Amos Comenius Gymnasium in Bonn
Abschluss Abitur
2000 - 2001 Zivildienst am Zoologischen Forschungsinstitut und
Museum Alexander Koenig in Bonn
2001 - 2003 Westfälische Wilhelms Universität in Münster,
Grundstudium der Biologie
2003 - 2006 Rheinisch-Westfälische Technische Hochschule in
Aachen, Hauptstudium der Biologie
2005 - 2005 Studentische Hilfskraft am Institut für Biologie II,
Lehrstuhl für Zoologie und Tierphysiologie,
RWTH Aachen
2006 - 2006 Diplomarbeit am Institut für Biologie II
Oktober 2006 Abschluss zum Diplom-Biologen
2006 - 2010 Promotion am Institut für Biologie II